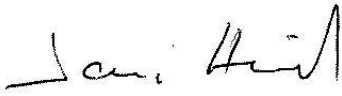




OPERATIONS REPORT

Issue 2/2024 rev. 1

Reporting period: July – December 2024

Authors			
Prepared by			
NAME		INSTITUTE	
Jari Hovila		FMI	
Contributions			
NAME		INSTITUTE	
Jari Hovila, Jukka Kujanpää, Kaisa Lakkala		FMI	
Axel Schmidt, Matthias Hofmann, Birgit Wunschheim		DLR	
Olaf Tuinder, Robert van Versendaal		KNMI	
Helge Jønych-Sørensen		DMI	
Katerina Garane, MariLiza Koukouli, Konstantinos Michailidis		AUTH	
Jeroen van Gent, José Granville, François Hendrick, Jean-Christopher Lambert, Bavo Langerock, Gaia Pinardi, Tijl Verhoelst		BIRA-IASB	
Andy Delcloo		KMI	
Peggy Tesche-Achtert		DWD	
Anne Boynard, Cathy Clerbaux, Maya George, Camille Viatte		LATMOS	
Rosa Astoreca, Pierre-François Coheur, Daniel Hurtmans, Catherine Wespes		ULB	
Carlos Vicente		EUMETSAT	
Approved by			
AC SAF Technical Manager	Jari Hovila / FMI	06/06/2025	 <i>Signature</i>

Document change log

Revision	Date	Description of change
1	06/06/2025	Initial revision

List of abbreviations

AC SAF	Satellite Application Facility on Atmospheric Composition Monitoring
ARP	Absorbing Aerosol Index from PMDs data product
ARP-A	Absorbing Aerosol Index from PMDs data product from Metop-A
ARP-B	Absorbing Aerosol Index from PMDs data product from Metop-B
ARP-C	Absorbing Aerosol Index from PMDs data product from Metop-C
ARS	Absorbing Aerosol Height data product
ARS-A	Absorbing Aerosol Height data product from Metop-A
ARS-B	Absorbing Aerosol Height data product from Metop-B
ARS-C	Absorbing Aerosol Height data product from Metop-C
ATMOS	Atmospheric Parameters Measured by in-Orbit Spectroscopy (DLR data service)
ATO	Assimilated Total Ozone
AUTH	Aristotle University of Thessaloniki
BIRA-IASB	Belgian Institute for Space Aeronomy
BrO	Bromine Oxide
CDOP	Continuous Development and Operations phase
CDR	Climate Data Record
CO	Carbon Monoxide
DLR	German Aerospace Center
DMI	Danish Meteorological Institute
DWD	German Weather Service
ECMWF	European Centre for Medium-Range Weather Forecasts
EDC	EUMETSAT Data Centre
EDD	Erythematous Daily Dose
EUMETCast	EUMETSAT's primary dissemination mechanism for the near real-time delivery of satellite data and products
EUMETSAT	European Organisation for the Exploitation of Meteorological Satellites
EUV	European UV product/data record
FMI	Finnish Meteorological Institute
GOME	Global Ozone Monitoring Experiment
H ₂ O	Water Vapour
HCHO	Formaldehyde
HNO ₃	Nitric acid
HR	High resolution
KMI	Royal Meteorological Institute of Belgium
KNMI	Royal Netherlands Meteorological Institute
L1b	Level 1b data product
L1c	Level 1c data product
L2	Level 2 data product

L3	Level 3 data product
LATMOS	Laboratoire Atmosphères, Milieux, Observations Spatiales
LER	Lambertian-equivalent reflectivity data record
NHP	Near Real-time High-resolution Ozone Profile data product
NO2	Nitrogen Dioxide
NRT	Near Real-time
NTO	Near Real-time Total Column data product
NUV	Near Real-time UV index data product
O3	Ozone
O3M SAF	Satellite Application Facility on Ozone and Atmospheric Chemistry Monitoring
OHP	Offline High-resolution Ozone Profile data product
OHP-A	Offline High-resolution Ozone Profile data product from Metop-A
OHP-B	Offline High-resolution Ozone Profile data product from Metop-B
OHP-C	Offline High-resolution Ozone Profile data product from Metop-C
OEM	Optimal Estimation Method
OPERA	Ozone Profile Retrieval Algorithm
OTO	Offline Total Column data product
OUV	Offline Surface UV data product
OUV-A	Offline Surface UV data product from Metop-A
OUV-AB	Offline Surface UV data product from Metop-A and Metop-B
OUV-B	Offline Surface UV data product from Metop-B
OUV-BC	Offline Surface UV data product from Metop-B and Metop-C
PDU	Product Dissemination Unit
PGE	Product Generation Element
PMD	Polarisation Measurement Device
RD	Reference Document
RMS	Root Mean Square
RMSE	Root Mean Square Error
SACS	Support to Aviation Control Service
SCD	Slant Column Density
SO2	Sulphur Dioxide
TOC	Total Ozone Column data product
TrOC	Global Tropospheric Ozone Column data product
TTrOC	Tropical Tropospheric Ozone Column data product
ULB	Université libre de Bruxelles
UTC	Coordinated Universal Time

TABLE OF CONTENTS

1.	INTRODUCTION	8
1.1.	Scope	8
1.2.	Reporting period	8
1.2.1.	Highlights	8
1.3.	Reference documents	8
1.4.	Definition of terms	11
1.5.	Accuracy requirements of AC SAF products	12
2.	PROCESSING CENTRE: FMI	18
2.1.	Offline surface UV	18
2.1.1.	Availability	18
2.1.2.	Timeliness	18
2.2.	Services, main events and anomalies	19
3.	PROCESSING CENTRE: DLR	22
3.1.	NRT and offline total/tropospheric trace gas columns, tropical tropospheric ozone	22
3.1.1.	Availability	22
3.1.2.	Timeliness	24
3.2.	Services, main events and anomalies	26
4.	PROCESSING CENTRE: KNMI	28
4.1.	NRT and offline ozone profiles, absorbing aerosol height and index, global tropospheric ozone	28
4.1.1.	Availability	28
4.1.2.	Timeliness	29
4.2.	Services, main events and anomalies	31
5.	PROCESSING CENTRE: DMI	33
5.1.	NRT clear-sky and cloud-corrected UV index	33
5.1.1.	Availability	33
5.1.2.	Timeliness	33
5.2.	Services, main events and anomalies	34
6.	PROCESSING CENTRE: EUMETSAT	35
6.1.	NRT IASI CO, SO ₂ , HNO ₃ and ozone profile	35
6.1.1.	Availability	35
6.1.2.	Timeliness	36
6.2.	Services, main events and anomalies	37
7.	VALIDATION AND QUALITY MONITORING	39
7.1.	GOME-2 total ozone column products	39
7.1.1.	Total ozone column validation	39
7.1.2.	Validation website	45
7.1.3.	Online quality monitoring	47
7.2.	GOME-2 tropospheric ozone products	47
7.3.	GOME-2 trace gas products	51
7.3.1.	Online quality monitoring	76
7.4.	GOME-2 ozone profile products	81
7.4.1.	Online quality monitoring	83
7.5.	GOME-2 aerosol products	85
7.5.1.	Online quality monitoring	91
7.6.	GOME-2 UV products	92

7.6.1.	Online quality monitoring.....	92
7.7.	IASI NRT products.....	94
8.	LIST OF AC SAF USERS.....	119
8.1.	FMI archive	119
8.2.	DLR archive	131
8.3.	DMI (NUV product via FTP)	143
8.4.	KNMI (unofficial NRT AAI via FTP).....	143
8.5.	Known international projects that use EUMETCast or WMO/GTS	143
8.6.	EUMETCast	144
9.	UPDATES DURING THE REPORTING PERIOD.....	145
9.1.	Software updates.....	145
9.2.	Hardware updates	145
9.3.	Documentation updates	145
10.	CHANGES IN APPEARANCE AND CONTENT OF THE WEB PORTAL.....	146
APPENDIX 1.....		147
APPENDIX 2.....		155

1. Introduction

1.1. Scope

The scope of this document is to summarise the operational activities concerning the products in operation and the associated services during the reporting period to see that the general requirements applicable to these services and products of the AC SAF [RD1, RD2, RD3] are fulfilled. Intended readers of this document are the members of AC SAF project team, Review Board of the annual Operations Review, AC SAF Steering Group and EUMETSAT OPS/WG as well as the users of the AC SAF products.

Operations Reports include information about product availability/timeliness, quality assurance, website usage, and delivery statistics. Main events, major anomalies and software/hardware updates are reported also. AC SAF Operations Report is published twice a year.

1.2. Reporting period

This Operations Report covers the period July – December 2024.

1.2.1. Highlights

New products

- 20 September: IASI CO and SO₂ level 2 climate data records (https://acsaf.org/datarecords/iasi_co_cdr.php and https://acsaf.org/datarecords/iasi_so2_cdr.php) released

1.3. Reference documents

Table 1.1. Operations Report reference documents

Reference	Title	Issued	Reporting period
RD1	Product Requirements Document (SAF/AC/FMI/RQ/PRD/001)	20/12/2023	N/A
RD2	Service Specification (SAF/AC/FMI/RQ/SESP/001)	15/05/2024	N/A
RD3	EUMETSAT Operational Services Specification (EUM/OPS/SPE/20/109969)	16/02/2023	N/A
RD4	O3M SAF Validation Report for NRT, offline and reprocessed total ozone columns	11/12/2015	January 2007 – December 2014
RD5	AC SAF Validation Report for NRT, offline, reprocessed and level 3 total/tropospheric NO ₂ columns	10/11/2017	Metop-A: January 2007 – July 2015 Metop-B: January 2013 – July 2015

Reference	Title	Issued	Reporting period
RD6	O3M SAF Validation Report for Metop-A NRT and offline coarse/high-resolution ozone profiles	20/02/2012	January 2007 – May 2011
RD7	O3M SAF Validation Report for Metop-B NRT and offline coarse/high-resolution ozone profiles	30/06/2013	December 2012 – April 2013
RD8	O3M SAF Validation Report for Metop-B NRT UV indexes	27/05/2013	May 2013
RD9	O3M SAF Validation Report for NRT, offline and reprocessed total SO ₂ columns	09/12/2015	January 2007 – December 2014
RD10	O3M SAF Validation Report for offline and reprocessed total BrO columns	09/12/2015	January 2007 – December 2014
RD11	O3M SAF Validation Report for NRT, offline and reprocessed total HCHO columns	30/10/2015	January 2007 – July 2015
RD12	O3M SAF Validation Report for offline and reprocessed total H ₂ O columns	30/10/2015	January 2007 – August 2015
RD13	O3M SAF Validation Report for NRT and offline aerosol products	25/06/2013	January 2007 – May 2013
RD14	O3M SAF Validation Report for Metop-B offline UV products	03/02/2015	June 2012 – May 2013
RD15	AC SAF Validation Report for GOME-2 surface LER product	27/03/2019	MSC: February 2007 – June 2018 PMD: April 2008 – June 2018
RD16	O3M SAF Validation Report for offline tropospheric ozone columns (cloud slicing)	03/07/2015	January 2007 – December 2014
RD17	O3M SAF Validation Report for NRT and offline tropospheric ozone columns (ozone profiles)	09/09/2015	January 2007 – December 2014
RD18	O3M SAF Validation Report for NRT IASI CO	17/11/2015	September 2015 – November 2015
RD19	AC SAF Validation Report for NRT IASI SO ₂	17/11/2017	Metop-A: January 2007 – December 2013 June 2017 – October 2017 Metop-B: June 2017 – December 2017

Reference	Title	Issued	Reporting period
RD20	AC SAF Validation Report for Metop-C offline tropical tropospheric ozone columns	05/06/2020	February – December 2019
RD21	AC SAF Validation Report for Metop-C NRT and offline global tropospheric ozone columns	05/06/2020	February – December 2019
RD22	AC SAF Validation Report for Metop-C NRT and offline high-resolution ozone profiles	05/06/2020	February – December 2019
RD23	AC SAF Validation Report for Metop-C NRT and offline total ozone columns	25/05/2020	February – July 2019
RD24	AC SAF Validation Report for Metop-C NRT and offline total/tropospheric nitrogen dioxide columns	25/11/2019	February – July 2019
RD25	AC SAF Validation Report for Metop-C NRT and offline total formaldehyde columns	19/05/2020	February – July 2019
RD26	AC SAF Validation Report for Metop-C offline total bromine monoxide columns	19/05/2020	February – July 2019
RD27	AC SAF Validation Report for Metop-C offline total water vapour columns	30/03/2020	February – July 2019
RD28	AC SAF Validation Report for NRT, offline and reprocessed absorbing aerosol height products	03/07/2020	2007-2019
RD29	AC SAF Validation Report for Metop-C NRT and offline absorbing aerosol index from PMDs products	09/10/2019	January – October 2019
RD30	AC SAF Validation Report for Metop-C NRT and offline total sulphur dioxide products	21/01/2021	February – July 2019
RD31	AC SAF Validation Report for NRT IASI total O ₃ and O ₃ profiles	28/02/2022	December 2019 – November 2020
RD32	AC SAF Validation Report for NRT IASI HNO ₃	26/04/2022	December 2019 – December 2021

Online documents:

[Service Specification](#), [Validation Reports](#)

1.4. Definition of terms

Availability is based on the definition in the EUMETSAT Operational Services Specification [RD3].

Product-specific clarifications:

- For NRT products, the monthly availability limit is 97.5 %. The availability is calculated as a “worst case scenario”:

$$\frac{\text{in time processed and disseminated L2 PDUs}}{\text{received L1b PDUs} + \text{missed L1b PDUs marked as “reception confirmed” in the EUMETCast sendlist}}$$

- For offline products, the monthly availability limit is 95.5 %. The availability is defined by the ratio of the number of in time processed, archived and quality-approved L2 products to the number of orbits for which L1b PDUs have been received per month.
- NUV and OUV are daily L3 products, and availability is defined as the fraction of days in a month with products fulfilling the timeliness requirements
- TTrOC is a monthly L3 product and availability is 100 % or 0 % depending on whether the product fulfills the timeliness requirement or not

Timeliness defines whether the product is near real time (NRT) product which is disseminated or ready for download in three hours from sensing at the latest or offline product which is available for download in two weeks after sensing at the latest, during system availability. System unavailability will in most cases not lead to loss of data but to delays with respect to the specified timeliness. In practice, timeliness of a product is determined by calculating the time from sensing to EUMETCast or archive upload. In the Operations Reports, the timeliness is presented as monthly average, minimum and maximum values.

Accuracy of a satellite product is defined as a comparison of the mean/median bias (absolute and/or relative differences) of the product against ground-based and/or satellite-based reference data. Precision around the accuracy is given as a spread around the averaged bias (either through standard deviation or other robust metrics).

1.5. Accuracy requirements of AC SAF products

The following table lists all operational AC SAF products and their accuracy requirements as defined in [RD2]. Also results of the semi-annual online quality assessment are reported.

Table 1.2. Accuracy requirements and validation results of AC SAF products

Product identifier	Product name	Threshold accuracy	Target accuracy	Optimal accuracy	Achieved accuracy according to online quality assessment (Section 7)
O3M-41.1	NRT total O3	20 %	4 % (SZA < 80°) 6 % (SZA > 80°)	1.5 %	For SZA < 80°: Mean rel. bias: +0.7 % Max rel. bias (SZA=75°-80°): +2.5 % For SZA > 80°: Mean rel. bias: +1.2 % w.r.t. Brewer ground reference
O3M-300					For SZA < 80°: Mean rel. bias: +1.6 % Max rel. bias (SZA=70°-75°): +3.1 % For SZA > 80°: Mean rel. bias: +2.8 % w.r.t. Brewer ground reference
O3M-50.1	NRT total NO2	20 % of annual mean	8 – 15 % of annual mean	4 – 8 % of annual mean	Abs. bias of -0.25×10^{15} molec/cm ² (GOME-2B) and -0.15×10^{15} molec/cm ² (GOME-2C) w.r.t. NDACC ZLS-DOAS. This corresponds to target accuracy reached.
O3M-338					
O3M-52.1	NRT tropospheric NO2	50 %	30 %	20 %	Between optimal and threshold accuracy depending on the pollution levels (for the MAX-DOAS station subset tested here).
O3M-341					
O3M-55.1	NRT total SO2	100 %	50 % (SZA < 70°)	30 %	50 % (SZA < 70°) 50 % (SZA < 70°)
O3M-374					

Product identifier	Product name	Threshold accuracy	Target accuracy	Optimal accuracy	Achieved accuracy according to online quality assessment (Section 7)
O3M-177	NRT total HCHO	100 %	50 % (polluted)	30 %	Between optimal and threshold accuracy depending on the pollution levels (for the MAX-DOAS station subset tested here).
O3M-344					
O3M-47.1	NRT high-resolution ozone profile	30 % in stratosphere 70 % in troposphere	15 % in stratosphere 30 % in troposphere	10 % in stratosphere 25 % in troposphere	
O3M-311					
O3M-78	NRT absorbing aerosol height	3 km (layer height < 10 km)	2 km (layer height < 10 km)	1 km (layer height < 10 km)	
O3M-364		4 km (layer height > 10 km)	3 km (layer height > 10 km)	2 km (layer height > 10 km)	
O3M-72.1	NRT absorbing aerosol index from PMDs	1.0 index points	0.5 index points	0.2 index points	0.5 index points
O3M-362					
O3M-409	NRT UV index, clear-sky	20 %	10 %	5 %	Deviation of the global average UV index for the reporting period from the preceding 8 years average was -3.14 % for NUV/CLEAR and 1.00 % for NUV/CLOUD
O3M-410	NRT UV index, cloud-corrected				
O3M-80	NRT IASI CO	25 % (normal conditions) 50 % (high pollution or low signal)	12 % (normal conditions) 20 % (high pollution or low signal)	5 % (normal conditions) 10 % (high pollution or low signal)	Accuracy is estimated at 7 % for the entire NDACC network. During local winter months with high solar zenith angle measurements the target accuracy can be exceeded but remains below the threshold accuracy of 25 %. For high latitude sites the biases fall within the target accuracy of 20 %. For the high pollution site Xianghe (near Beijing), the accuracy is estimated at 12 %.
O3M-352					
O3M-57	NRT IASI SO ₂	200 % (below 10 km)	100 % (below 10 km)	50 % (below 10 km)	
O3M-377		100 % (above 10 km)	35 % (above 10 km)	20 % (above 10 km)	

Product identifier	Product name	Threshold accuracy	Target accuracy	Optimal accuracy	Achieved accuracy according to online quality assessment (Section 7)
O3M-81	NRT IASI HNO ₃	50 %	35 %	10 %	Accuracy is estimated at 14 % for the entire NDACC network. Higher biases reaching 20 % are observed at tropical NDACC sites and in the southern hemisphere (Lauder and Wollongong). Lower relative biases below 10 % at high latitude sites.
O3M-336					Similar as for O3M-81
O3M-44	NRT IASI total O ₃	10 %	5 %	1 %	
O3M-306					
O3M-49	NRT IASI ozone profile	30 % in stratosphere 50 % in troposphere	15 % in stratosphere 30 % in troposphere	5 % in stratosphere 10 % in troposphere	
O3M-315					
O3M-06.1	Offline total O ₃	20 %	4 % (SZA < 80°) 6 % (SZA > 80°)	1.5 %	
O3M-42.1					Same as for NRT total O ₃
O3M-301					
O3M-07.1	Offline total NO ₂	20 % of annual mean	8 – 15 % of annual mean	4 – 8 % of annual mean	
O3M-51.1					Same as for NRT total NO ₂
O3M-339					
O3M-37.1	Offline tropospheric NO ₂	50 %	30 %	20 %	
O3M-53.1					Same as for NRT tropospheric NO ₂
O3M-342					

Product identifier	Product name	Threshold accuracy	Target accuracy	Optimal accuracy	Achieved accuracy according to online quality assessment (Section 7)
O3M-09.1	Offline total SO ₂	100 %	50 % (SZA < 70°)	30 %	
O3M-56.1					Same as for NRT total SO ₂
O3M-375					
O3M-08.1	Offline total BrO	50 %	30 %	15 %	Generally within the target requirements for the S5p comparisons, within optimal accuracy for comparisons to Harestua ZSL-DOAS.
O3M-82.1					
O3M-317					
O3M-10.1	Offline total HCHO	100 %	50 % (polluted cond.)	30 %	
O3M-58.1					Same as for NRT total HCHO
O3M-345					
O3M-12.1	Offline total H ₂ O	25 %	10 %	5 %	
O3M-86.1					
O3M-386					
O3M-35	Offline tropical tropospheric ozone	50 %	25 %	15 %	
O3M-43					
O3M-302					
O3M-303	Offline L3 daily averaged total O ₃	20 %	4 % (SZA < 80°) 6 % (SZA > 80°)	1.5 %	Same as for the offline L2 total O ₃
O3M-388	Offline L3 monthly averaged total O ₃				

Product identifier	Product name	Threshold accuracy	Target accuracy	Optimal accuracy	Achieved accuracy according to online quality assessment (Section 7)
O3M-340	Offline L3 daily averaged total NO ₂	20 %	8 %	5 %	Same as for the offline L2 total NO ₂
O3M-389	Offline L3 monthly averaged total NO ₂				
O3M-343	Offline L3 daily averaged tropospheric NO ₂	50 %	30 %	20 %	Same as for the offline L2 tropospheric NO ₂
O3M-390	Offline L3 monthly averaged tropospheric NO ₂				
O3M-376	Offline L3 daily averaged total SO ₂	100 %	50 % (SZA < 70°)	30 %	Same as for the offline L2 total SO ₂
O3M-397	Offline L3 monthly averaged total SO ₂				
O3M-318	Offline L3 daily averaged total BrO	50 %	30 %	15 %	Same as for the offline L2 total BrO
O3M-391	Offline L3 monthly averaged total BrO				
O3M-387	Offline L3 daily averaged total H ₂ O	25 %	10 %	5 %	Same as for the offline L2 total H ₂ O
O3M-393	Offline L3 monthly averaged total H ₂ O				
O3M-346	Offline L3 daily averaged total HCHO	100 % (polluted cond.)	50 % (polluted cond.)	30 % (polluted cond.)	Same as for the offline L2 total HCHO
O3M-394	Offline L3 monthly averaged total HCHO				
O3M-39.1	Offline high-resolution ozone profile	30 % in stratosphere 70 % in troposphere	15 % in stratosphere 30 % in troposphere	10 % in stratosphere 25 % in troposphere	
O3M-48.1					Same as for NRT high-resolution ozone profile
O3M-312					

Product identifier	Product name	Threshold accuracy	Target accuracy	Optimal accuracy	Achieved accuracy according to online quality assessment (Section 7)
O3M-172	NRT global tropospheric ozone	50 %	20 %	15 %	
O3M-174					
O3M-304					
O3M-173	Offline global tropospheric ozone	50 %	20 %	15 %	
O3M-175					
O3M-305					
O3M-69	Offline absorbing aerosol height	3 km (layer height < 10 km) 4 km (layer height > 10 km)	2 km (layer height < 10 km) 3 km (layer height > 10 km)	1 km (layer height < 10 km) 2 km (layer height > 10 km)	
O3M-79					GOME2 - EARLINET 40.6 % (<1km) 65.0 % (<2km) 83.2 % (<3km)
O3M-365					
O3M-63.1	Offline absorbing aerosol index from PMDs	1.0 index points	0.5 index points	0.2 index points	
O3M-73.1					Same as for NRT AAI
O3M-363					
O3M-450 – O3M-464	Offline surface UV	50 %	20 %	10 %	Average value of the global erythemal daily dose during the reporting period deviated -3.41 % from the long-term average. See Figure 7.28.

Latest validation reports for all pre-operational and operational AC SAF products are listed in Section 1.3.

2. Processing centre: FMI

2.1. Offline surface UV radiation

Offline surface UV radiation (OUV) product is a L3 multi-mission (Metop-B+C) product consisting of 15 sub-products which are listed in Table 2.1. Since they are all archived in the same file, single entries in the tables in the following sections represent them all.

Table 2.1. OUV sub-products

Product Identifier	Product Name	Product Acronym
O3M-450	Offline UV daily dose, erythemat (CIE) weighting	MM-O-UV_DD_CIE
O3M-451	Offline UV daily dose, plant response weighting	MM-O-UV_DD_PLANT
O3M-452	Offline UV daily dose, DNA damage weighting	MM-O-UV_DD_DNA
O3M-453	Offline UV daily dose, UVA range (315-400 nm)	MM-O-UV_DD_UVA
O3M-454	Offline UV daily dose, UVB range (280-315 nm)	MM-O-UV_DD_UVB
O3M-455	Offline UV daily maximum dose rate, erythemat (CIE) weighting	MM-O-UV_MDSR_CIE
O3M-456	Offline UV daily maximum dose rate, plant response weighting	MM-O-UV_MDSR_PLANT
O3M-457	Offline UV daily maximum dose rate, DNA damage weighting	MM-O-UV_MDSR_DNA
O3M-458	Offline UV daily maximum dose rate, UVA range (315-400 nm)	MM-O-UV_MDSR_UVA
O3M-459	Offline UV daily maximum dose rate, UVB range (280-315 nm)	MM-O-UV_MDSR_UVB
O3M-460	Offline UV solar noon UV index	MM-O-UV_NOON_UVI
O3M-461	Offline UV daily maximum ozone photolysis rate	MM-O-UV_MPHR_O3
O3M-462	Offline daily maximum nitrogen dioxide photolysis rate	M-O-UV_MPHR_NO2
O3M-463	Offline UV daily dose, vitamin D weighting	MM-O-UV_DD_VITD
O3M-464	Offline UV daily maximum dose rate, vitamin D weighting	MM-O-UV_MDSR_VITD

2.1.1. Availability

Availability requirement for OUV has been defined in Section 1.4. The availability statistics of FMI products are presented in Table 2.2. If the availability requirement has been violated, those values are marked with red colour, identified by numbers and reported in Table 2.7.

Table 2.2. Availability of OUV product during the reporting period

7/2024	8/2024	9/2024	10/2024	11/2024	12/2024
100 %	100 %	100 %	100 %	100 %	100 %

2.1.2. Timeliness

Timeliness indicates the elapsed time between sensing and product dissemination. Timeliness requirement is 15 days for offline products. If the requirement has been violated, those values are

marked with red colour. In addition, the violations are identified by numbers and reported in Table 2.7 if they have caused the availability values to drop below the allowed limits.

Note: timeliness violations are not listed as anomalies if the availability is above the limit.

The values in Table 2.3 indicate the elapsed times (days, hours and minutes in the format [ddT]hh:mm) from sensing to archive upload. In each cell, the values from top to bottom represent observed monthly average, minimum and maximum times.

Table 2.3. Timeliness of OUV product during the reporting period

7/2024	8/2024	9/2024	10/2024	11/2024	12/2024
avg: 04T01:15 min: 04T00:32 max: 04T01:37	avg: 04T01:15 min: 04T01:12 max: 04T02:12	avg: 04T01:13 min: 04T00:17 max: 04T01:17	avg: 04T01:17 min: 04T00:17 max: 04T01:22	avg: 04T01:16 min: 04T00:22 max: 04T01:22	avg: 04T01:13 min: 04T00:22 max: 04T01:27

2.2. Services, main events and anomalies

Table 2.4. FMI service statistics related to product archiving, ordering and AC SAF Helpdesk

Description of service / event	7/2024	8/2024	9/2024	10/2024	11/2024	12/2024
Product ordering ¹						
Number of users (cumulative)	698	704	711	717	720	722
Number of orders	17	21	17	24	4	7
Number of ordered products	OHP: 439 ARS: 9973 ARP: 3 OUV subset: 30 OUV time-series: 79	OHP: 28 ARS: 1812 ARP: 89 OUV subset: 31 OUV time-series: 11686	OHP: 468 ARS: 4049 ARP: 93 OUV subset: 31	OHP: 70 OUV subset: 572 OUV time-series: 76004	ARP: 58 OUV time-series: 6	OHP: 2 OUV subset: 1539 OUV time-series: 6409
Ordered data volume	OHP: 110 GB ARS: 10.3 GB ARP: 17.6 MB OUV subset: 916 kB OUV time-series: 9.31 kB	OHP: 7.02 GB ARS: 1.88 GB ARP: 640 MB OUV subset: 947 kB OUV time-series: 960 kB	OHP: 117 GB ARS: 4.18 GB ARP: 674 MB OUV subset: 947 kB	OHP: 24.3 GB OUV subset: 2.20 GB OUV time-series: 10.4 MB	ARP: 41.1 MB OUV time-series: 4.40 kB	OHP: 504 MB OUV subset: 32.8 GB OUV time-series: 2.64 MB
Number of failed orders ²	0	0	0	0	0	0
Archive statistics ³						
Number of archived products (Metop-B)	OHP: 438 ARS: 438 ARP: 438	OHP: 438 ARS: 438 ARP: 438	OHP: 422 ARS: 422 ARP: 422	OHP: 438 ARS: 438 ARP: 438	OHP: 425 ARS: 425 ARP: 425	OHP: 439 ARS: 439 ARP: 439
Size of archived products (Metop-B)	OHP: 110 GB ARS: 454 MB ARP: 3.16 GB	OHP: 110 GB ARS: 453 MB ARP: 3.17 GB	OHP: 106 GB ARS: 433 MB ARP: 3.06 GB	OHP: 110 GB ARS: 449 MB ARP: 3.18 GB	OHP: 107 GB ARS: 435 MB ARP: 3.08 GB	OHP: 110 GB ARS: 448 MB ARP: 3.16 GB
Number of archived products (Metop-C)	OHP: 439 ARS: 439 ARP: 439	OHP: 432 ARS: 432 ARP: 432	OHP: 422 ARS: 422 ARP: 422	OHP: 438 ARS: 438 ARP: 438	OHP: 423 ARS: 423 ARP: 423	OHP: 433 ARS: 433 ARP: 433
Size of archived products (Metop-C)	OHP: 110 GB ARS: 457 MB ARP: 3.19 GB	OHP: 109 GB ARS: 449 MB ARP: 3.14 GB	OHP: 106 GB ARS: 436 MB ARP: 3.08 GB	OHP: 110 GB ARS: 452 MB ARP: 3.20 GB	OHP: 106 GB ARS: 436 MB ARP: 3.08 GB	OHP: 109 GB ARS: 448 MB ARP: 3.15 GB

Number of archived multi-mission products	OUV: 31	OUV: 31	OUV: 30	OUV: 31	OUV: 30	OUV: 31
Size of archived multi-mission products	OUV: 528 MB	OUV: 540 MB	OUV: 545 MB	OUV: 595 MB	OUV: 561 MB	OUV: 551 MB
GOME-2 L1b PDU rolling archive statistics ⁴						
PDUs archived / PDUs “reception confirmed” (Metop-B)	14797/14855 99.6 %	14723/14791 99.5 %	14263/14261 >100 %	14879/14879 100 %	14383/14383 100 %	14740/14746 100 %
PDUs archived / PDUs “reception confirmed” (Metop-C)	14778/14836 99.6 %	14608/14665 99.6 %	14261/14239 >100 %	14880/14876 >100 %	14377/14376 >100 %	14675/14674 >100 %
Helpdesk statistics						
Number of emails	0	0	2	1	3	0
Number of email threads	-	-	1	1	2	-
Average response time ([ddT]hh:mm)	-	-	03T08:20 ⁵	00:20	01T19:42	-

¹ More detailed information about the orders is available in Appendix 1

² Failed orders are detailed in Appendix 2

³ Based on sensing start time

⁴ For Level 1b products, the availability is defined as the number of archived L1b PDUs divided by the number of L1b PDUs with status “reception confirmed” in the EUMETCast sendlist. PDUs received via EUMETCast Terrestrial may increase the ratio above 100 %.

⁵ Helpdesk operator was on sick leave

Data archive statistics since 2008 are illustrated in Figure 2.1.

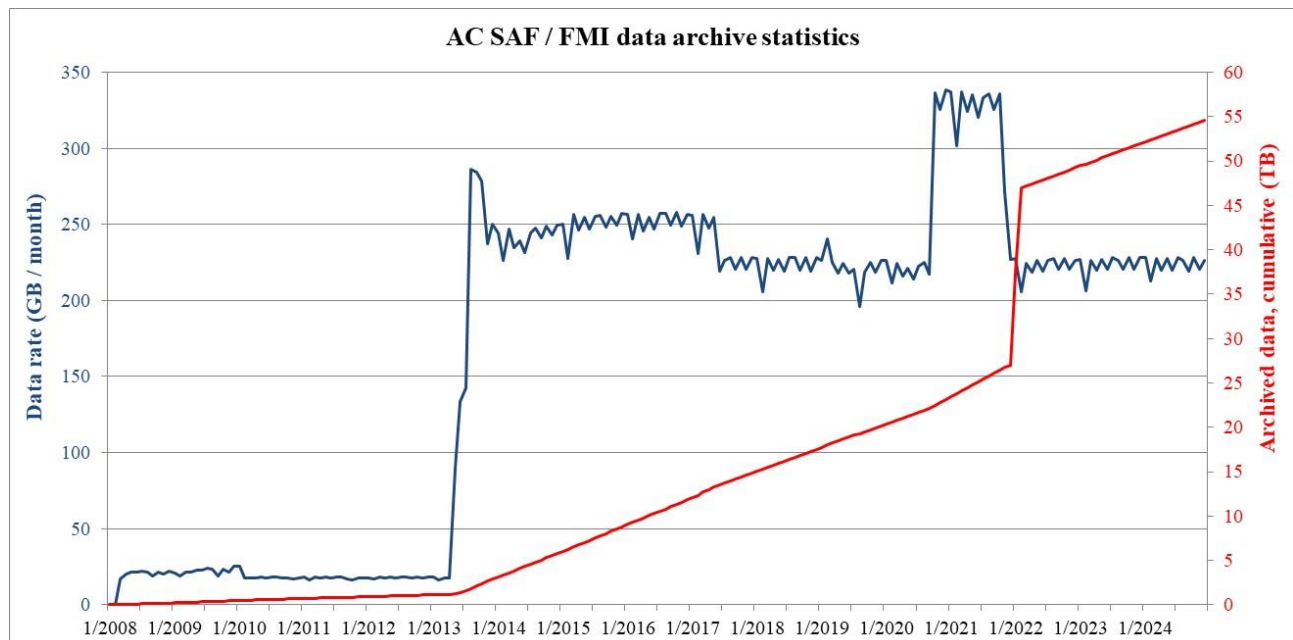


Figure 2.1. FMI data archive statistics: data rate and cumulative amount of data

Sudden increase in the cumulative amount of archived data in January – February 2022 is due to archiving of Metop-A/B high-resolution ozone profile data record R1.

Events affecting the data rate are presented in Table 2.5.

Table 2.5. Events affecting the FMI archive data rate

Date	Event	Data rate (GB/month)
03/2008	Archiving of OOP-A started	19.1 – 22.2
06/2009	Archiving of OUV-A started	19.2 – 23.8
11/2009	Archiving of ARS-A started	25.3
02/2010	Compression of OOP-A started	16.2 – 18.3
05/2013	Archiving of OHP-A started	133 – 142
08/2013	Archiving of OOP-B, OHP-B and ARS-B started	279 – 284
11/2013	Archiving of ARP-A and ARP-B started. KNMI implements shuffling algorithm in the hdf5 compression	226 – 250
03/2014	Archiving of OUV-A discontinued, archiving of OUV-B started	227 – 250
02/2015	OPERA algorithm update, tropospheric integrated profiles added	247 – 257
06/2017	Archiving of OOP-A and OOP-B discontinued	206 – 229
10/2020	Archiving of ARS-C, ARP-C and OHP-C started	302 – 338
11/2021	Archiving of OHP-A, ARS-A and ARP-A discontinued	206 – 228
01/2023	Archiving of IASI-B/C L3 CO started	206 – 228

Table 2.6 lists the main events (product/service/hardware/software updates etc.) at FMI during the reporting period.

Table 2.6. Main events at FMI during the reporting period

Date	Description
	<i>Nothing to report.</i>

Table 2.7 lists the main local and external anomalies during the reporting period. Corrective and preventive actions should be provided also when applicable.

Table 2.7. Main local and external anomalies affecting FMI systems and performance during the reporting period

ID	Time period	Description
		<i>Nothing to report.</i>

3. Processing centre: DLR

3.1. NRT and offline total/tropospheric trace gas columns, tropical tropospheric ozone

This section reports availability and timeliness of the operational NRT and offline L2 and L3 products processed for GOME-2 on Metop-B and Metop-C.

3.1.1. Availability

For Level 1b products, the availability is defined as the number of L1b PDUs with status “reception confirmed”, i.e. EUMETSAT received these L1b PDUs through its EUMETCast reference receiving station, divided by the total number of L1b PDUs listed in the EUMETCast sendlist.

Availability for offline L2 and L3 products has been defined in Section 1.4. The availability statistics of DLR products are presented in Table 3.1 and Table 3.2. If the availability requirements have been violated, those values are marked with red colour, identified by numbers and reported in Table 3.7.

Table 3.1. Availability of Metop-B total and tropospheric trace gas column products during the reporting period

Product Identifier	Product Name	7/2024	8/2024	9/2024	10/2024	11/2024	12/2024
L1b	PDUs received / PDUs “reception confirmed”	14855/14855 100 %	14790/14791 99.9 %	14261/14261 100 %	14879/14879 100 %	14383/14383 100 %	14746/14746 100 %
O3M-41.1	NRT total O3	100 %	99.9 %	99.7 %	99.9 %	100 %	100 %
O3M-50.1	NRT total NO2						
O3M-52.1	NRT tropospheric NO2						
O3M-55.1	NRT total SO2						
O3M-177.0	NRT total HCHO						
O3M-42.1	Offline total O3	99.6 %	98.4 %	99.1 %	99.3 %	99.8 %	99.3 %
O3M-51.1	Offline total NO2						
O3M-53.1	Offline tropospheric NO2						
O3M-56.1	Offline total SO2						
O3M-58.1	Offline total HCHO						
O3M-82.1	Offline total BrO						
O3M-86.1	Offline total H2O						
O3M-43	Offline tropical tropospheric ozone	100 %	100 %	100 %	100 %	100 %	100 %

Table 3.2. Availability of Metop-C total and tropospheric trace gas column products during the reporting period

Product Identifier	Product Name	7/2024	8/2024	9/2024	10/2024	11/2024	12/2024
L1b	PDU received / PDUs “reception confirmed”	14807/14836 99.8 %	14645/14665 99.9 %	14225/14239 99.9 %	14856/14876 99.9 %	14371/14376 99.9 %	14671/14674 99.9 %
O3M-300	NRT total O3	99.7 %	99.8 %	99.5 %	99.9 %	99.9 %	99.9 %
O3M-338	NRT total NO2						
O3M-341	NRT tropospheric NO2						
O3M-374	NRT total SO2						
O3M-344	NRT total HCHO						
O3M-301	Offline total O3	99.6 %	98.3 %	99.1 %	99.3 %	98.8 %	99.8 %
O3M-339	Offline total NO2						
O3M-342	Offline tropospheric NO2						
O3M-375	Offline total SO2						
O3M-345	Offline total HCHO						
O3M-317	Offline total BrO						
O3M-386	Offline total H2O						
O3M-302	Offline tropical tropospheric ozone	100 %	100 %	100 %	100 %	100 %	100 %

3.1.2. Timeliness

Timeliness indicates the elapsed time between sensing and product dissemination. Timeliness requirements are 3 hours for NRT products, 14 days for the offline tropical tropospheric ozone product and 15 days for the other offline products. If the requirements have been violated, those values are marked with red colour. In addition, the violations are identified by numbers and reported in Table 3.7 if they have caused the availability values to drop below the allowed limits.

Note: timeliness violations are not listed as anomalies if the availability is above the limit.

The values in Table 3.3 and Table 3.4 indicate the elapsed times (days, hours and minutes in the format [ddT]hh:mm) from sensing to EUMETCast (NRT) or AC SAF FTP site (offline) upload. For the offline tropical tropospheric ozone product, however, the values indicate the elapsed time from the end of the preceding month to product upload to the AC SAF FTP site. Timeliness requirement for those products is currently 14 days.

In each cell, the values from top to bottom represent observed monthly average, minimum and maximum times.

Table 3.3. Timeliness of Metop-B total and tropospheric trace gas column products during the reporting period

Product Identifier	Product Name	7/2024	8/2024	9/2024	10/2024	11/2024	12/2024
O3M-41.1	NRT total O3	avg: 00:54 min: 00:31 max: 01:50	avg: 00:57 min: 00:29 max: 02:06	avg: 00:58 min: 00:29 max: 07:13	avg: 00:57 min: 00:29 max: 01:50	avg: 00:53 min: 00:37 max: 02:07	avg: 00:53 min: 00:32 max: 02:07
O3M-50.1	NRT total NO2						
O3M-52.1	NRT tropospheric NO2						
O3M-55.1	NRT total SO2						
O3M-177.0	NRT total HCHO						
O3M-42.1	Offline total O3	avg: 01T03:16 min: 01T00:55 max: 01T15:39	avg: 01T01:32 min: 01T00:54 max: 01T08:10	avg: 03T02:10 min: 01T00:24 max: 13T10:20	avg: 01T01:18 min: 01T01:02 max: 01T01:13	avg: 01T01:31 min: 01T00:45 max: 03T17:32	avg: 01T02:15 min: 01T00:52 max: 02T06:24
O3M-51.1	Offline total NO2						
O3M-53.1	Offline tropospheric NO2						
O3M-56.1	Offline total SO2						
O3M-58.1	Offline total HCHO						
O3M-82.1	Offline total BrO						
O3M-86.1	Offline total H2O						
O3M-43	Offline tropical tropospheric ozone	18T17:34 (1)	24T15:34 (1)	44T17:32 (1)	13T17:32	15T18:33 (1)	23T18:33 (1)

Table 3.4. Timeliness of Metop-C total and tropospheric trace gas column products during the reporting period

Product Identifier	Product Name	7/2024	8/2024	9/2024	10/2024	11/2024	12/2024
O3M-300	NRT total O3	avg: 01:37 min: 00:35 max: 02:17	avg: 01:42 min: 00:34 max: 02:11	avg: 01:43 min: 00:40 max: 07:45	avg: 01:43 min: 00:46 max: 02:05	avg: 01:39 min: 01:09 max: 01:56	avg: 01:36 min: 01:07 max: 01:54
O3M-338	NRT total NO2						
O3M-341	NRT tropospheric NO2						
O3M-374	NRT total SO2						
O3M-344	NRT total HCHO						
O3M-301	Offline total O3	avg: 01T03:38 min: 01T00:54 max: 01T18:14	avg: 01T05:44 min: 01T00:22 max: 03T18:24	avg: 01T02:58 min: 01T00:46 max: 08T23:27	avg: 01T01:18 min: 01T01:03 max: 01T01:15	avg: 01T01:36 min: 01T01:00 max: 01T19:23	avg: 01T02:07 min: 01T01:02 max: 02T05:25
O3M-339	Offline total NO2						
O3M-342	Offline tropospheric NO2						
O3M-375	Offline total SO2						
O3M-345	Offline total HCHO						
O3M-317	Offline total BrO						
O3M-386	Offline total H2O						
O3M-302	Offline tropical tropospheric ozone	18T17:34 (1)	24T15:34 (1)	44T17:33 (1)	13T17:33	15T18:33 (1)	23T18:33 (1)

3.2. Services, main events and anomalies

Table 3.5. DLR service statistics related to product archiving and ordering

Description of service / event	7/2024	8/2024	9/2024	10/2024	11/2024	12/2024
Archive statistics ²						
Number of archived products (cumulative) – according to product insertion time	551817	552689	553540	554414	555263	556140
Size of archived products (TB, cumulative)	17.55	17.60	17.64	17.69	17.73	17.78
Number of missing orbit products – according to sensing time	0	0	0	0	1	0
Number of archived products with good/poor/error ³ quality assessed per month – according to product insertion time	868/1/10	846/8/18	768/24/59	834/12/28	842/8/5	877/0/2
Online Access ¹						
Number of FTP (ATMOS/VELA) subscribers	629	634	642	646	650	650
Number of FTP (ATMOS/VELA) downloads	247415	145571	(*)	(*)	(*)	(*)
Downloaded data volume (GB)	2485.6	965.88	(*)	(*)	(*)	(*)

¹ NTO product and OTO product is stored at the DLR for external search and download

² O3MOTO product (collection GOME.TC, Metop missions) is archived and available to non-NRT users

³ good: max. 2 PDUs missing, poor/error: more than 2 PDUs missing

(*) Due to a server upgrade, the respective log information for retrieving the number of FTP downloads from 08/2024 up to including 05/2025 is irrecoverably lost; preventive action: incorporation of log file availability into monitoring system

Table 3.6 lists the main events (product/service/hardware/software updates etc.) at DLR during the reporting period.

Table 3.6. Main events at DLR during the reporting period

Date	Event
	<i>Nothing to report.</i>

Table 3.7 lists the main and external local anomalies at DLR during the reporting period. Corrective and preventive actions should be provided also when applicable.

Table 3.7. Main local and external anomalies affecting DLR systems and performance during the reporting period

ID	Time period	Description
1	July – December 2024	<p>The timeliness of ≤ 2 weeks as specified in the currently applicable version (2.1) of the Product Requirements Document has been violated consistently (except for 10/2024 for both missions Metop-B and Metop-C) in the reporting period. The generation of the tropospheric ozone products is triggered manually after a certain and not fully fixed time period after all L2 data covering the respective month plus its nominal 14 days timeliness have passed.</p> <p>Corrective action: None</p> <p>Preventive action: A first discussion about the potential adaption of the timeliness requirement for this product type (O3M-43) has been held in the Operations Review 16 end of 2024. During the Operations Review a final check on the user needs with regards to the product availability has been suggested by the project team. DLR clarified the user needs. However, final feedback towards the project team and clarification is pending.</p>

4. Processing centre: KNMI

4.1. NRT and offline ozone profiles, absorbing aerosol height and index, global tropospheric ozone

4.1.1. Availability

For Level 1b products, the availability is defined as the number of unique L1b PDUs received either via EUMETCast Satellite or EUMETCast Terrestrial (demonstrational dissemination service), divided by the number of L1b PDUs not marked as “not sent” in the EUMETCast Satellite sendlist. This approximation presumes that all PDUs marked as “sent not confirmed” are still available via EUMETCast Terrestrial. Availability is higher than 100 % if there are more PDUs received from Terrestrial than is indicated by the Satellite sendlists.

Availability for offline L2 products has been defined in Section 1.4. The availability statistics of KNMI products are presented in Table 4.1 and Table 4.2. If the availability requirements have been violated, those values are marked with red colour, identified by numbers and reported in Table 4.9.

Tropospheric ozone products are included in the ozone profile products and have the same statistics. The same applies to scattering aerosol index products which are included in the absorbing aerosol index products.

Table 4.1. Availability of Metop-B L1b PDUs, ozone profile products and aerosol products during the reporting period

Product Identifier	Product Name	7/2024	8/2024	9/2024	10/2024	11/2024	12/2024
EUMETCast							
L1b	PDUs received / sent	14857/14855 >100 %	14793/14791 >100 %	14263/14261 >100 %	14879/14879 100 %	14383/14383 100 %	14748/14746 >100 %
O3M-47.1	NRT high-resolution ozone profile	100 %	100 %	100 %	100 %	100 %	100 %
O3M-78	NRT absorbing aerosol height	100 %	100 %	100 %	100 %	100 %	100 %
O3M-72.1	NRT absorbing aerosol index from PMDs	100 %	100 %	100 %	100 %	100 %	100 %
WMO/GTS							
O3M-47.1	NRT high-resolution ozone profile	100 %	100 %	100 %	100 %	100 %	100 %
FMI archive							
O3M-48.1	Offline high-resolution ozone profile	100 %	100 %	100 %	100 %	100 %	100 %
O3M-79	Offline absorbing aerosol height	100 %	100 %	100 %	100 %	100 %	100 %
O3M-73.1	Offline absorbing aerosol index from PMDs	100 %	100 %	100 %	100 %	100 %	100 %

Table 4.2. Availability of Metop-C L1b PDUs, ozone profile products and aerosol products during the reporting period

Product Identifier	Product Name	7/2024	8/2024	9/2024	10/2024	11/2024	12/2024
EUMETCast							
L1b	PDUs received / sent	14841/14836 >100 %	14667/14665 >100 %	14261/14239 >100 %	14880/14876 >100 %	14377/14376 >100 %	14675/14674 >100 %
O3M-311	NRT high-resolution ozone profile	100 %	100 %	100 %	100 %	100 %	100 %
O3M-364	NRT absorbing aerosol height	100 %	100 %	100 %	100 %	100 %	100 %
O3M-362	NRT absorbing aerosol index from PMDs	100 %	100 %	100 %	100 %	100 %	100 %
WMO/GTS							
O3M-311	NRT high-resolution ozone profile	100 %	100 %	100 %	100 %	100 %	100 %
FMI archive							
O3M-312	Offline high-resolution ozone profile	100 %	100 %	100 %	100 %	100 %	100 %
O3M-365	Offline absorbing aerosol height	100 %	100 %	100 %	100 %	100 %	100 %
O3M-363	Offline absorbing aerosol index from PMDs	100 %	100 %	100 %	100 %	100 %	100 %

4.1.2. Timeliness

Timeliness indicates the elapsed time between sensing and product dissemination. Timeliness requirements are 3 hours for NRT products and 15 days for offline products. If the requirements have been violated, those values are marked with red colour. In addition, the violations are identified by numbers and reported in Table 4.9 if they have caused the availability values to drop below the allowed limits.

Note: timeliness violations are not listed as anomalies if the availability is above the limit.

The values in Table 4.3 and Table 4.4 indicate elapsed times (days, hours and minutes in the format [ddT]hh:mm) from sensing to EUMETCast and WMO/GTS (NRT) or archive upload (offline). In each cell, the values from top to bottom represent observed monthly average, minimum and maximum times.

Tropospheric ozone products are included in the ozone profile products and have the same statistics.

Table 4.3. Timeliness of Metop-B ozone profile and aerosol products during the reporting period

Product Identifier	Product Name	7/2024	8/2024	9/2024	10/2024	11/2024	12/2024
EUMETCast							
O3M-47.1	NRT high-resolution ozone profile	avg: 01:05 min: 00:32 max: 02:04	avg: 01:07 min: 00:31 max: 02:32	avg: 01:05 min: 00:30 max: 02:01	avg: 01:08 min: 00:30 max: 02:07	avg: 01:06 min: 00:30 max: 02:20	avg: 01:06 min: 00:29 max: 02:27
O3M-78	NRT absorbing aerosol height	avg: 00:52 min: 00:30 max: 01:49	avg: 00:55 min: 00:30 max: 02:05	avg: 00:54 min: 00:29 max: 01:46	avg: 00:55 min: 00:29 max: 01:50	avg: 00:53 min: 00:29 max: 02:06	avg: 00:53 min: 00:29 max: 02:06
O3M-72.1	NRT absorbing aerosol index from PMDs	avg: 00:52 min: 00:30 max: 01:49	avg: 00:55 min: 00:30 max: 02:05	avg: 00:54 min: 00:29 max: 01:46	avg: 00:55 min: 00:29 max: 01:50	avg: 00:53 min: 00:29 max: 02:07	avg: 00:53 min: 00:29 max: 02:06
WMO/GTS							
O3M-47.1	NRT high-resolution ozone profile	avg: 01:06 min: 00:34 max: 02:05	avg: 01:08 min: 00:32 max: 02:23	avg: 01:06 min: 00:31 max: 02:02	avg: 01:09 min: 00:31 max: 02:08	avg: 01:07 min: 00:31 max: 02:21	avg: 01:07 min: 00:31 max: 02:27
FMI archive							
O3M-48.1	Offline high-resolution ozone profile	avg: 12:46 min: 06:51 max: 02T03:02	avg: 08:59 min: 06:42 max: 02T02:57	avg: 07:38 min: 06:45 max: 02T02:24	avg: 07:43 min: 06:57 max: 02T02:18	avg: 07:41 min: 06:51 max: 02T02:18	avg: 07:30 min: 06:51 max: 08:39
O3M-79	Offline absorbing aerosol height	avg: 12:44 min: 06:49 max: 02T02:55	avg: 08:58 min: 06:52 max: 02T03:04	avg: 07:38 min: 06:43 max: 02T02:19	avg: 07:42 min: 06:55 max: 02T02:55	avg: 07:40 min: 06:49 max: 02T02:55	avg: 07:28 min: 06:55 max: 08:52
O3M-73.1	Offline absorbing aerosol index from PMDs	avg: 12:40 min: 06:37 max: 02T03:16	avg: 08:54 min: 06:40 max: 02T02:52	avg: 07:34 min: 06:34 max: 02T02:49	avg: 07:40 min: 06:52 max: 02T02:43	avg: 07:39 min: 06:49 max: 02T02:43	avg: 07:26 min: 06:49 max: 08:52

Table 4.4. Timeliness of Metop-C ozone profile and aerosol products during the reporting period

Product Identifier	Product Name	7/2024	8/2024	9/2024	10/2024	11/2024	12/2024
EUMETCast							
O3M-311	NRT high-resolution ozone profile	avg: 01:45 min: 00:37 max: 02:27	avg: 01:50 min: 00:34 max: 02:41	avg: 01:49 min: 00:34 max: 02:16	avg: 01:53 min: 00:33 max: 02:27	avg: 01:50 min: 00:34 max: 02:13	avg: 01:47 min: 00:40 max: 02:41
O3M-364	NRT absorbing aerosol height	avg: 01:34 min: 00:35 max: 02:16	avg: 01:38 min: 00:34 max: 02:10	avg: 01:37 min: 00:34 max: 02:06	avg: 01:40 min: 00:33 max: 01:59	avg: 01:38 min: 00:34 max: 01:59	avg: 01:35 min: 00:40 max: 01:52
O3M-362	NRT absorbing aerosol index from PMDs	avg: 01:34 min: 00:35 max: 02:16	avg: 01:38 min: 00:34 max: 02:10	avg: 01:37 min: 00:34 max: 02:06	avg: 01:40 min: 00:33 max: 01:59	avg: 01:38 min: 00:34 max: 01:59	avg: 01:35 min: 00:40 max: 01:53

Product Identifier	Product Name	7/2024	8/2024	9/2024	10/2024	11/2024	12/2024
WMO/GTS							
O3M-311	NRT high-resolution ozone profile	avg: 01:46 min: 00:38 max: 02:28	avg: 01:51 min: 00:35 max: 02:42	avg: 01:49 min: 00:35 max: 02:20	avg: 01:53 min: 00:34 max: 02:28	avg: 01:50 min: 00:35 max: 02:15	avg: 01:48 min: 00:40 max: 02:30
FMI archive							
O3M-312	Offline high-resolution ozone profile	avg: 14:33 min: 07:24 max: 02T03:53	avg: 12:40 min: 07:29 max: 02T03:56	avg: 10:38 min: 06:54 max: 02T03:41	avg: 11:56 min: 07:15 max: 02T03:47	avg: 10:29 min: 06:24 max: 02T03:32	avg: 08:41 min: 07:14 max: 02T03:21
O3M-365	Offline absorbing aerosol height	avg: 14:31 min: 07:19 max: 02T03:43	avg: 12:39 min: 07:19 max: 02T03:46	avg: 10:37 min: 06:49 max: 02T03:31	avg: 11:54 min: 07:22 max: 02T03:37	avg: 10:29 min: 06:19 max: 02T03:31	avg: 08:40 min: 07:16 max: 02T03:16
O3M-363	Offline absorbing aerosol index from PMDs	avg: 14:29 min: 07:22 max: 02T03:42	avg: 12:38 min: 07:13 max: 02T03:42	avg: 10:36 min: 06:19 max: 02T03:43	avg: 11:51 min: 07:22 max: 02T03:31	avg: 10:27 min: 05:49 max: 02T03:25	avg: 08:36 min: 07:10 max: 02T03:22

4.2. Services, main events and anomalies

Tropospheric ozone products are included in the ozone profile products and have the same statistics.

Table 4.5. Number of products sent to FMI archive¹

Product Identifier	Product Name	Metop satellite	7/2024	8/2024	9/2024	10/2024	11/2024	12/2024
O3M-48.1	Offline high-resolution ozone profile	B	438	438	422	438	425	439
O3M-312		C	439	432	422	438	423	433
O3M-79	Offline absorbing aerosol height	B	438	438	422	438	425	439
O3M-365		C	439	432	422	438	423	433
O3M-73.1	Offline absorbing aerosol index from PMDs	B	438	438	422	438	425	439
O3M-363		C	439	432	422	438	423	433

Table 4.6. Number of products stored locally at KNMI²

Product Identifier	Product Name	Metop satellite	7/2024	8/2024	9/2024	10/2024	11/2024	12/2024
O3M-47.1	NRT high-resolution ozone profile	B	8627	8668	8384	8736	8479	8731
O3M-311		C	8563	8480	8329	8662	8381	8627
O3M-78	NRT absorbing aerosol height	B	8627	8668	8384	8736	8479	8731
O3M-364		C	8563	8480	8329	8662	8381	8627

Product Identifier	Product Name	Metop satellite	7/2024	8/2024	9/2024	10/2024	11/2024	12/2024
O3M-72.1	NRT absorbing aerosol index from PMDs	B	8627	8668	8384	8736	8479	8731
O3M-362		C	8563	8480	8329	8662	8381	8627
O3M-48.1	Offline high-resolution ozone profile	B	438	438	422	438	425	439
O3M-312		C	439	432	422	438	423	433
O3M-79	Offline absorbing aerosol height	B	438	438	422	438	425	439
O3M-365		C	439	432	422	438	423	433
O3M-73.1	Offline absorbing aerosol index from PMDs	B	438	438	422	438	425	439
O3M-363		C	439	432	422	438	423	433

Table 4.7. EUMETCast and WMO/GTS uploads³

Product Identifier	Product Name	Metop satellite	7/2024	8/2024	9/2024	10/2024	11/2024	12/2024
O3M-47.1	NRT high-resolution ozone profile	B	8627/8627	8668/8668	8384/8384	8736/8736	8479/8479	8731/8731
O3M-311		C	8563/8563	8480/8480	8329/8329	8662/8662	8381/8381	8627/8627
O3M-78	NRT absorbing aerosol height	B	8627	8668	8384	8736	8479	8731
O3M-364		C	8563	8480	8329	8662	8381	8627
O3M-72.1	NRT absorbing aerosol index from PMDs	B	8627	8668	8384	8736	8479	8731
O3M-362		C	8563	8480	8329	8662	8381	8627

¹ Products are archived in HDF5 format.

² Products are stored for 3 years (in HDF5 and BUFR formats).

³ NRT high-resolution ozone profile is disseminated via EUMETCast and WMO/GTS in BUFR format. NRT absorbing aerosol index and NRT absorbing aerosol index from PMDs are disseminated only via EUMETCast (in HDF5 and BUFR formats).

Table 4.8 lists the main events (product/service/hardware/software updates etc.) at KNMI during the reporting period.

Table 4.8. Main events at KNMI during the reporting period

Date	Description
	<i>Nothing to report.</i>

Table 4.9 lists the main local and external anomalies at KNMI during the reporting period. Corrective and preventive actions should be provided also when applicable.

Table 4.9. Main local and external anomalies affecting KNMI systems and performance during the reporting period

ID	Time period	Description
		<i>Nothing to report.</i>

5. Processing centre: DMI

5.1. NRT clear-sky and cloud-corrected UV index

5.1.1. Availability

NUV product is required to be produced every day, either on the basis of new GOME ATO input or in the case of ATO delivery failure based on back-up total ozone data (ECMWF or climatology).

Availability requirement for NUV has been defined in Section 1.4. The availability statistics of DMI products are presented in Table 5.1. If the requirement is violated, those values are marked with red colour, identified by numbers and reported in Table 5.5.

Table 5.1. Availability of NRT UV products during the reporting period

Product Identifier	Product Name	7/2024	8/2024	9/2024	10/2024	11/2024	12/2024
O3M-409	NRT UV index, clear-sky	100 %	100 %	100 %	100 %	100 %	96.8 % (1)
O3M-410	NRT UV index, cloud-corrected						

5.1.2. Timeliness

Timeliness requirement for NUV says that the final NUV product is to be delivered to users no later than 04:00 UTC. The timeliness reported in Table 5.2 is calculated as the time difference (hours and minutes in format hh:mm) between 04:00 UTC and the time when the NUV products are available to users. Thus **positive** values refer to situations where the timeliness requirement is violated, and marked in red colour. In addition, the violations are identified by numbers and reported in Table 5.5 if they have caused the availability values to drop below the allowed limits.

Days where no products are produced or could be delivered to users (as indicated in Table 5.1) are not included in Table 5.2.

From top to bottom, the values in Table 5.2 represent observed monthly average, minimum and maximum time differences.

Table 5.2. Timeliness of NRT UV products during the reporting period

Product Identifier	Product Name	7/2024	8/2024	9/2024	10/2024	11/2024	12/2024
O3M-409	NRT UV index, clear-sky	avg: -00:54 min: -00:54 max: -00:53	avg: -00:54 min: -00:54 max: -00:53	avg: -00:54 min: -00:54 max: -00:53	avg: -00:54 min: -00:53 max: -00:54	avg: -00:54 min: -00:54 max: -00:53	avg: -00:52 min: -00:54 max: -00:33
O3M-410	NRT UV index, cloud-corrected						

5.2. Services, main events and anomalies

Table 5.3. Number of products stored locally at DMI¹

Description of service / event	7/2024	8/2024	9/2024	10/2024	11/2024	12/2024
Storage statistics						
Number of stored products (NRT UV index, clear-sky)	31	31	30	31	30	31
Number of stored products (NRT UV index, cloud-corrected)	31	31	30	31	30	31
Total size of stored products (MB)	248	248	240	248	240	248

¹ NUV products are stored at the DMI at least until the end of the Metop programs.

Table 5.4 lists the main events (product/service/hardware/software updates etc.) at DMI during the reporting period.

Table 5.4. Main events at DMI during the reporting period

Date	Event
	<i>Nothing to report.</i>

Table 5.5 lists the main local and external anomalies at DMI during the reporting period. Corrective and preventive actions should be provided also when applicable.

Table 5.5. Main local and external anomalies affecting DMI systems and performance during the reporting period

ID	Time period	Description
1	31/12/2024	<p>The end-of-year diagnostic tool was for unknown reason running in endless loop and the transfer of the NUV product to the web server failed. The product was produced and saved but not transferred to users.</p> <p>Corrective action: The diagnostic tool was stopped.</p> <p>Preventive action: The tool shall in the future only be executed manually during daytime.</p>

6. Processing centre: EUMETSAT

6.1. NRT IASI CO, SO₂, HNO₃ and ozone profile

6.1.1. Availability

For Level 1c products, the availability is defined as the number of available PDUs divided by the number of maximum expected PDUs.

For NRT products, the availability requirement is 97.5 % and it is defined by the ratio of the number of in time processed and disseminated products to the number of maximum expected input products (L1c PDUs) per month.

The availability statistics of EUMETSAT products are presented in Table 6.1 and Table 6.2. If the availability requirements have been violated, those values are marked with **red** colour, identified by numbers and reported in Table 6.7 and/or Table 6.8.

Note that in the frame of this product processing centre being the EUMETSAT HQ in Darmstadt, the L1c data is directly available to the L2+ algorithm, i.e., its availability is not dependable of EUMETCast dissemination, which can sometimes be translated into higher L2+ availability than the applicable L1c, depending on the data which has been successfully disseminated. Furthermore, since there is no relay of information from *Satellite* processing centres, the L2 product availability in the following tables concern the end-to-end availability as they were recorded in the EUMETSAT Reference Receiving Stations.

Table 6.1. Availability of Metop-B L1c PDUs and IASI NRT products during the reporting period

Product Identifier	Product Name	7/2024	8/2024	9/2024	10/2024	11/2024	12/2024
L1c	PDUs available / PDUs expected	14865/14880	14612/14880	14397/14400	14797/14880	14382/14400	14666/14880
L1c	Availability	99.9 %	98.2 %	100 %	99.4 %	99.9 %	98.6 %
O3M-80	NRT IASI CO	99.9 %	98.2 %	99.9 %	99.4 %	99.8 %	98.4 %
O3M-57	NRT IASI SO ₂	99.9 %	98.2 %	99.9 %	99.4 %	99.8 %	98.4 %
O3M-81	NRT IASI HNO ₃	99.9 %	98.2 %	99.9 %	99.4 %	99.8 %	98.4 %
O3M-49	NRT IASI ozone profile	99.9 %	98.2 %	99.9 %	99.4 %	99.8 %	98.4 %

Table 6.2. Availability of Metop-C L1c PDUs and IASI NRT products during the reporting period

Product Identifier	Product Name	7/2024	8/2024	9/2024	10/2024	11/2024	12/2024
L1c	PDUs available / PDUs expected	14765/14880	14578/14880	14311/14400	14874/14880	14296/14400	12261/14880
L1c	Availability	99.2 %	97.9 %	99.4 %	100 %	99.3 %	82.4 % (1)
O3M-352	NRT IASI CO	99.2 %	98.0 %	99.3 %	100 %	99.3 %	82.3 % (1)
O3M-377	NRT IASI SO ₂	99.2 %	98.0 %	99.3 %	100 %	99.3 %	82.3 % (1)
O3M-336	NRT IASI HNO ₃	99.2 %	98.0 %	99.3 %	100 %	99.3 %	82.3 % (1)
O3M-315	NRT IASI ozone profile	99.2 %	98.0 %	99.3 %	100 %	99.3 %	82.3 % (1)

6.1.2. Timeliness

Timeliness indicates the elapsed time between sensing and product dissemination. Timeliness requirement is 3 hours for NRT products. If the requirements have been violated, those values are marked with red colour. In addition, the violations are identified by numbers and reported in Table 6.8 if they have caused the availability values to drop below the allowed limits.

Note: timeliness violations are not listed as anomalies if the availability is above the limit.

The values in Table 6.3 and Table 6.4 indicate elapsed times (hours and minutes in the format hh:mm) from sensing to EUMETCast Reference Receiving Station, i.e., end-to-end timeliness. In each cell, the values from top to bottom represent observed monthly average, minimum and maximum times.

Table 6.3. Timeliness of Metop-B IASI NRT products during the reporting period

Product Identifier	Product Name	7/2024	8/2024	9/2024	10/2024	11/2024	12/2024
O3M-80	NRT IASI CO	avg: 01:04 min: 00:35 max: 02:07	avg: 01:03 min: 00:34 max: 02:44	avg: 01:03 min: 00:34 max: 02:36	avg: 01:03 min: 00:34 max: 01:49	avg: 01:02 min: 00:35 max: 02:40	avg: 01:02 min: 00:35 max: 03:21
O3M-57	NRT IASI SO ₂	avg: 01:04 min: 00:35 max: 02:07	avg: 01:03 min: 00:34 max: 02:44	avg: 01:03 min: 00:34 max: 02:36	avg: 01:03 min: 00:34 max: 01:49	avg: 01:02 min: 00:35 max: 02:40	avg: 01:02 min: 00:35 max: 03:21
O3M-81	NRT IASI HNO ₃	avg: 01:04 min: 00:35 max: 02:07	avg: 01:03 min: 00:34 max: 02:44	avg: 01:03 min: 00:34 max: 02:36	avg: 01:03 min: 00:34 max: 01:49	avg: 01:02 min: 00:35 max: 02:40	avg: 01:02 min: 00:35 max: 03:21
O3M-49	NRT IASI ozone profile	avg: 01:04 min: 00:35 max: 02:07	avg: 01:03 min: 00:34 max: 02:44	avg: 01:03 min: 00:34 max: 02:36	avg: 01:03 min: 00:34 max: 01:49	avg: 01:02 min: 00:35 max: 02:40	avg: 01:02 min: 00:35 max: 03:21

Table 6.4. Timeliness of Metop-C IASI NRT products during the reporting period

Product Identifier	Product Name	7/2024	8/2024	9/2024	10/2024	11/2024	12/2024
O3M-352	NRT IASI CO	avg: 01:36 min: 00:43 max: 02:15	avg: 01:35 min: 00:52 max: 02:40	avg: 01:35 min: 00:44 max: 02:20	avg: 01:37 min: 00:54 max: 02:14	avg: 01:33 min: 00:55 max: 02:09	avg: 01:17 min: 00:53 max: 03:03 (2)
O3M-377	NRT IASI SO2	avg: 01:36 min: 00:43 max: 02:15	avg: 01:35 min: 00:52 max: 02:40	avg: 01:35 min: 00:44 max: 02:20	avg: 01:37 min: 00:54 max: 02:14	avg: 01:33 min: 00:55 max: 02:10	avg: 01:17 min: 00:53 max: 03:03 (2)
O3M-336	NRT IASI HNO3	avg: 01:36 min: 00:43 max: 02:15	avg: 01:35 min: 00:52 max: 02:40	avg: 01:35 min: 00:44 max: 02:20	avg: 01:37 min: 00:54 max: 02:14	avg: 01:33 min: 00:55 max: 02:10	avg: 01:17 min: 00:53 max: 03:03 (2)
O3M-315	NRT IASI ozone profile	avg: 01:36 min: 00:43 max: 02:15	avg: 01:35 min: 00:52 max: 02:40	avg: 01:35 min: 00:44 max: 02:20	avg: 01:37 min: 00:54 max: 02:14	avg: 01:33 min: 00:55 max: 02:10	avg: 01:17 min: 00:53 max: 03:03 (2)

6.2. Services, main events and anomalies

Table 6.5. Number of products stored locally at EUMETSAT¹

Product Identifier	Product Name	Metop satellite	7/2024	8/2024	9/2024	10/2024	11/2024	12/2024
O3M-80	NRT IASI CO	B	14865	14604	14398	14786	14374	14653
O3M-352		C	14765	14576	14319	14869	14296	12252
O3M-57	NRT IASI SO2	B	14865	14604	14398	14786	14374	14653
O3M-377		C	14765	14576	14319	14869	14296	12252
O3M-81	NRT IASI HNO3	B	14865	14604	14398	14786	14373	14653
O3M-336		C	14765	14576	14319	14869	14296	12252
O3M-49	NRT IASI ozone profile	B	14865	14604	14398	14786	14374	14653
O3M-315		C	14765	14576	14319	14869	14296	12252

¹ PDUs are concatenated back to orbit-based products before being stored

Table 6.6. EUMETCast uploads¹

Product Identifier	Product Name	Metop satellite	7/2024	8/2024	9/2024	10/2024	11/2024	12/2024
O3M-80	NRT IASI CO	B	14865	14604	14398	14786	14374	14653
O3M-352		C	14765	14576	14319	14869	14296	12252
O3M-57	NRT IASI SO ₂	B	14865	14604	14398	14786	14374	14653
O3M-377		C	14765	14576	14319	14869	14296	12252
O3M-81	NRT IASI HNO ₃	B	14865	14604	14398	14786	14373	14653
O3M-336		C	14765	14576	14319	14869	14296	12252
O3M-49	NRT IASI ozone profile	B	14865	14604	14398	14786	14374	14653
O3M-315		C	14765	14576	14319	14869	14296	12252

¹ NRT IASI products are disseminated via EUMETCast (in BUFR format)

Table 6.7 lists the main events (product/service/hardware/software updates etc.) at EUMETSAT during the reporting period.

Table 6.7. Main planned activities at EUMETSAT during the reporting period

ID	Date	Description
1	11 – 16 December	Metop-C IASI instrument decontamination

Table 6.8 lists the main local and external anomalies at EUMETSAT during the reporting period. Corrective and preventive actions should be provided also when applicable.

Table 6.8. Main local and external anomalies affecting EUMETSAT systems and performance during the reporting period

ID	Time period	Description
2	11 – 16 December	Metop-C IASI instrument decontamination

7. Validation and quality monitoring

This section describes the validation status and validation/quality monitoring activities of NRT and offline data products during the reporting period. Validation reports for data records are found from <https://acsaf.org/valreps.html>

Reference documents are listed in Section 1.3 and accuracy requirements in Section 1.5.

7.1. GOME-2 total ozone column products

Table 7.1. Validation status of total ozone column products

Product Identifier	Product Name	Accuracy	Reference	Validating Institute	Correlative data sources
O3M-41.1	NRT total O3	Fulfil threshold accuracy requirement	RD4	AUTH	World Ozone Mapping Centre
O3M-300			RD23		
O3M-06.1	Offline total O3	Fulfil threshold accuracy requirement	RD4	AUTH	World Ozone and Ultraviolet Radiation Data Center (WOUDC), of the World Meteorological Organization, (WMO), Global Atmosphere Watch, (GAW)
O3M-42.1					
O3M-301			RD23		

Validation results can be found in more detail on the AC SAF validation & quality assessment website at http://acsaf.physics.auth.gr/eumetsat/validation/near_real and <http://acsaf.physics.auth.gr/eumetsat/validation/offline>

7.1.1. Total ozone column validation

This summary presents the validation activities for total ozone column products (TOCs), reported by the GOME-2/Metop-B and GOME-2/Metop-C instruments (hereafter GOME-2B and GOME-2C, respectively). Members of the Laboratory of Atmospheric Physics of the Aristotle University of Thessaloniki ([LAP/AUTH](#)), Thessaloniki, Greece, involved in the validation activities include Professor, Dr. Dimitris Balis, Special Teaching Fellow & Researcher, Dr. Katerina Garane and Research Associate, Dr. MariLiza Koukouli.

During the reporting period, the operational validation of offline total ozone and NRT total ozone products continued as per previous periods.

7.1.1.1 Update of database for reference ground-based data

For the nominal validation, the ground-based TOCs from Brewer, Dobson and M-124 instruments reported to the World Ozone and Ultraviolet Radiation Data Centre ([WOUDC](#)), are employed. WOUDC is one of the World Data Centres which are part of the Global Atmosphere Watch ([GAW](#)) programme of the World Meteorological Organization ([WMO](#)). For the quality of the reference ground-based data used for the validation of the total ozone products, updated information were extracted from recent inter-comparisons and calibration records. This continuously updated selection of ground-based measurements has already been used numerous times in the validation and analysis of global total ozone records such as the inter-comparison between the OMI/Aura TOMS and OMI/Aura DOAS algorithms [Balis *et al.*, 2007a], the validation of ten years of GOME/ERS-2 ozone record [Balis *et al.*, 2007b], the validation of the updated version of the OMI/Aura TOMS algorithm [Antón *et al.*, 2009], the GOME-2/Metop-A validation [Loyola *et al.*,

2011; Koukouli *et al.*, 2012], the GOME-2B validation [Hao *et al.*, 2014] and the evaluation of the European Space Agency's Ozone Climate Change Initiative project [O₃-CCI] TOCs [Koukouli *et al.*, 2015, Garane *et al.*, 2018], as well as in TROPOMI/S5P TOCs validation [Garane *et al.*, 2019]. In all the aforementioned works, LAP/AUTH assumes the leading role in the validation efforts. The number of WOUDC ground-based stations used in the full operational periods of the two instruments, alongside the mean difference between ground- and space-based TOC estimates is given in Table 7.2.

The comparisons and validation results with respect to the M-124 instruments are available via the [validation website](#), but not shown herein for reasons of brevity.

7.1.1.2 Validation results for the offline total ozone products

GOME-2B and GOME-2C OTO data for the period December 2012 (or January 2019 for GOME-2C) to December 2024 have been downloaded, quality-assured and pre-processed in order to perform the validation strategies. The GDP-4.8 algorithm is the latest version of the GDP-4.x suite of algorithms that have been used for the operational processing of GOME-2B total ozone columns. GOME-2C is processed with GDP-4.9. The main differences between GDP-4.8 and GDP-4.9 concern the SO₂ vertical column retrieval. For ozone only minor updates have been performed, such as the optimization of the slit function, the introduction of a pseudo absorber for possible orbital variations of the resolution etc. Therefore, the ozone columns from GOME-2C can be assumed to be similar to the respective data from GOME-2B, analyzed with the previous version of the algorithm.

This period's satellite-to-ground-based measurements comparisons were performed and added to the existing time series. The majority of the quality-assured ground-based Brewer and Dobson TOCs are reported to the WOUDC repository between 3 and 6 months after measurement, which accounts for the last couple of months missing from the comparative plots shown below. This is a common reporting feature, quite unavoidable.

In Figure 7.1, left column of figures, the status of GOME-2B and GOME-2C TOCs since the beginning of each individual mission is shown in the form of a monthly mean time-series of the percentage differences between each sensor and ground-based observations. Panel a shows the co-locations with Brewer Northern Hemisphere (NH) stations, panel c with Dobson NH stations and panel e with Dobson Southern Hemisphere (SH) stations. The plots shown in the right column of Figure 7.1 (panels (b), (d) and (f), show the common time period of operation of the GOME-2B and GOME-2C sensors, hence since the beginning of 2019 onwards.

The monthly mean percentage differences of the two sensors with respect to the ground network range between:

GOME-2B

- 1a) -1 to +3 % before 2022, and
- 1b) continuously decreasing afterwards, up to -3.5 % in July 2024.

GOME-2C

- 2a) 0 to +2.5 % for the first year of the GOME-2C operation,
- 2b) which is shifted to +1.5 to +4 % after March 2020,

depending on the season and the ground-based reference.

This seasonality in the differences between satellite and ground-based is more pronounced in the Dobson co-locations (panels c – f) and is a well-known feature which appears in most operational

and scientific satellite TOC comparisons, see for e.g. the validation of the OMI/Aura products [Balis *et al.*, 2007a], the GOME/ERS-2 product [Balis *et al.*, 2007b] and even the recent GOME/ERS-2, SCIAMACHY/Envisat and GOME-2A ESA products [Koukouli *et al.*, 2015, Garane *et al.*, 2018]. The reasons have to do with the treatment of the variability of the stratospheric temperature and how that affects the ozone absorption coefficients used in the different algorithms [Fragkos *et al.*, 2013; Serdyuchenko *et al.*, 2014]. Hence, when the stratospheric temperature deviates strongly from what is assumed by the algorithms, which is usually the case during the winter months, the differences between ground and satellite increase. See the work of Koukouli *et al.*, 2016, and discussion therein, on this topic.

The well-known reason for the Dobson total ozone seasonality could be treated following a methodology (see Komhyr *et al.*, 1993 and Koukouli *et al.*, 2016) that is utilized by the LAP/AUTH validation chain to post-correct the Dobson ground-based measurements for their effective temperature dependence, but the correction is always dependent on the temperature dataset that is used for its implementation. Additionally, the official repositories such as WOUDC do not provide temperature corrected data and to keep our validation analysis compatible with other studies and validation reports on various other sensors, it was chosen to use the Dobson ground-based dataset as originally provided by WOUDC.

Using the ground-based measurements as a common reference, Figure 7.1 leads to the noticeable difference in the agreement levels between the two sensors in the NH, which is different before and after spring of 2020:

- Before that point, the deviation of the two sensors was $\sim 0 - 1$ %, with GOME-2C reporting higher TOCs during summer months by up to ~ 0.8 % with respect to GOME-2B.
- Since March 2020, their deviation especially during summer months gradually increases up to ~ 4 %, with GOME-2B reporting continuously lower TOCs than GOME-2C. The increased difference between the two sensors has a seasonal dependence, being lower during winter months (~ 0.5 % for January 2020 going up to ~ 3 % for December 2024) and higher during summer months (~ 1.6 % for June 2020 up to ~ 4 % in July 2024).

In the SH (panels c and f) an increased difference, especially pronounced during the local spring-summer months, is also seen since March or April 2020, going up to ~ 3.5 % in December 2024, with GOME-2B reporting continuously lower TOCs than GOME-2C.

The explanation of GOME-2B continuously decreasing total ozone observations since early 2020 is also confirmed by direct satellite-to-satellite comparisons (not shown here) and is under investigation by the algorithm team.

The observed drift between the two GOME-2 instruments is likely caused by the degradation of the L1 data. For the ozone slant column density (SCD) fit, two pseudo absorbers were added by the algorithm team in the non-operational DOAS retrieval, which improved the observed drift in the SCDs between the two instruments. A large-scale test in the official testing environment is in preparation. This test will also include the AMF part. Once a reasonable amount of data has been processed, they will be provided to AUTH for comparison to ground based observations. It is expected that the changes will be in the order of the allowed uncertainty range. Based on a successful validation phase, the updated dataset will be released as operational product.

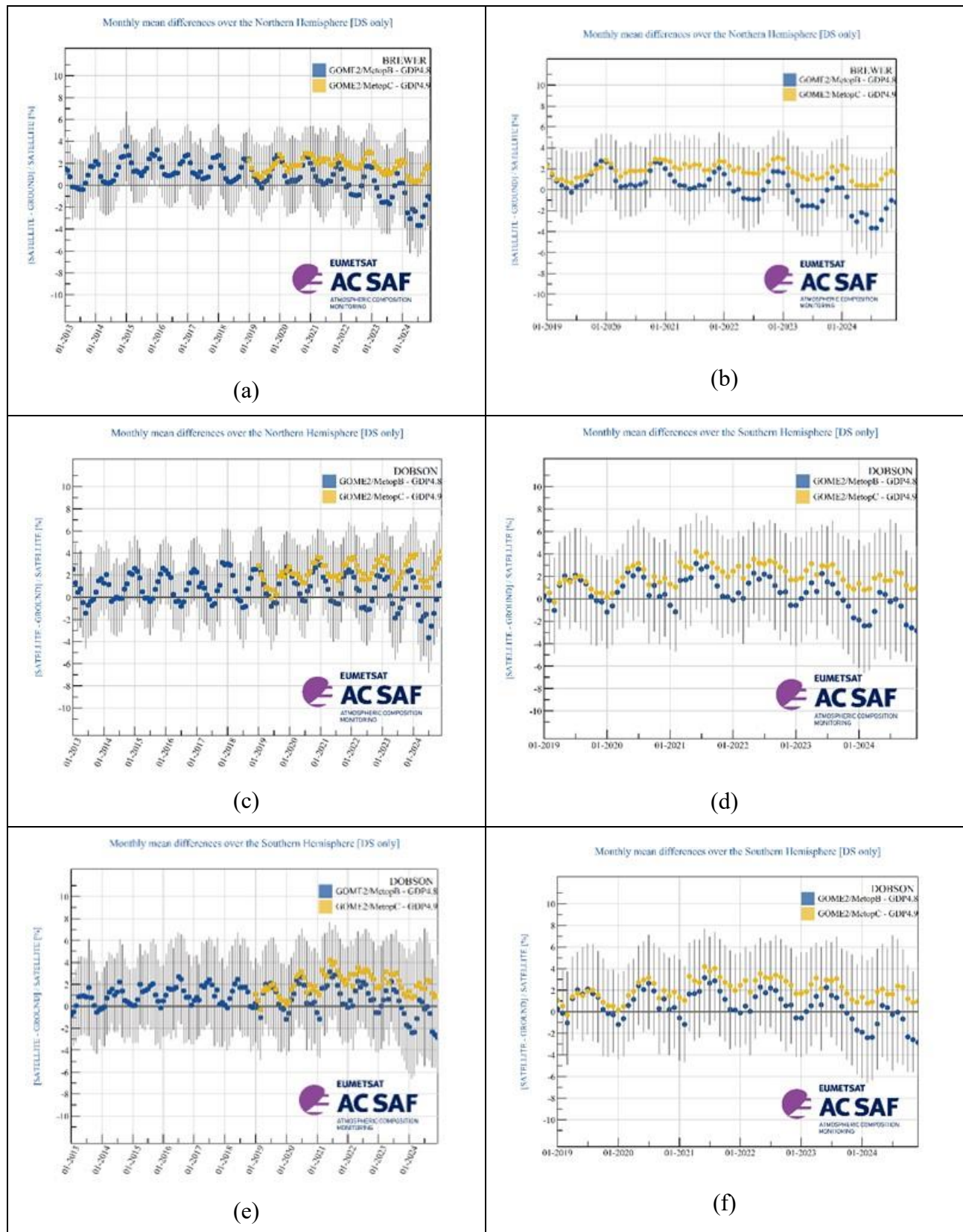


Figure 7.1. Hemispherical time-series of the monthly mean percentage differences between GOME-2B GDP-4.8 (blue symbols) and GOME-2C GDP-4.9 (orange symbols) total ozone products against ground-based observations. Panels a – d: Northern Hemisphere, panels e and f: Southern Hemisphere. Brewer co-locations are shown in panels a and b (Northern Hemisphere only). Dobson co-locations are

shown in panels c – f. The difference between the left and the right column of figures is the time period covered.

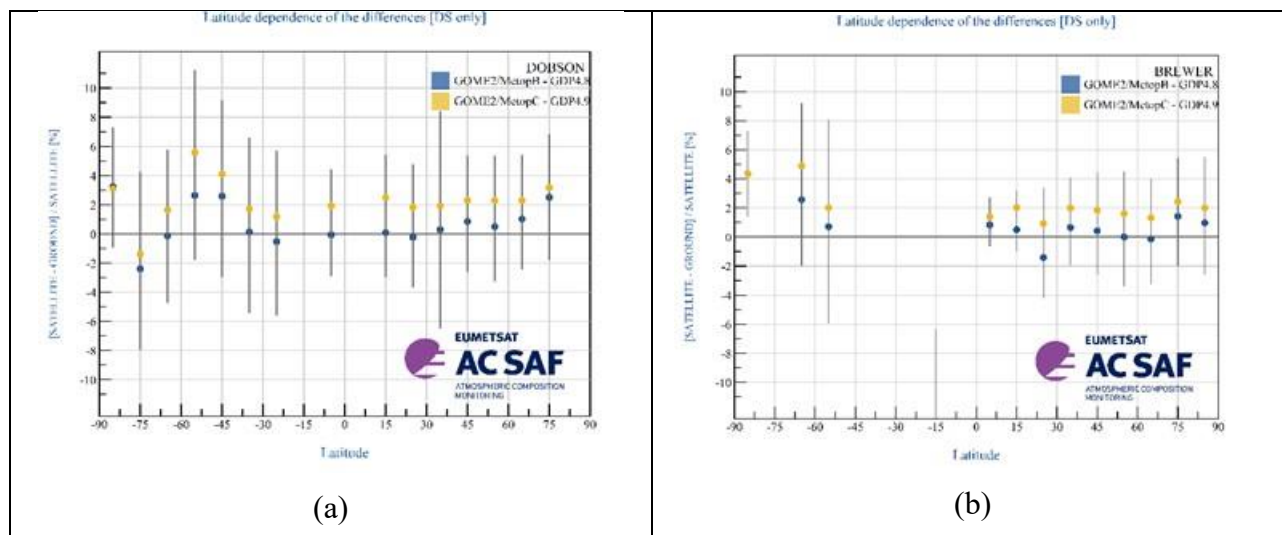


Figure 7.2. The latitudinal dependency of the differences for the Dobson (panel a) and the Brewer network (panel b). The Brewer SH mean biases are greyed-out because the limited number of stations in this part of the earth cannot provide reliable validation results.

In the latitudinal plot (Figure 7.2), it is shown that the overall agreement of both sensors to the ground-based measurements is within 0 – 2 % in the tropics and mid-latitudes. Additionally, it is noticeable that the comparisons of GOME-2C with respect to ground-based measurements have almost no dependency on latitude, having a very stable relative mean bias of ~2 % for the NH stations and for co-locations northwards ~40°S. The TOC underestimation of GOME-2B with respect to GOME-2C is also shown to be global, but it appears to be more evident for the mid-latitudes and the tropics, where GOME-2B reports lower TOCs by about 1 – 2 % with respect to GOME-2C.

It should be noted that the co-locations used in Figure 7.2 cover the time-period of the two sensors operating in tandem, since January 2019. The respective latitudinal plot made with co-locations covering only 2024 (not shown here), when the divergence between the two sensors is stronger, indicates that these recently-increased differences between the GOME-2B and GOME-2C total ozone observations result almost equally from all latitude belts.

7.1.1.3 Tables of statistics

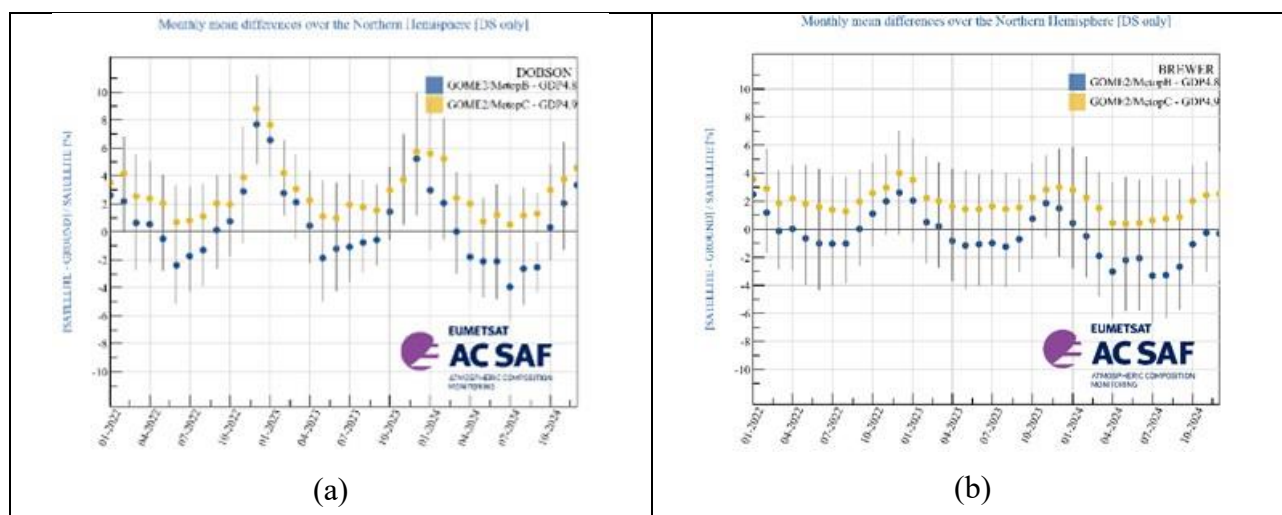
In Table 7.2, the summary statistics for the GOME-2B and GOME-2C comparisons against co-located total ozone observations from the Dobson and Brewer stations presented in the previous section, are enumerated. The number of individual daily common observations for the Dobsons apply to the entire globe, whereas the Brewer comparisons depict only the NH. As can be noted, the relative differences between GOME-2B and Brewer and Dobson stations is quite stable, with an average mean difference of about $+0.6 \pm 4.5$ %. GOME-2C has a higher mean relative bias with respect to ground-based measurements, of $+1.3$ to $+2.2 \pm 4.5$ %. Nevertheless, **both total ozone products are within the product accuracy requirements (4 % for $\text{SZA} < 80^\circ$ and 8 % for $\text{SZA} > 80^\circ$).**

Table 7.2. Summary statistics for the respective time period of operation of each sensor, based on GOME-2B and GOME-2C OTO data compared to WOUDC Brewer & Dobson observations

		Brewer	Dobson
GOME-2B 01/2013 – 12/2024	# stations:	68	64
	# obs:	193 000	133 000
	Mean Rel. Bias (%):	0.4 ± 4.4	0.7 ± 4.9
	Compliance with the product requirements:		
	Mean Rel. Bias for SZA $\leq 80^\circ$:	0.7 %	0.7 %
	Mean Rel. Bias for SZA $> 80^\circ$:	1.2 %	2.0 %
GOME-2C 01/2019 – 12/2024	# stations:	57	52
	# obs:	86 000	57 500
	Mean Rel. Bias (%):	1.3 ± 4.2	2.2 ± 4.9
	Compliance with the product requirements:		
	Mean Rel. Bias for SZA $\leq 80^\circ$:	1.6 %	2.2 %
	Mean Rel. Bias for SZA $> 80^\circ$:	2.8 %	3.4 %

7.1.1.4 Validation results for the NRT total ozone products

The GOME-2B and GOME-2C NRT total ozone products are continuously validated against Brewer and Dobson TOCs routinely deposited in the World Meteorological Organisation (WMO) [Ozone Mapping Centre](#), also hosted by the Laboratory of Atmospheric Physics, AUTH. The comparative datasets that cover the last two-three years of observations, are updated weekly and they are operationally available by the [online quality monitoring tool operated by AUTH](#). Some indicative plots are shown in Figure 7.3.



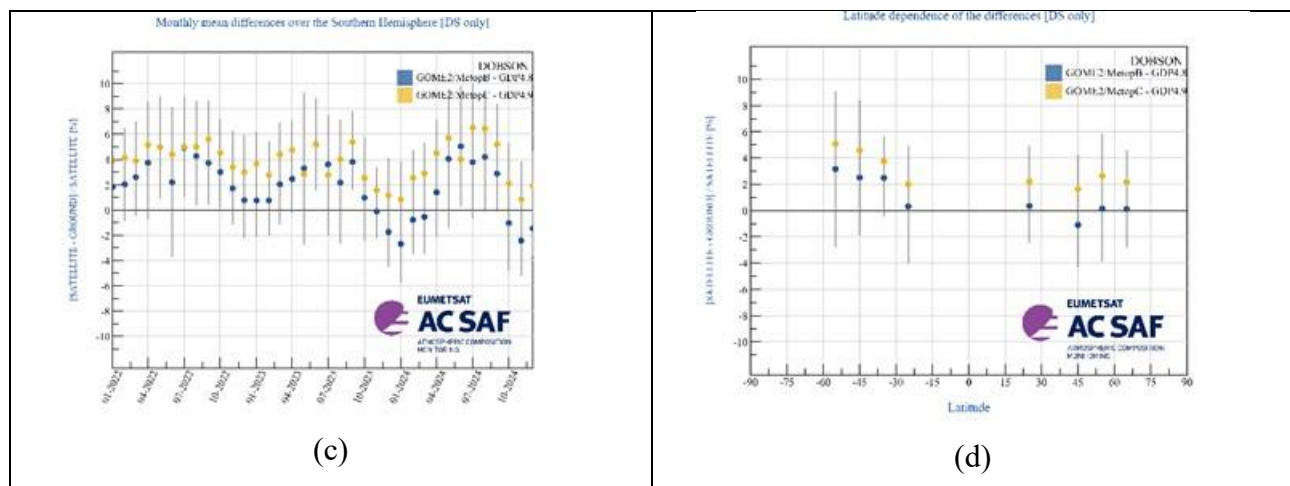


Figure 7.3. The percentage differences of the GOME-2B (blue) and GOME-2C (orange) NRT total ozone observations against the Dobson (panels a, c, and d) and Brewer (panel b) ground-based co-located measurements. Panels (a) and (c) show the Dobson NH (panel a) and SH (panel c) monthly mean timeseries. Panel (b) shows the Brewer NH monthly mean timeseries. The Dobson latitudinal dependency plot is shown in panel (d), made with co-locations since January 2022.

7.1.2. Validation website

The [AC SAF Ozone Validation & Quality Assessment](#) was launched on the initiation of the project's CDOP 2 phase in 2013. The validation webpages host the validation results of GOME-2A GDP-4.8, GOME-2B GDP4.8 and GOME-2C GDP4.9 near real-time and offline total ozone data. Currently, the validation results are available until March 2025.

The validation website will soon include validation results for the IASI CDR total ozone dataset, processed by EUMETSAT. Currently, the adjustment of the validation chain to ingest IASI is in progress.

The website and the processing algorithms that run behind it are routinely inspected and quality controlled. All the necessary actions, needed to keep it at its current good state, are taken by the LAP/AUTH team.

References:

Antón, M., Loyola, D., López, M., Vilaplana, J. M., Bañón, M., Zimmer, W., and Serrano, A.: Comparison of GOME-2/MetOpA total ozone data with Brewer spectroradiometer data over the Iberian Peninsula, *Annales Geophysicae*, 27, 1377–1386, 2009.

<https://doi.org/10.5194/angeo-27-1377-2009>

Balis, D., Kroon M., Koukouli, M.E., Brinksma, E. J., Labow, G., Veefkind, J. P., and McPeters, R. D.: Validation of Ozone Monitoring Instrument total ozone column measurements using Brewer and Dobson spectrophotometer ground-based observations, *J. Geophys. Res.*, 112, D24S46, 2007a.

<https://doi.org/10.1029/2007JD008796>

Balis, D., Lambert, J-C., Van Roozendael, M., Spurr, R., Loyola, D., Livschitz, Y., Valks, P., Amiridis, V., Gerard, P., Granville, J., and Zehner, C.: Ten years of GOME/ERS-2 total ozone data – The new GOME data processor (GDP) version 4: 2. Ground-based validation and comparisons with TOMS V7/V8, *J. Geophys. Res.*, vol. 112, D07307, 2007b.

<https://doi.org/10.1029/2005JD006376>

Fragkos, K., Bais, A. F., Balis, D., Meleti, C., and Koukouli, M. E.: The effect of three different absorption cross-sections and their temperature dependence on total ozone measured by a mid-latitude Brewer spectrophotometer, *Atmos. Ocean*, 53, 2015.

<https://doi.org/10.1080/07055900.2013.847816>

Hao, N., Koukouli, M. E., Inness, A., Valks, P., Loyola, D. G., Zimmer, W., Balis, D. S., Zyrichidou, I., Van Roozendaal, M., Lerot, C., and Spurr, R. J. D.: GOME-2 total ozone columns from MetOp-A/MetOp-B and assimilation in the MACC system, *Atmos. Meas. Tech.*, 7, 2937-2951, 2014.

<https://doi.org/10.5194/amt-7-2937-2014>

Koukouli, M. E., Balis, D. S., Loyola, D., Valks, P., Zimmer, W., Hao, N., Lambert, J.-C., Van Roozendaal, M., Lerot, C., and Spurr, R. J. D.: Geophysical validation and long-term consistency between GOME-2/MetOp-A total ozone column and measurements from the sensors GOME/ERS-2, SCIAMACHY/ENVISAT and OMI/Aura, *Atmos. Meas. Tech.*, 5, 2169-2181, 2012.

<https://doi.org/10.5194/amt-5-2169-2012>

Koukouli, M. E., Lerot, C., Granville, J., Goutail, F., Lambert, J.-C., Pommereau, J.-P., Balis, D., Zyrichidou, I., Van Roozendaal, M., Coldewey-Egbers, M., Loyola, D., Labow, G., Frith, S., Spurr, S., and Zehner, C.: Evaluating a new homogeneous total ozone climate data record from GOME/ERS-2, SCIAMACHY/Envisat and GOME-2/MetOp-A, *J. Geophys. Res. Atmos.*, 120, 12296-12312, 2015.

<https://doi.org/10.1002/2015JD023699>

Koukouli, M. E., Zara, M., Lerot, C., Fragkos, K., Balis, D., van Roozendaal, M., Allart, M. A. F., and van der A, R. J.: The impact of the ozone effective temperature on satellite validation using the Dobson spectrophotometer network, *Atmos. Meas. Tech.*, 9, 2055-2065, 2016.

<https://doi.org/10.5194/amt-9-2055-2016>

Loyola, D. G., Koukouli, M. E., Valks, P., Balis, D. S., Hao, N., Van Roozendaal, M., Spurr, R. J. D., Zimmer, W., Kiemle, S., Lerot, C., and Lambert, J.-C.: The GOME-2 total column ozone product: Retrieval algorithm and ground-based validation, *J. Geophys. Res.*, 116, 2011.

<https://doi.org/10.1029/2010JD014675>

Serdyuchenko, A., Gorshelev, V., Weber, M., Chehade, W., and Burrows, J. P.: High spectral resolution ozone absorption cross-sections – Part 2: Temperature dependence, *Atmos. Meas. Tech.*, 7, 625–636, 2014.

<https://doi.org/10.5194/amt-7-625-2014>

Garane, K., Lerot, C., Coldewey-Egbers, M., Verhoelst, T., Koukouli, M. E., Zyrichidou, I., Balis, D. S., Danckaert, T., Goutail, F., Granville, J., Hubert, D., Keppens, A., Lambert, J.-C., Loyola, D., Pommereau, J.-P., Van Roozendaal, M., and Zehner, C.: Quality assessment of the Ozone_cci Climate Research Data Package (release 2017) – Part 1: Ground-based validation of total ozone column data products, *Atmos. Meas. Tech.*, 11, 1385-1402, 2018.

<https://doi.org/10.5194/amt-11-1385-2018>

Garane, K., Koukouli, M.-E., Verhoelst, T., Lerot, C., Heue, K.-P., Fioletov, V., Balis, D., Bais, A., Bazureau, A., Dehn, A., Goutail, F., Granville, J., Griffin, D., Hubert, D., Keppens, A., Lambert, J.-C., Loyola, D., McLinden, C., Pazmino, A., Pommereau, J.-P., Redondas, A., Romahn, F., Valks, P., Van Roozendaal, M., Xu, J., Zehner, C., Zerefos, C., and Zimmer, W.: TROPOMI/S5P total ozone column data: global ground-based validation and consistency with other satellite missions, *Atmos. Meas. Tech.*, 12, 5263–5287, 2019.

<https://doi.org/10.5194/amt-12-5263-2019>

7.1.3. Online quality monitoring

The online quality monitoring tool is operational and consists of the continuous generation of plots showing the slant column density (SCD) distribution, the vertical column density (VCD) distribution as well as the root mean square (RMS) as histograms per sensing day as well as time series per sensing month. These plots are generated for three different geographic regions, the Pacific ocean (25-15S, 210-250E), the Sahara desert (20-30N, 0-30E) and global, in order to represent typical extremes of ground reflectivity and atmospheric conditions as well as the global mean. The plots are generated per sensing instrument (GOME-2B, GOME-2C) and per product (O3, NO2, BrO, HCHO, SO2, H2O).

The online quality monitoring plots are published in PDF format on the DLR AC SAF FTP server (acsaf.eoc.dlr.de) using the following directory schemes:

```
/oq/GOME-2[BC]/[O3 NO2 BrO HCHO SO2 H2O]/daily/YYYY/MM/DD/[global sahara
pacific]/*.[vcd scd rms]_hist.pdf
/oq/GOME-2[BC]/[O3 NO2 BrO HCHO SO2 H2O]/monthly/YYYY/MM/[global sahara pacific]/
*.[vcd scd rms]_series.pdf
```

More information about quality monitoring of the operational GOME-2 total ozone columns by other AC SAF and external partners is available at the following websites:

- <https://acsaf.org> → Validation & QA → QM websites
- http://acsaf.physics.auth.gr/eumetsat/validation/near_real
- <http://acsaf.physics.auth.gr/eumetsat/validation/offline>
- <https://www.temis.nl/acsaf/vod.php>

7.2. GOME-2 tropospheric ozone products

Table 7.3. Validation status of tropospheric ozone products

Product Identifier	Product Name	Accuracy	Reference	Validating Institute	Correlative data sources
O3M-35	Offline tropical tropospheric ozone	Fulfil target accuracy requirement	RD16	KMI	Ozonesonde data from SHADOZ , NDACC , NILU and WOUDC
O3M-43					
O3M-302			RD20		
O3M-174	NRT global tropospheric ozone	Fulfil target accuracy requirement	RD17	KMI	Ozonesonde data from SHADOZ , NDACC , NILU and WOUDC
O3M-304			RD21		
O3M-173	Offline global tropospheric ozone	Fulfil target accuracy requirement	RD17	KMI	Ozonesonde data from SHADOZ , NDACC , NILU and WOUDC
O3M-175					
O3M-305			RD21		

Validation activities summary for global tropospheric ozone:

This summary contains validation results of the GOME-2B and GOME-2C high resolution (HR) global tropospheric ozone column (TrOC) products, retrieved by the Ozone Profile Retrieval Algorithm (OPERA) at KNMI. It covers the time period January 2024 – December 2024. Validation results are shown from two TrOC products, i.e. the tropopause related product and a

fixed altitude TrOC product. The TrOC products are derived from the daily operational ozone profile product.

Since these TrOC products are derived from the OPERA ozone profile product, OPERA averaging kernel smoothing has been applied to the ground-based reference profiles before calculating comparison statistics. This AVK smoothing is expected to reduce the vertical smoothing difference error between satellite and ground-based measurements. The outcome is summarized at the end of this section.

The global tropospheric ozone column (TrOC) product has the following user requirements:

- Threshold accuracy: within 50 %
- Target accuracy: within 20 %
- Optimal accuracy: within 15 %

This summary was made available by Dr. Andy Delcloo from KMI. More information on how these values are extracted is available in the [validation report](#). The collocation data used are the same as for the ozone profiles (Figure 7.22).

The statistics on the accuracy of the GOME-2B and GOME-2C HR tropospheric ozone column products (tropopause related) for different latitude belts, validated against $X_{AVK-sonde}$, are shown in Table 7.4 and Table 7.5.

Table 7.4. Relative differences (RD) and standard deviation (STDEV) are shown (in percent) together with the absolute difference (DU) on the accuracy of the GOME-2B HR tropospheric ozone column products (tropopause related) for five different latitude belts, validated against $X_{AVK-sonde}$

January – December 2024		GOME-2B HR		
	RD (%)	STDEV (%)	AD (DU)	STDEV (DU)
Northern Polar Region	-7.53	29.0	-1.49	8.32
Northern Mid-Latitudes	3.12	29.2	1.26	8.45
Tropical region	22.1	33.8	4.61	7.46
Southern Mid-Latitudes	0.53	33.2	0.29	6.27
Southern Polar Region	-18.7	34.4	-3.33	5.15

Table 7.5. Relative differences (RD) and standard deviation (STDEV) are shown (in percent) together with the absolute difference (DU) on the accuracy of the GOME-2C HR tropospheric ozone column products (tropopause related) for five different latitude belts, validated against $X_{AVK-sonde}$

January – December 2024		GOME-2C HR		
	RD (%)	STDEV (%)	AD (DU)	STDEV (DU)
Northern Polar Region	-3.35	14.2	-1.03	4.00
Northern Mid-Latitudes	3.96	17.9	1.05	5.41
Tropical region	48.0	38.8	9.48	7.34
Southern Mid-Latitudes	-1.2	24.9	-0.17	4.92
Southern Polar Region	-19.1	30.8	-2.89	4.78

The statistics on the accuracy of the GOME-2B and GOME-2C HR tropospheric ozone column products (fixed altitude) for different latitude belts, validated against $X_{\text{AVK-sonde}}$, are shown in Table 7.6 and Table 7.7.

Table 7.6. Relative differences (RD) and standard deviation (STDEV) are shown (in percent) together with the absolute difference (DU) on the accuracy of the GOME-2B HR tropospheric ozone column products (fixed altitude) for five different latitude belts, validated against $X_{\text{AVK-sonde}}$

January – December 2024		GOME-2B HR		
	RD (%)	STDEV (%)	AD (DU)	STDEV (DU)
Northern Polar Region	-2.11	12.9	-0.35	2.35
Northern Mid-Latitudes	0.94	14.2	0.28	2.51
Tropical region	17.1	33.7	1.54	3.20
Southern Mid-Latitudes	-1.11	16.2	-0.18	1.73
Southern Polar Region	-9.02	23.3	-1.07	1.42

Table 7.7. Relative differences (RD) and standard deviation (STDEV) are shown (in percent) together with the absolute difference (DU) on the accuracy of the GOME-2C HR tropospheric ozone column products (fixed altitude) for five different latitude belts, validated against $X_{\text{AVK-sonde}}$

January – December 2024		GOME-2C HR		
	RD (%)	STDEV (%)	AD (DU)	STDEV (DU)
Northern Polar Region	-1.80	6.21	-0.33	1.10
Northern Mid-Latitudes	1.11	9.28	0.14	1.61
Tropical region	40.9	40.5	3.53	3.55
Southern Mid-Latitudes	-1.72	10.9	-0.27	1.22
Southern Polar Region	-10.7	12.4	-0.57	0.90

For the GOME-2B and GOME-2C TrOC products, most of these products comply with the target accuracy requirement. Only for the tropical region (GOME-2C), this is obviously not the case. Between all sensors, there is a clear offset visible in the results. Also here, a degradation correction will be necessary to correct for this offset.

Validation activities summary for tropical tropospheric ozone:

No new reference data was available when this report was published.

This summary contains validation results of the GOME-2B and GOME-2C tropical tropospheric ozone column (TTrOC) products, using the cloud slicing method. The tropospheric ozone retrieval is based on the GOME-2 ozone columns as derived by the GOME Data Processor (GDP, version 4.8) and covers the tropical latitude belt (20S – 20N). This product is available on a monthly basis and has a resolution of 1.25° latitude x 2.5° longitude.

The tropical tropospheric ozone column product has the following user requirements:

- Threshold accuracy: within 50 %
- Target accuracy: within 25 %
- Optimal accuracy: within 15 %

This summary was made available by Dr. Andy Delcloo from KMI. More information on how these values are extracted is available in the [validation report](#). The collocation data used are the same as for the ozone profiles (Figure 7.22).

The time period covered is January 2022 – December 2023 for the GOME-2B and GOME-2C offline TTrOC products.

In Table 7.8 and Table 7.9, the statistics on the accuracy of the GOME-2B/C tropical tropospheric ozone column products for different stations under consideration are shown, showing some general statistics for both datasets.

It is shown that for GOME-2C, most of the stations are within the optimal accuracy (15 %). The correlation varies between 0.3 and 0.7 with a rmse between 2.9 and 7.8 DU. These TTrOC products still fulfill the user requirements.

Table 7.8. Relative Differences (RD), standard deviation (STDEV), correlation, bias and RMSE are shown on the accuracy of the GOME-2B TTrOC product for the time period January 2022 – December 2023

Station	RD (%)	STDEV (%)	Correlation	Bias (DU)	RMSE (DU)
Paramaribu	3.61	28.2	0.43	0.59	5.32
Samoa	20.1	28.8	0.56	2.82	5.18
Ascension Island	4.04	13.0	0.83	1.10	3.44
Kuala Lumpur	-6.62	12.1	0.73	-1.47	2.98
Nairobi	15.9	12.1	0.67	2.66	3.09
Natal	6.44	21.5	0.80	1.93	5.47

Table 7.9. Relative Differences (RD), standard deviation (STDEV), correlation, bias and RMSE are shown on the accuracy of the GOME-2C TTrOC product for the time period January 2022 – December 2023

Station	RD (%)	STDEV (%)	Correlation	Bias (DU)	RMSE (DU)
Paramaribu	11.1	21.5	0.66	1.96	4.21
Samoa	14.4	23.1	0.66	1.83	3.49
Ascension Island	3.16	27.0	0.50	0.80	7.80
Kuala Lumpur	9.85	18.7	0.35	1.32	2.94
Nairobi	17.4	10.6	0.70	3.01	3.37
Natal	8.66	27.9	0.65	1.75	5.58

7.3. GOME-2 trace gas products

Table 7.10. Validation status of trace gas products

Product Identifier	Product Name	Accuracy	Reference	Validating Institute	Correlative data sources
O3M-50.1	NRT total NO ₂	Fulfil threshold accuracy requirement	RD5	BIRA-IASB	NDACC zenithSky measurements
O3M-338			RD24		
O3M-52.1	NRT tropospheric NO ₂	Fulfil threshold accuracy requirement	RD5	BIRA-IASB	BIRA-IASB and other MAXDOAS stations
O3M-341			RD24		
O3M-55.1	NRT total SO ₂	Fulfil threshold accuracy requirement	RD9	AUTH	
O3M-374			RD30		
O3M-177	NRT total HCHO	Fulfil threshold accuracy requirement	RD11	BIRA-IASB	BIRA-IASB and other MAXDOAS stations
O3M-344			RD25		
O3M-51.1	Offline total NO ₂	Fulfil threshold accuracy requirement	RD5	BIRA-IASB	NDACC zenithSky measurements
O3M-339			RD24		
O3M-37.1	Offline tropospheric NO ₂	Fulfil threshold accuracy requirement	RD5	BIRA-IASB	BIRA-IASB and other MAXDOAS stations
O3M-53.1					
O3M-342			RD24		
O3M-09.1	Offline total SO ₂	Fulfil threshold accuracy requirement	RD9	AUTH	
O3M-56.1					
O3M-375			RD30		
O3M-08.1	Offline total BrO	Fulfil threshold accuracy requirement	RD10	BIRA-IASB	BIRA-IASB Harestua zenithSky station and satellite comparisons
O3M-82.1					
O3M-317			RD26		
O3M-10.1	Offline total HCHO	Fulfil target accuracy requirement	RD11	BIRA-IASB	BIRA-IASB and other MAXDOAS stations
O3M-58.1					
O3M-345			RD25		
O3M-12.1	Offline total H ₂ O	Fulfil threshold accuracy requirement	RD12	FMI, DLR	IGRA , COSMIC-SuomiNet , SSM/I
O3M-86.1					Comparison against GOME-2B water vapour data
O3M-386			RD27		

Validation activities summary:

This summary presents validation activities for offline total and tropospheric NO₂, total HCHO, and total BrO data products of GOME-2B/C as performed at BIRA-IASB and SO₂ data as performed at AUTH.

The authors of this summary are Gaia Pinardi (for tropospheric NO₂ and HCHO validation), Jean-Christopher Lambert, José Granville and Tijl Verhoelst (for total/stratospheric NO₂ validation), François Hendrick and Jeroen van Gent (for BrO validation) and Jeroen van Gent and MariLiza Koukouli (for quality assessment).

Validation exercises are performed following the protocols described in the original Metop-A, Metop-B and Metop-C [validation reports](#) and updated in Pinardi *et al.* (AMT 2020) and Verhoelst *et al.* (AMT 2021), and the results presented in this report are based on updates of the correlative datasets with the last available – and sometimes improved – versions. While illustrations at a few stations are included in this report, all the updated figures are reported on the [BIRA-IASB trace gases validation server](#).

Update of database for reference data

For this report, the validation database was updated with ground-based NDACC UVVIS ZenithSky NO₂ data (as usual) and MAXDOAS NO₂ and HCHO data from BIRA, KNMI and IUPB (as collected for the NIDFORVAL S5p validation project and already used in Pinardi *et al.* (AMT 2020), Verhoelst *et al.* (AMT 2021) and De Smedt *et al.* (ACP 2021), in order to cover as much as possible the period until end of 2024. BIRA-IASB ZenithSky BrO data at Harestua could not be updated for this report, due to BIRA-IASB change of personnel and only the comparisons of GOME-2 to TROPOMI BrO VCD are updated.

ZenithSky NO₂ total columns are collected from the NDACC Data Host Facility (to where the data have to be uploaded by instrument Pis within 1 year after data acquisition) and from the SAOZ rapid delivery operational facility operated by LATMOS. The SAOZ at Bauru (Brazil) is unfortunately no longer operational. The ground-based data are then quality assessed and post-processed at BIRA-IASB in preparation for the data comparisons. This preparation includes calculation of the effective ground-based airmasses with which GOME-2 data co-locations will be sought.

The BIRA-IASB MAXDOAS ground-based dataset are automatically retrieved with an improved version of the bePRO profiling algorithm (Clémer *et al.*, 2010; Hendrick *et al.*, 2014, Vlemmix *et al.*, 2015) developed within the EU FP7 NORS and QA4ECV projects (aiming at rapid delivery of improved NO₂ and HCHO profiles), and is progressively shifting to the FRM4DOAS analysis chain. The FRM4DOAS (Fiducial Reference Measurements for Ground-Based DOAS Air-Quality Observations) is an ESA activity aiming at the development of the first centralised NRT processing system for MAX-DOAS instruments operated within the international Network for the Detection of Atmospheric Composition Change (NDACC). It includes the launch of the NDACC MAX-DOAS Processing Service in a demonstration mode, focusing on tropospheric and stratospheric NO₂ vertical profiles, total O₃ columns, and tropospheric HCHO profiles as target MAX-DOAS products for the first phase of the project (July 2016 – August 2021), see <https://frm4doas.aeronomie.be/>. The lower tropospheric profiles and vertical columns processing chain rely on parallel runs of optimal-estimation based MMF (Friedrich *et al.*, 2019) and parametrized approach MAPA (Beirle *et al.*, 2019) algorithms and testings of their results coherence. The service is running in a best-effort mode at the time of writing for a limited number of stations belonging to the project partners, and only tropospheric NO₂ and total O₃ are to the NDACC RD database. More details can be found in Van Roozendael *et al.* 2024.

IUPB and KNMI sites are retrieved respectively with the QA4ECV database approach (https://uv-vis.aeronomie.be/groundbased/QA4ECV_MAXDOAS/index.php), as discussed and used in Pinardi *et al.* (AMT 2020) and Verhoelst *et al.* (AMT 2021) for NO₂ and De Smedt *et al.* (ACP 2021) for HCHO. This approach only provides VCD columns, and profiles are not retrieved. These datasets

are also used for the online validation of S5p (<https://mpc-vdaf-server.tropomi.eu/no2/no2-offl-maxdoas> and <https://mpc-vdaf-server.tropomi.eu/hcho/hcho-offl-maxdoas>).

The NO₂ and HCHO datasets include the following ground-based stations:

- OHP (from June 2007 to July 2014 with the geometrical approximation, and since August 2014 to March 2017 with the bePRO profiling tool)
- Uccle (from April 2011 to March 2016 with a miniMAXDOAS instrument (Uccle-miniDOAS) and from end of January 2017 to February 2020 with a scientific grade MAXDOAS: Uccle-SG)
- Bujumbura (from November 2013 to July 2017; since then the instrument had a power failure and only limited operations and data transfer was possible)
- LePort, on Reunion Island (from April 2016 to 10 January 2018). The instrument has been reinstalled in June 2018 on the Maito site, and data analysis from the FRM4DOAS analysis chain was tested, but it is not adapted for tropospheric (NO₂, HCHO) gases validation at this mountaneous site and is not used for this report.
- Xianghe (from March 2010 to July 2018 and from October 2019 to August 2022). Since November 2021 the retrievals in the UV are of bad quality and the UV channel broke down early 2022. SO₂ MAXDOAS profiles were also analysed for the whole time-series (2010 to Oct. 2021), although the SO₂ levels are very low now in China nowadays.
- Kinshasa (from December 2019 to December 2024). The instrument and the FRM4DOAS processing is described in Yombo Phaka *et al.*, 2023.
- IUPB Bremen and Athens and KNMI Cabauw and De Bilt data used here covers the periods from April/May 2018 to end of December 2024 for NO₂ and the KNMI also for HCHO.

Status of GOME-2B and GOME-2C tropospheric NO₂

Comparisons with ground-based MAXDOAS instruments is performed similarly as in previous [validation report](#). In Pinardi *et al.* (2020) it is shown that best results are achieved by filtering out the largest pixels and selecting only pixels covering the stations. For GOME-2, the selection includes keeping only pixels with a size of less than 100 km, while selecting pixels over the station, only slightly changes the results, as generally pixels with their center within 50 km, are covering the station. This improvement of the biases comes at the expenses of a strongly reduced number of pixels (see AC SAF Operations Report 1/2020).

Only BIRA MAXDOAS station from Kinshasa can be used over 2024, and we also used some available MAXDOAS data from KNMI and IUPB, as presented above.

Figure 7.4 shows example of results for GOME-2B and GOME-2C for Kinshasa. Monthly mean differences are calculated for every year and for the whole time-series in order to see the evolution in time of the bias. Table 7.11 reports the median differences and the spread (half the percentile 68) at the stations, with and without the smoothing, and the figures for all the stations can be found on the [BIRA-IASB validation web server](#).

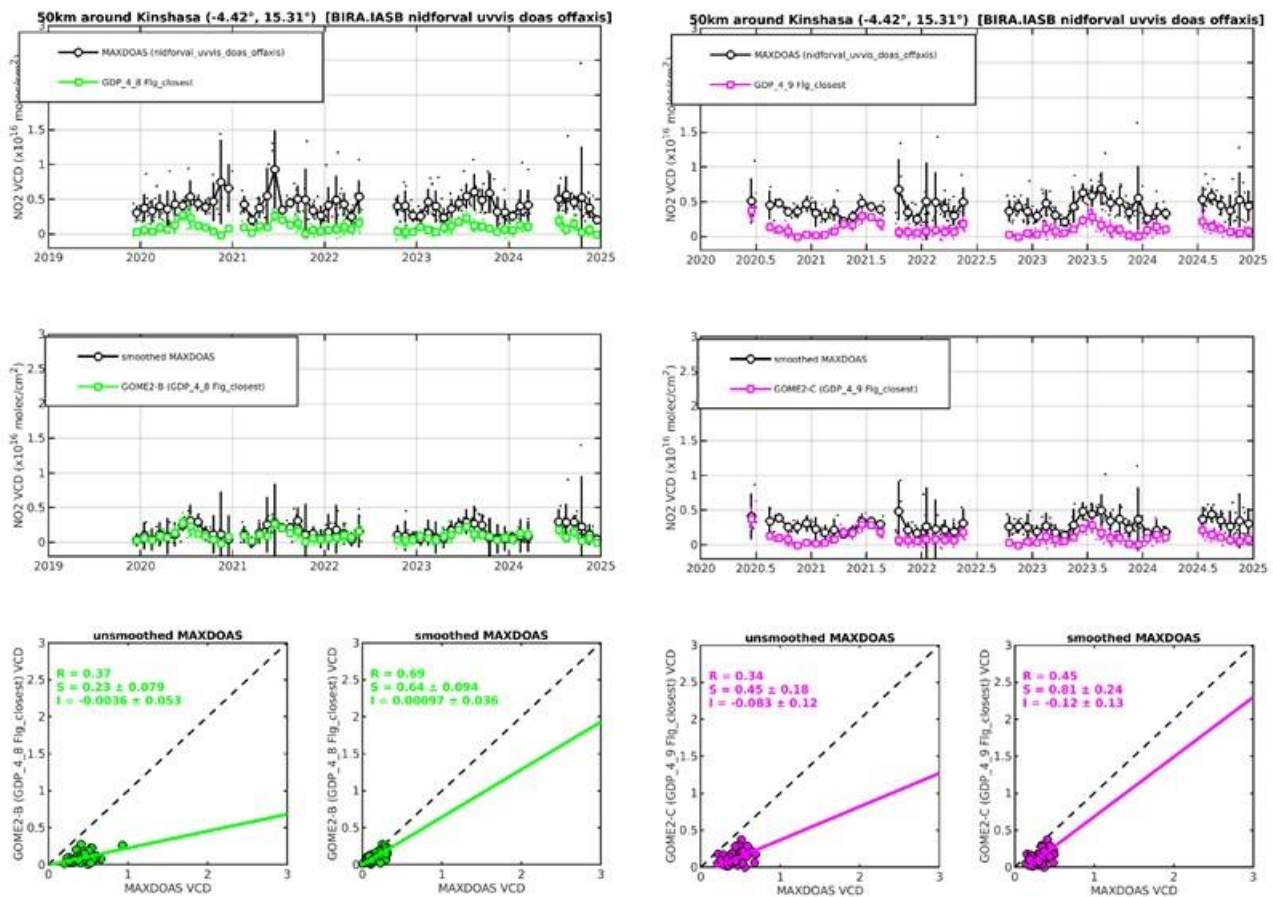


Figure 7.4. Illustration for the Kinshasa MAXDOAS versus GOME-2B GDP-4.8 (left) and GOME-2C GDP-4.9 (right) tropospheric NO₂ comparisons.

Table 7.11. Median Absolute Differences (AD=SAT-GB, in 10¹⁵ molec/cm²), Relative Differences (RD, in %) and spread (0.5*IP68) on the accuracy of GOME-2B and GOME-2C tropospheric NO₂ products when comparing to MAXDOAS data (NOT cloud filtered). Values for the last 12 months are given, and the values for the whole time-series are reported in brackets for comparison. Results for both the original comparisons (pixels over the station, for pixels smaller than 100 km side) and for the smoothed comparisons are reported. Only the first rows are stations with recent data (in bold below), the others are given as examples of past results.

	GOME-2B			GOME-2C		
	AD (×10 ¹⁵)	RD (%)	SPREAD (%)	AD (×10 ¹⁵)	RD (%)	SPREAD (%)
Bremen (IUPB) Last 12 months: 12/2023 – 12/2024 [whole period: since 04/2018]	-2.5 [-2.2]	-56 [-41]	51.6 [53.0]	-1.3 [-2.1]	-38 [-45]	66.6 [43.3]
Athens (IUPB) Last 12 months: 1/2024 – 12/2024 [whole period: since 05/2018]	-1.8 [-1.6]	-40 [-38]	53 [38]	-2.2 [-2.0]	-45 [-39]	11 [30]
Cabauw (KNMI)	-0.5 [0.25]	11 [3.4]	55 [36]	-0.3 [-0.3]	-7 [-4.8]	34 [30]

	GOME-2B			GOME-2C		
Last 12 months: 12/2023 – 12/2024 [whole period: since 04/2018]						
De Bilt (KNMI) Last 12 months: 1/2024 – 12/2024 [whole period: since 04/2018]	-1.0 [-0.1]	-3.1 [-1.2]	32 [39]	-0.1 [-0.1]	-2.0 [-1.6]	55 [40]
Kinshasa * last 12 months: 1/2024 – 12/2024 [whole period: 12/2019 – 12/2024]	-3.1 [-3.1]	-80 [-80]	34.2 [29.0]	-3.2 [-3.2]	-75 [-78]	26.5 [26.5]
Kinshasa smoothed *	-0.5 [-0.4]	-47 [-30]	99 [65]	-2.0 [-1.7]	-67 [-67]	36 [37]
Uccle SG last 12 months: 03/2019 – 02/2020 [whole period: 02/2017 – 02/2020]	-1.2 [-1.4]	-16 [-20]	33 [36]	-	-	-
Uccle SG smoothed	-2.5 [-2.7]	-26 [-29]	38 [36]	-	-	-
Reunion Maito (last 12 months: 12/2018 – 11/2019) [whole period: 06/2018 – 11/2019]	-0.02 [-0.02]	-4.2 [-4.3]	76 [93]	-	-	-
Reunion Maito smoothed	-0.03 [-0.01]	-1.4 [-9]	85 [115]	-	-	-
Xianghe (last 12 months: 12/2020 – 07/2022) [whole period: 03/2010 – 07/2022]	0.9 [-0.8]	-4.9 [-4.4]	26 [25]	-0.3 [-0.8]	-1.2 [-9]	23 [21]
Xianghe smoothed	-2.2 [-3.8]	-17 [-18]	28 [36]	-2.1 [-2.4]	-13 [-21]	29 [36]
Bujumbura (last 12 months: 07/2016 – 07/2017) [whole period: 11/2013 – 07/2017]	-3.4 [-3.2]	-83 [-81]	42 [28]	-	-	-
Bujumbura smoothed	-2 [-1.8]	-70 [-74]	21 [35]	-	-	-
OHP (last 12months: 03/2016 – 03/2017)	-0.7 [-0.6]	-37 [-28]	34 [36]	-	-	-

	GOME-2B			GOME-2C		
[whole period: 08/2014 – 03/2017]						
OHP smoothed	-0.5 [-0.4]	-36 [-24]	41 [39]	-	-	-
Reunion LePort Last 12 months: 12/2016 – 12/2017) [whole period: 04/2016 – 12/2017]	-1.4 [-1.4]	-83 [-84]	25 [25]	-	-	-
Reunion LePort smoothed	-0.41 [-0.42]	-59 [-60]	22 [25]	-	-	-
Uccle minDOAS (last 12 months: 03/2015 – 03/2016) [whole period: 04/2011 – 03/2016]	-2.6 [-3]	-26 [-31]	25 [24]	-	-	-
Uccle minDOAS smoothed	-3.6 [-3.3]	-29 [-33]	20 [30]	-	-	-

* The Kinshasa site had to be processed with a different satellite pixels selection (closest valid flagged pixel instead of valid pixel over the site) to have enough daily coincidences and allow meaningful comparisons.

From Figure 7.4 it can be seen, that GOME-2C scatter plot is similar to what obtained with GOME-2B (confirming past results from Xianghe), although the statistics are slightly different, probably due to the presence in GOME-2B period of a few larger NO₂ columns (between $1 - 2 \times 10^{15}$ molec/cm²) that strongly influence the regression analysis (Pinardi *et al.*, 2020). There are some differences in the absolute and relative differences for GOME-2B and GOME-2C and for the last 12 months compared to the whole period. These depend from one station to the other (ie. -7 % bias for GOME-2C compared to 11 % for GOME-2B in Cabauw, -38 % compared to -56 % for Bremen and -2 % compared to -3.1 % for De Bilt).

The biases results are usually within or close to the requirements (target accuracy requirement of 30 % in polluted conditions and optimal accuracy of 20 %), as it was the case for the other sensors for Xianghe and Uccle in the past. Kinshasa, Cabauw and De Bilt sites are remote sites, with low levels of NO₂ pollution and low biases, while Bremen and Athens are more urban polluted sites, with biases around the -40 % levels, with a spatial comparison mismatch (horizontal dilution component) as highlighted in Pinardi *et al.* (2020) and also seen for other BIRA-IASB sites in the past. Beijing and OHP report about 50 % biases, while larger values are found for Bujumbura and Reunion, as previously (Pinardi *et al.*, 2014; NO₂ Validation Report 2015; Pinardi *et al.*, 2020). As before, smoothing the MAXDOAS profiles with the satellite averaging kernels is not always reducing the mean comparison differences, with an impact of ~10 – 20 % depending on the station (AC SAF Operations Report 1/2018, PT meeting of May 2018). The comparison improvement for Kinshasa is clear in Figure 7.4.

In terms of stability most of the stations report differences over time up to 15 % for both GOME-2B and GOME-2C, which is also about the level of difference between GOME-2B and GOME-2C (10 to 15 %, except Cabauw and Bremen in this case), and the levels we had in the past between

GOME-2A and GOME-2B. These biases could be partly reduced in the future with the improved GDP-4.9 GOME-2 algorithm (Liu *et al.*, 2019).

Status of GOME-2B and GOME-2C total (stratospheric) NO₂

Quality monitoring of the GOME-2 NO₂ total (stratospheric) column data is regularly carried out using correlative ground-based measurements collected from about 20 Zenith-Scattered-Light DOAS UV-visible (ZSL-DOAS) instruments affiliated with the Network for the Detection of Atmospheric Composition Change (NDACC). The NO₂ column validation protocol has already been described in previous AC SAF validation reports with its latest updates published in Verhoelst *et al.* (AMT 2021). This protocol includes the selection of GOME-2/NDACC co-located data pairs based on the air-mass matching technique, a model-based photochemical correction compensating for significant solar local time differences between GOME-2 mid-morning and NDACC twilight observations in polar summer, and a cloud-based filtering of NO₂ data over polluted stations aiming at the removal of pollution-affected pixels. At some stations, real-time processing of the ground-based observations still uses NO₂ absorption cross-sections at room temperature instead of stratospheric temperature. As a result, the retrieved total NO₂ column is affected by a negative systematic bias of 15 – 20 % with a seasonal component. Such data are removed. Thanks to this strict protocol, data comparisons can be carried out within a residual uncertainty of about $2 - 3 \times 10^{14}$ molec/cm² combining both the ground-based data uncertainty and comparison errors. This uncertainty is indicated by the shaded area on the pole-to-pole graphs. Drift estimates are performed using both a strict linear regression (but reporting on the autocorrelation ϕ in the residuals) and a regression including annual and semi-annual terms. The latter can for instance absorb the seasonally varying bias due to the fixed assumed effective temperature in the ZSL-DOAS retrievals.

Figure 7.5 shows the comparison of NO₂ column data at the NDACC Antarctic station of Dumont d'Urville, a station located on the polar circle, in a pristine environment without any known source of tropospheric NO₂. Comparison results at this station are representative of the validation of purely stratospheric data series, at moderate and large solar zenith angle, and over the full range of NO₂ stratospheric column values from winter lows of about 1×10^{14} molec/cm² (wintertime denoxification episodes) up to summer highs of 7×10^{15} molec/cm² (complete depletion of N₂O₅ into NO₂ due to polar midnight Sun). On a monthly median basis, and over the 16 years covered by the three satellites, the target bias of $3 - 5 \times 10^{14}$ molec/cm² hasn't often been exceeded, except occasionally in October when the station is overpassed frequently by the border of the polar vortex, thus when atmospheric variability contributes significant co-location mismatch noise and bias to the difference in stratospheric NO₂. The ground dataset shown in this figure is a composite dataset consisting of the NDACC reprocessed dataset extended through the last year by the near-real-time dataset (latmos_rt).

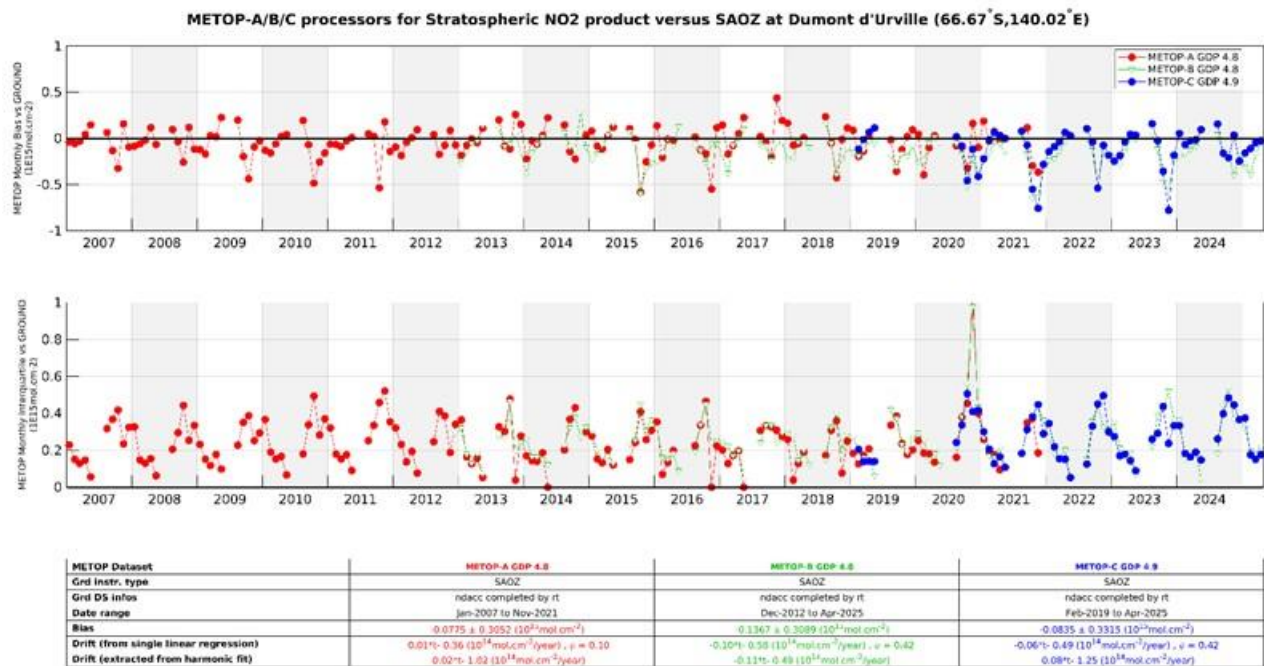


Figure 7.5. Comparison of NO₂ column data measured at the NDACC Antarctic station of Dumont d'Urville by the GOME-2 instruments) and by the CNRS/LATMOS ZSL-DOAS spectrometer. Top: time-series of the median NO₂ column difference per month; centre: time-series of the dispersion of the NO₂ column difference per month; bottom (table): summary statistics.

Figure 7.6 and Figure 7.7 display similar results obtained at the NDACC station of Izaña on Tenerife (Canary Islands) and the NDACC Southern Tropic station of Saint-Denis de la Réunion, thus in occasional presence of pollution and over a wider range of solar zenith angle. Again, the target bias of $3 - 5 \times 10^{14}$ molec/cm² has rarely been exceeded, except in very few cases.

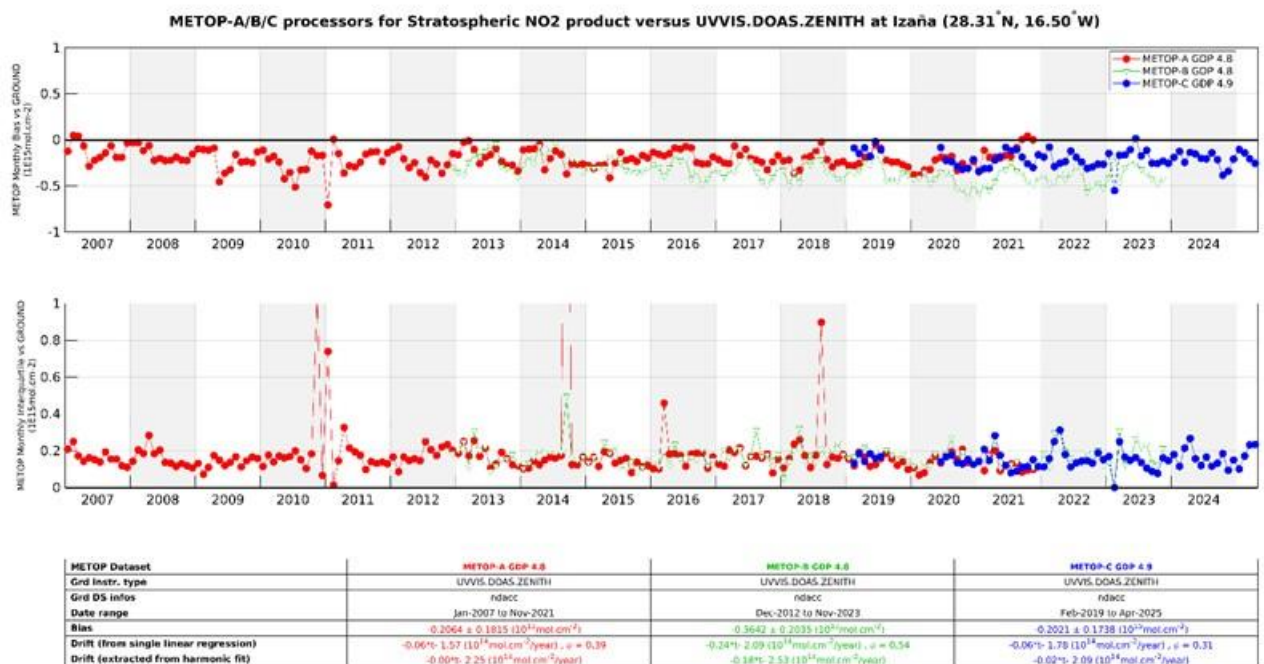


Figure 7.6. Same as Figure 7.5 but at the NDACC station of Izaña on Tenerife (Canary Islands).

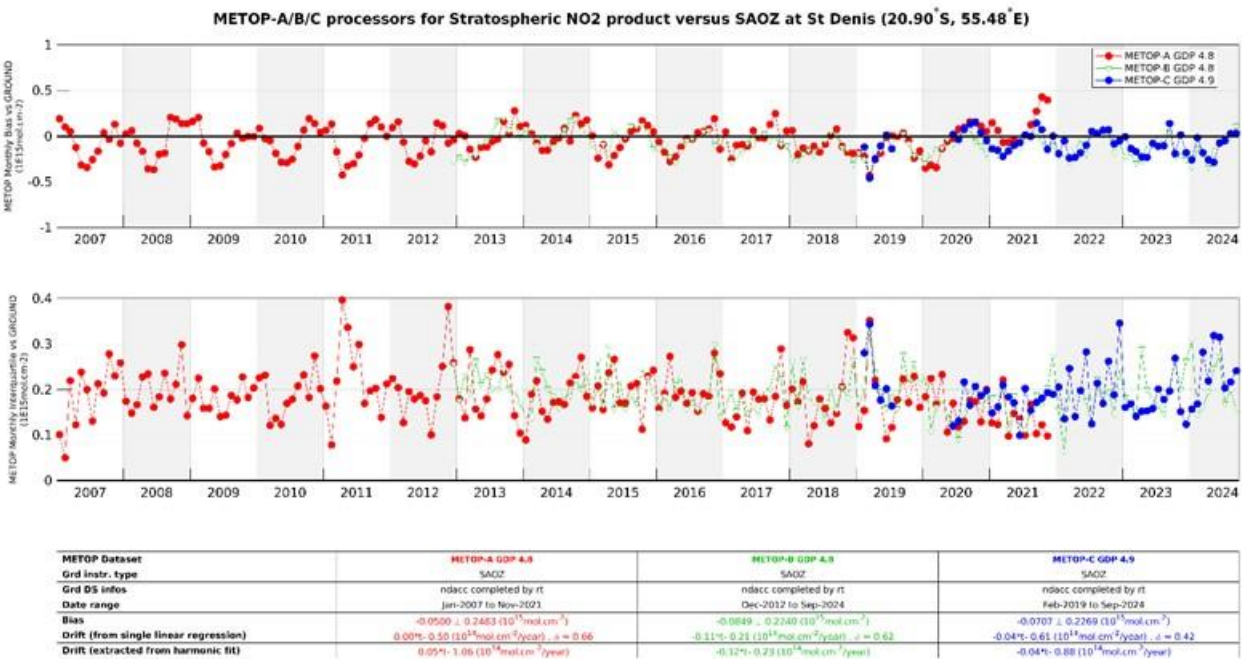


Figure 7.7. Same as Figure 7.5, but at the NDACC Southern Tropical station of Saint-Denis de la Reunion.

Figure 7.8 reports from pole to pole the median value and the dispersion of the differences between GOME-2 and NDACC ZSL-DOAS data, while Figure 7.9 displays, again from pole to pole, the linear drift between GOME-2A/B/C and NDACC data. Those graphs show the good long-term stability of the satellite NO₂ column data with respect to NDACC ZSL-DOAS data at all stations.

They also show that the target bias of $3 - 5 \times 10^{14}$ molec/cm² in unpolluted conditions is achieved at virtually all sites for all three satellites. Figure 7.7 also confirms the slight difference already noticed in previous validation reports between the biases observed respectively in the Southern and Northern hemispheres. Averaging median differences separately over the Northern and Southern Hemispheres concludes to an inter-hemispheric bias of about $2 - 3 \times 10^{14}$ molec/cm². GOME-2C NO₂ column data present a slightly more positive bias across all latitudes. Drift estimates show a bit more scatter for GOME-2C, in particular at high Northern latitudes, but the mission lifetime of GOME-2C is still relatively short for stable drift determination.

Note that for these global statistics visualized in Figure 7.8 and Figure 7.9, only ground instruments yielding co-locations with all 3 satellite instruments (on Metop-A/B/C) were used so as to limit selection biases between sounders.

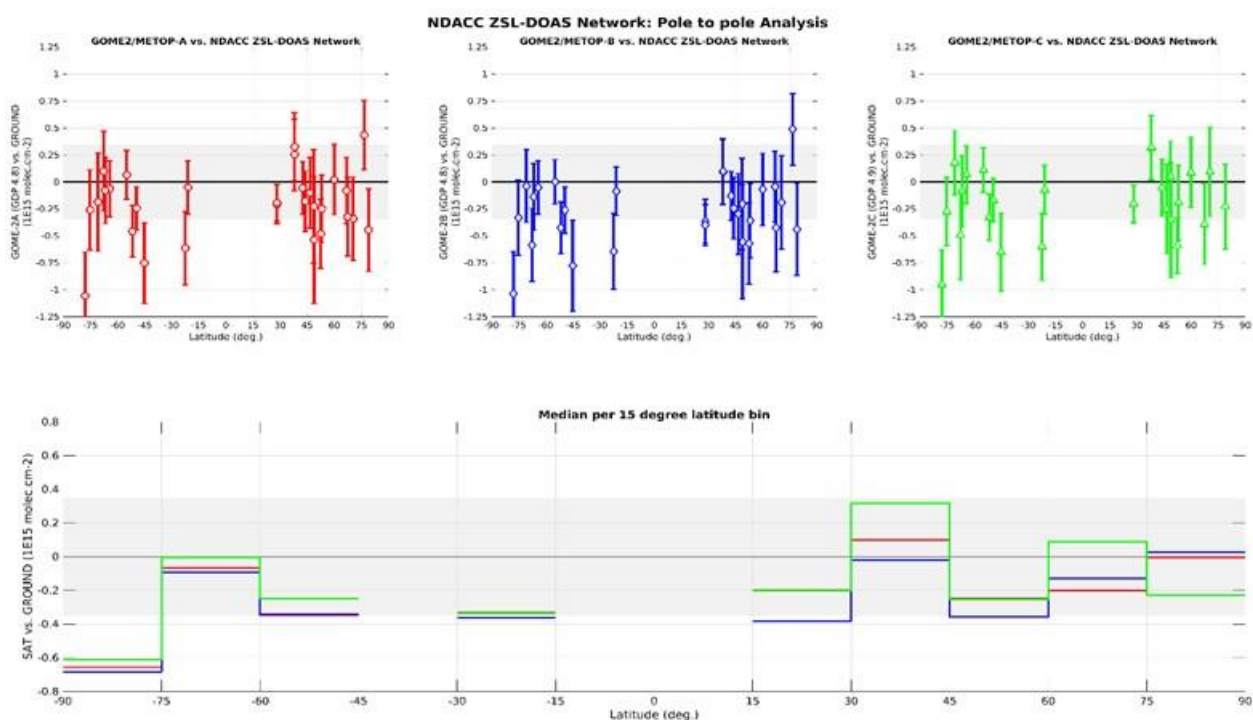


Figure 7.8. From pole to pole, median difference between the NO₂ column data reported by GOME-2A/B/C (red/blue/green) GDP-4.8 (GDP 4.9 for GOME-2C) and by ground-based ZSL-DOAS spectrometers at about 20 NDACC stations, calculated over 2007 – November 2021 for GOME-2A, 2012 – March 2025 for GOME-2B and 2019 – March 2025 for GOME-2C. Top: median difference at individual stations. Bottom: median difference averaged over 15° latitude bins.

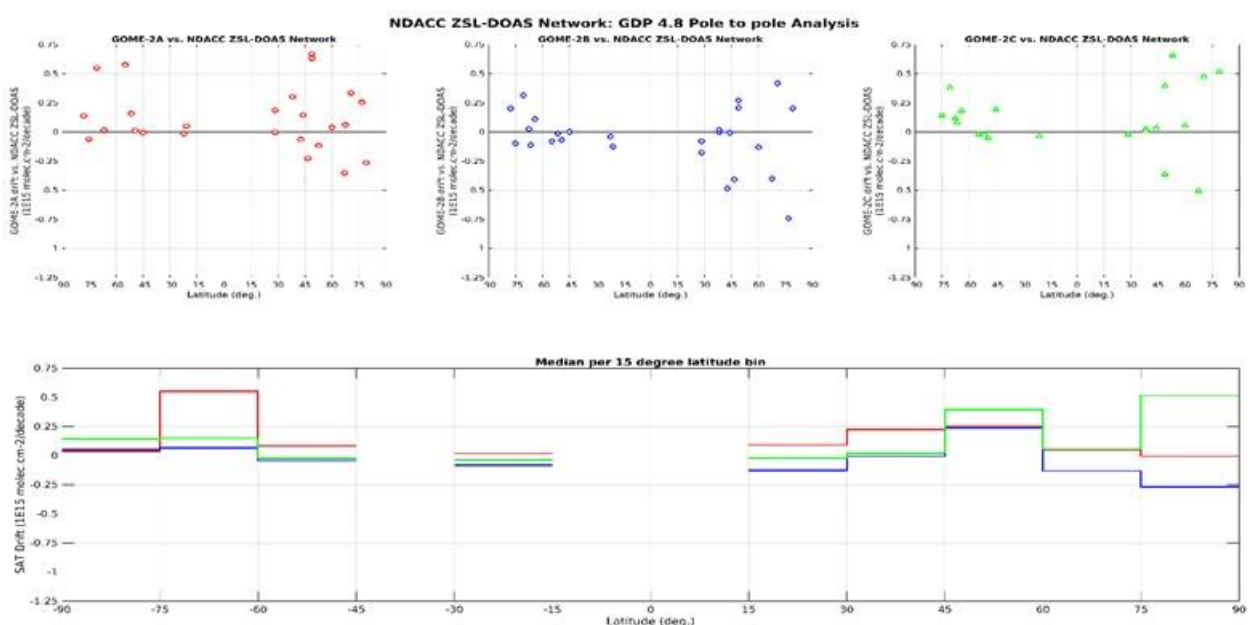


Figure 7.9. From pole to pole, linear drift from a regression model including annual and semi-annual harmonic terms of the difference between the NO₂ column data reported by GOME 2A/B/C (red/ blue/ green) GDP 4.8 (GDP 4.9 for GOME-2C) and by ground-based ZSL-DOAS spectrometers at about 20 NDACC stations, calculated over 2007 – November 2021 for GOME-2A, 2012 – March 2025 for GOME-2B and 2019 – March 2025 for GOME-2C. Top: linear drift estimates at individual stations. Bottom: same linear drift estimates but averaged over 15° latitude bins.

Status of GOME-2B and GOME-2C total HCHO

This validation exercise is an extension of what is presented in the [HCHO GDP-4.8 validation report](#), relying on correlative observations from MAX-DOAS instruments operated by BIRA-IASB at Xianghe, Bujumbura, Uccle (miniDOAS and SG), OHP and Reunion (Le Port and Maito). As discussed above, the only update possible from BIRA-IASB stations is the Kinshasa site, so the KNMI Cabauw and De Bilt sites are also included in this report. An illustration of the comparisons for De Bilt are presented in Figure 7.10, past figures can be found on the [BIRA validation web server](#) and a summary is presented in Table 7.12.

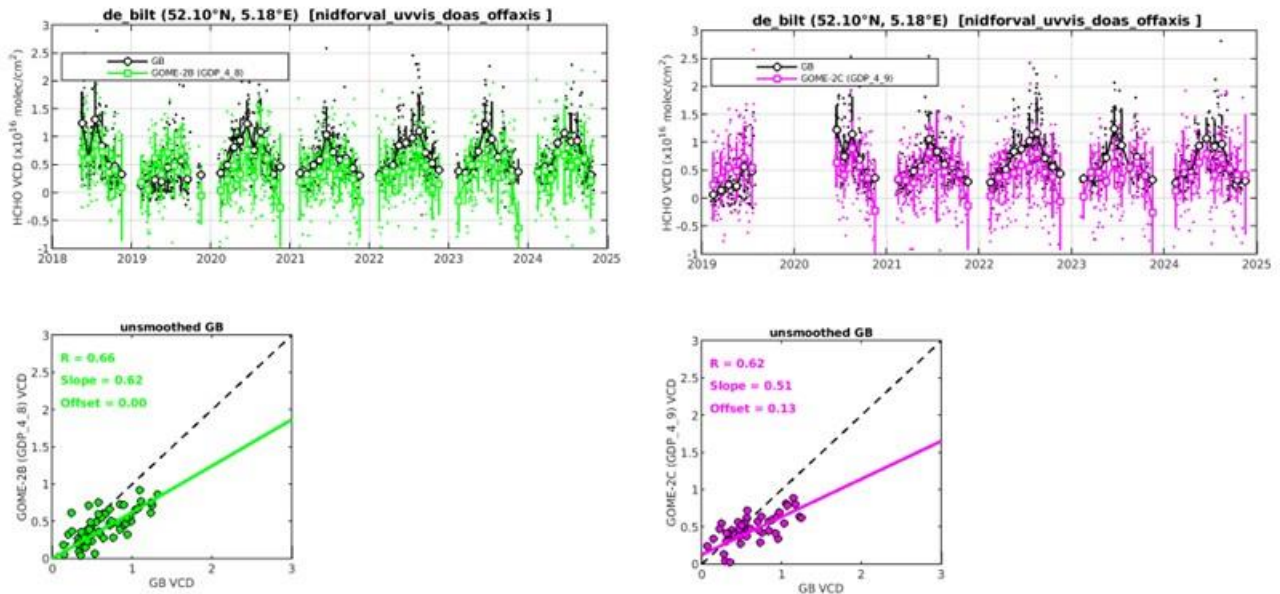


Figure 7.10. Illustration for the De Bilt MAXDOAS versus GOME-2B GDP-4.8 (left) and GOME-2C GDP-4.9 (right) HCHO comparisons.

Table 7.12. Summary of the mean biases (SAT-GB, in 10^{15} molec/cm²) between GOME-2B/C and MAX-DOAS HCHO VCDs. The values in parentheses correspond to the mean relative biases (in %) and R is the correlation coefficients and S the slope of the linear regression of the monthly mean points. Only the first two rows are stations with recent data (Cabauw, De Bilt and Kinshasa), the others are given as examples of past results.

	GOME-2B	GOME-2C
CABAUW (51.97°N, 4.93°E) (whole period: 04/2018 – 12/2024)	-1.7 ± 2 (-29 ± 44) R = 0.63, S = 0.62	-1.3 ± 2 (-23 ± 45) R = 0.63, S = 0.58
DE BILT (52.10°N, 5.18°E) (whole period: 05/2018 – 12/2024)	-2.3 ± 2.4 (-37 ± 56) R = 0.66, S = 0.62	-1.6 ± 2.5 (-28 ± 71) R = 0.62, S = 0.51
KINSHASA (4.42°S, 15.31°E) (whole period: 12/2019 – 12/2024)	-0.3 ± 3 (-2.4 ± 22) R = 0.79, S = 0.98	-0.1 ± 3.2 (-0.23 ± 23) R = 0.76, S = 0.74
UCCLE-SG (50.8°N, 4.3°E) (whole period: 02/2017 – 12/2019)	0.3 ± 1.6 (7 ± 52) R = 0.75, S = 0.96	-
With smoothing	1.6 ± 1.7 (49 ± 75) R = 0.76, S = 1.34	-
REUNION MAIDO (20.9°S, 55.3°E) (whole period: 06/2018 – 11/2019)	2.1 ± 0.8 (94 ± 54) R = 0.84, S = 1.17	-
With smoothing	1.7 ± 0.8 (68 ± 43) R = 0.69, S = 1.29	-
XIANGHE (39.7°N, 117.0°E) (whole period: 03/2010 – 12/2021)	-6.4 ± 2.7 (-48 ± 16) R = 0.88, S = 0.67	-8.9 ± 2.6 (-60 ± 21) R = 0.82, S = 0.76
With smoothing	0.59 ± 2.2 (-8 ± 31) R = 0.88, S = 1.19	-2.4 ± 2.7 (-29 ± 37) R = 0.79, S = 1.40
BUJUMBURA (3.0°S, 29.0°E) (whole period: 11/2013 – 07/2017)	-4.4 ± 2.2 (-32 ± 10) R = 0.88, S = 0.52	-
With smoothing	0.3 ± 2.0 (3.2 ± 25) R = 0.72, S = 0.65	-
OHP (whole period: 08/2014 – 03/2017)	0.3 ± 1.1 (4.2 ± 21) R = 0.90, S = 0.75	-
With smoothing	103.51 ± 1.0 (17 ± 22) R = 0.86, S = 1.01	-
REUNION LEPORT (20.9°S, 55.3°E) (whole period: 04/2016 – 12/2017)	103.51 ± 0.8 (39 ± 26) R = 0.80, S = 1.56	-

With smoothing	2.6 ± 0.1 (180 ± 56) $R = 0.78, S = 2.83$	-
UCCLE-miniDOAS (50.8°N, 4.3°E) (whole period: 04/2011 – 05/2015)	-0.6 ± 1.6 (-9.4 ± 29) $R = 0.76, S = 0.89$	-
With smoothing	-0.4 ± 1.7 (7.1 ± 34) $R = 0.73, S = 0.88$	-

Results obtained at Cabauw, De Bilt and Kinshasa confirm that both satellite instruments capture well the HCHO VCD seasonality. Results for GOME-2B and GOME-2C are similar (as shown also in the past for Xianghe), to within 10 %. Results for the whole period (shown here) and for the last 12 months generally show differences up to 15 % (not shown here, see the different figures for each station on the BIRA validation web server). In Reunion the signal is very small (less than $\sim 0.5 \times 10^{16}$ molec/cm²) and is more difficult to have firm conclusions.

A significant bias exists between GOME-2B/C and MAX-DOAS observations at the some of the stations (up to 50 %), but as already shown in the GDP-4.8 validation report, for some stations this bias can be significantly reduced when smoothing the MAX-DOAS profiles with the satellite column averaging kernels (see also values with smoothing in Table 7.12).

Status of GOME-2B and GOME-2C total BrO

GOME-2B/C total columns of BrO from GDP-4.8 (4.9 in the case of GOME-2C) operational product are usually compared to ground-based UV-visible zenith-sky measurements at Harestua, Norway (60°N, 11°E), as done in previous [validation report](#). The ground-based columns are derived from the vertical profiles retrieved by applying an OEM (Optimal Estimation Method) –based profiling technique to zenith-sky measurements at sunrise (Hendrick *et al.*, 2007). The instrument was temporarily off due to problems at the Harestua observatory since 09/12/2022 and is now back in operations since the end of April 2023 with a change of management at the Harestua Solar Observatory. Moreover, due to long-period sickness of key personnel, the ground-based BrO data could not yet be analyzed and this comparison with the GOME-2 instruments could not be updated for this report. We leave the results and discussion of the Operations Report 1/2022 further down in this section.

As a replacement, first introduced in the 2/2023 report, a comparison of total BrO columns from GOME-2B (GDP 4.8 product) and GOME-2C (GDP 4.9 product) on one hand and S5P/TROPOMI on the other hand is made below. The TROPOMI data derives from the total BrO retrieval algorithm TCBRO, developed at BIRA-IASB, that is currently running in the so-called pre-operational environment of the ESA S5P-PAL system (<https://data-portal.s5p-pal.com/>). For this, we use the high resolution (0.022°) TROPOMI BrO L3 monthly-averaged data from S5P-PAL.

For the satellite-satellite comparison, monthly average BrO VCD values over 2024 have been derived over a 150 km area around 12 well known ground stations, ranging in latitude from the northern to the southern polar region. The geographic locations of these stations are shown in Figure 7.11.

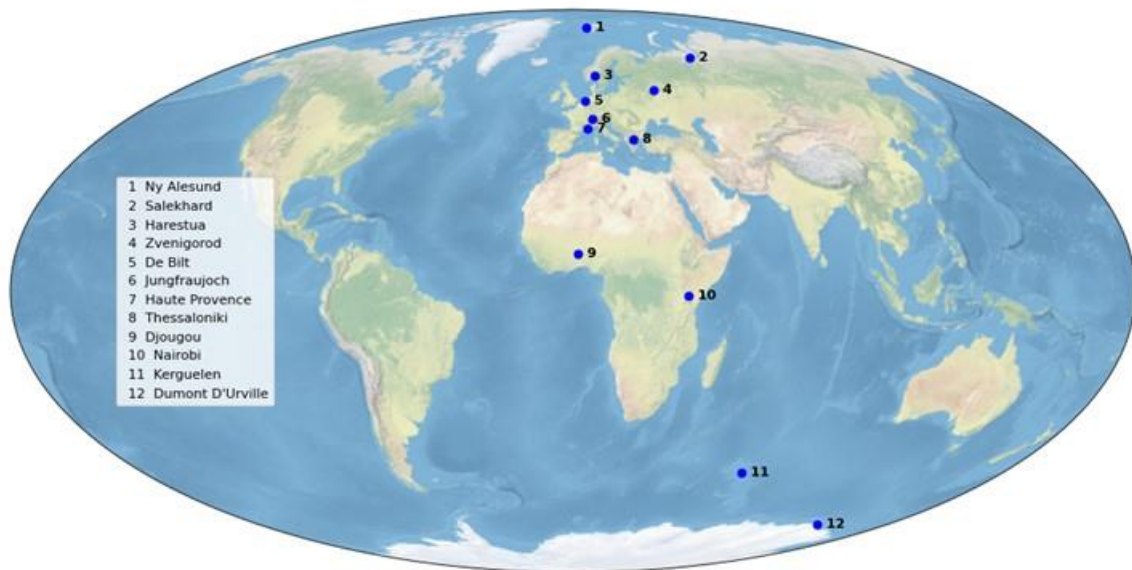
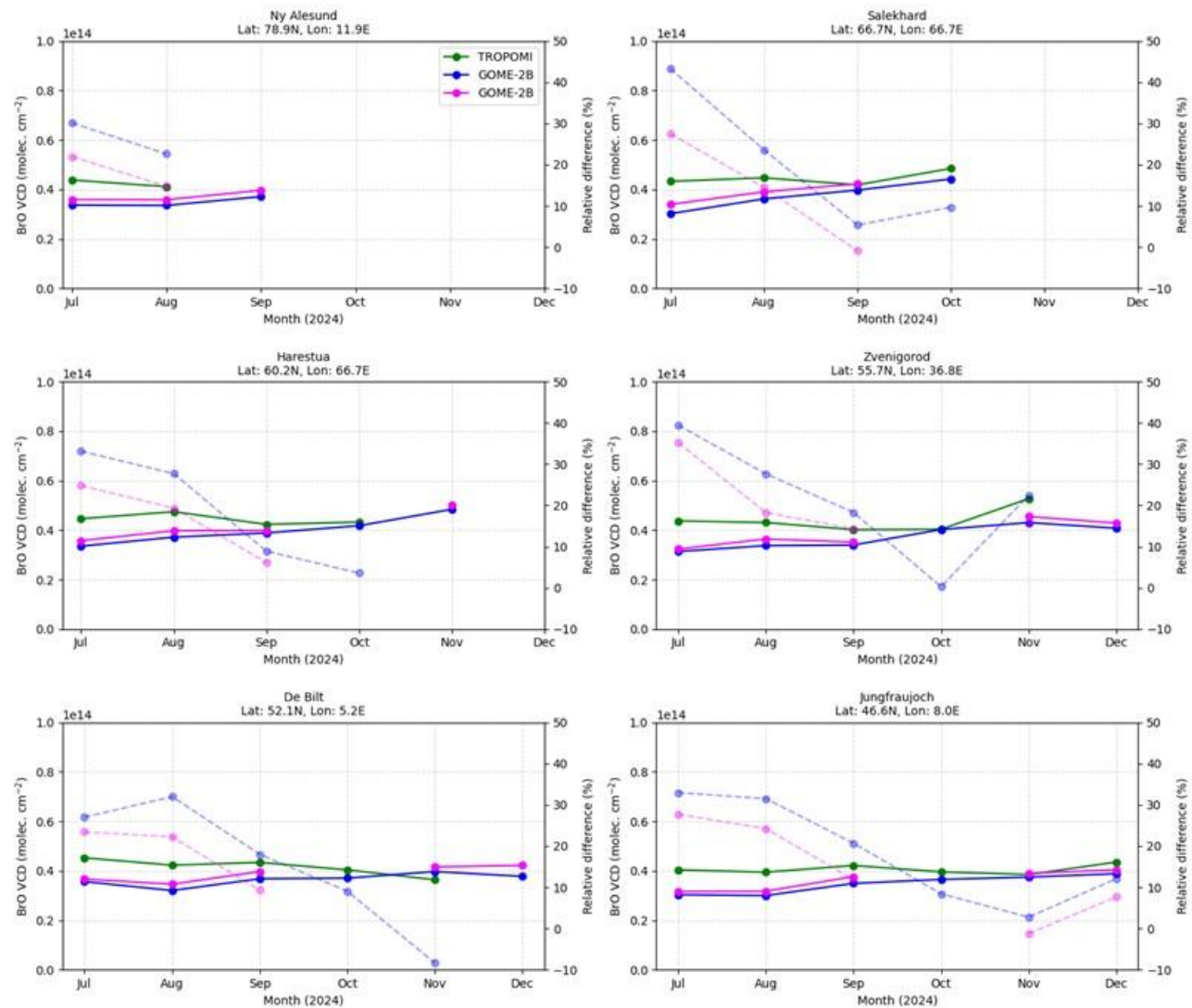


Figure 7.11. Location of the 12 stations for which overpass BrO VCD values were determined for the three sensors GOME-2B and GOME-2C and TROPOMI. VCD values were determined as average values over an area with a radius of 150 km from the station.

The actual comparison of the BrO VCD values for the three instruments is depicted in



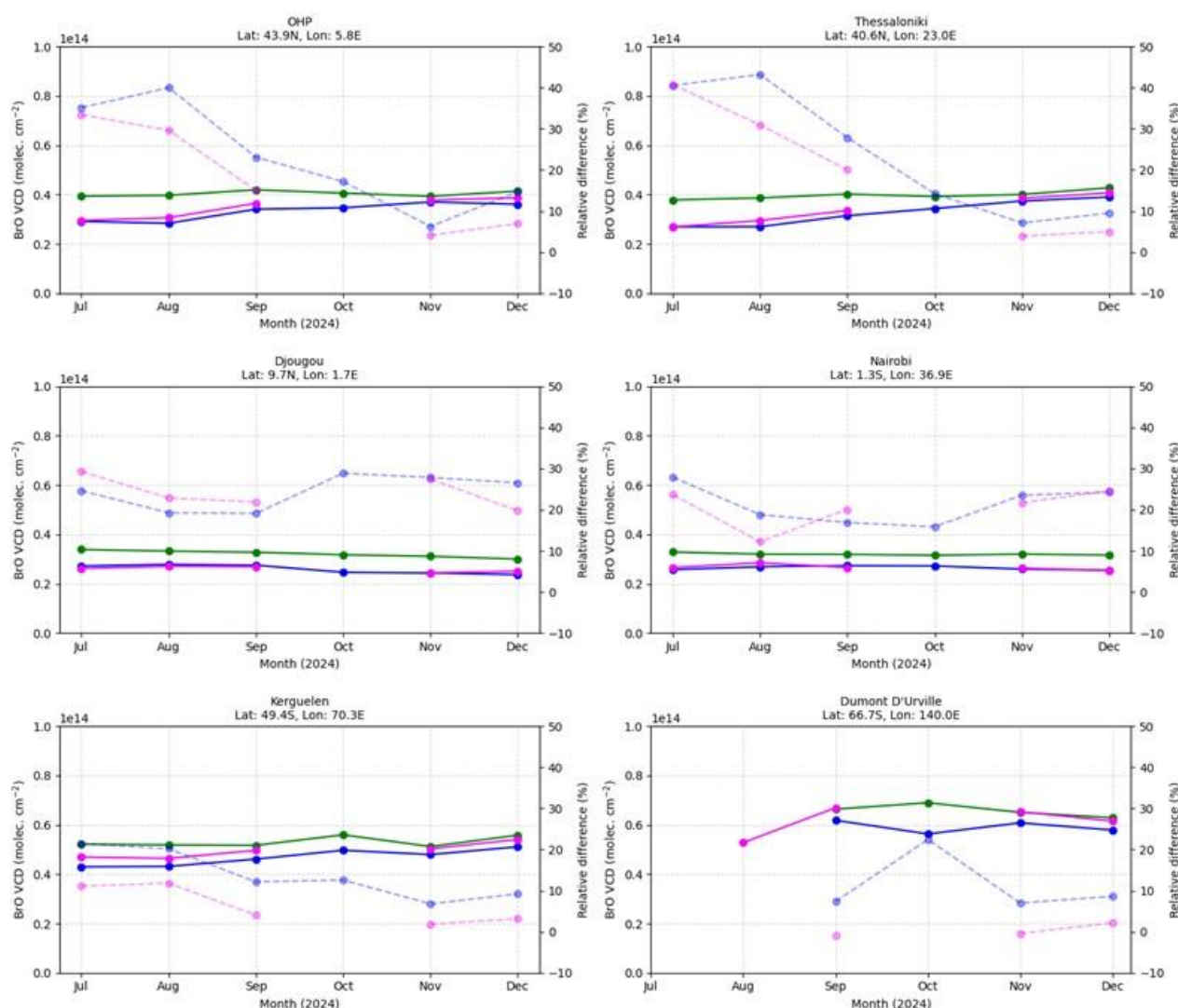


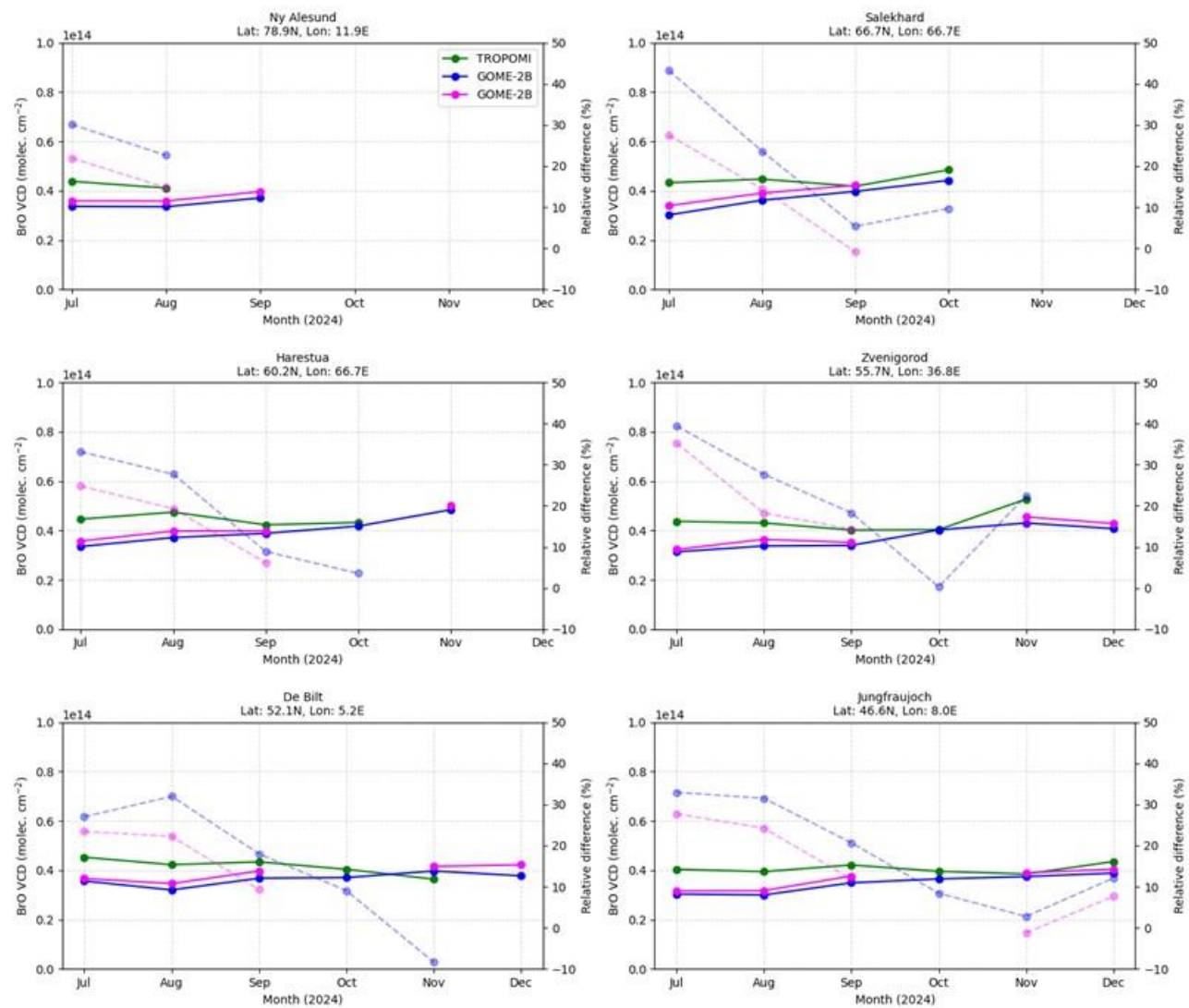
Figure 7.12.

Overall, the two GOME-2 instruments closely agree with each other. Although not always, the TROPOMI VCD values tend to be higher than the GOME-2 results. The results from the three instruments agree well, however, when it comes to the variation over the year.

The origin of the negative offset of the GOME-2 values with respect to TROPOMI is not clear, but may be due to simplified air-mass-factor treatment in the TROPOMI data. Comparisons of TROPOMI values with Harestua ground measurements for 2019 show a very good agreement (Van Gent and Hendrick, 2022). This agrees with the observed lower values for the GOME-2 instruments with respect to Harestua measurements, as shown in earlier editions of this report (see the results for 2022 below).

Unfortunately, the TROPOMI monthly-averaged data obtained from S5P-PAL seems to show more missing data points than when calculating those values manually. This is quite likely due to the fact that the S5P-PAL data is filtered for qa value > 0.5 , which, for example, eliminates pixels with large cloud cover or large solar angles. The data suffice, however for the intend of the comparison.

Overall, the deviation of the GOME-2 VCD's with respect to TROPOMI remains within the requirements of 30 %, although somewhat larger deviations are occasionally observed for GOME-2B in particular.



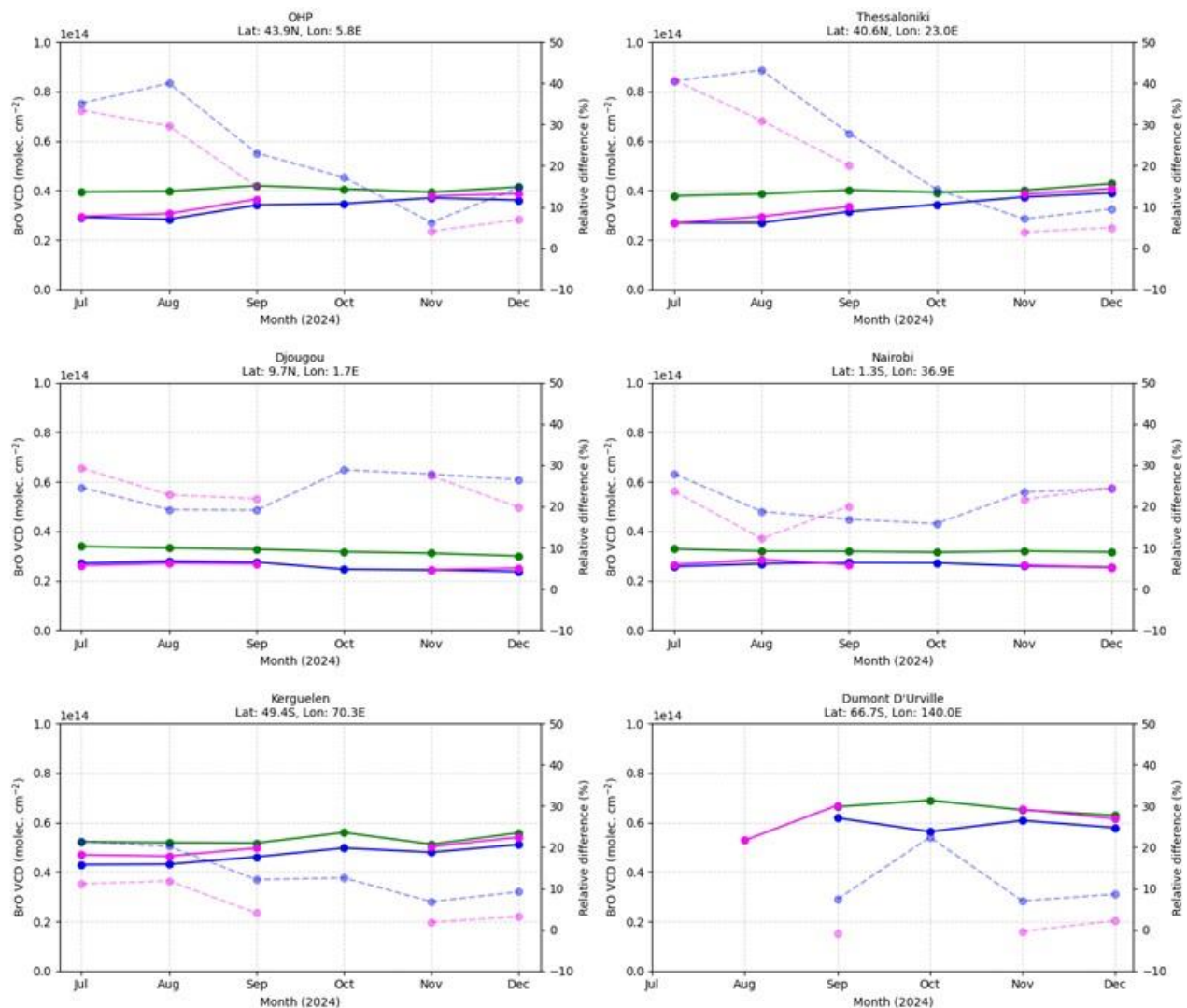


Figure 7.12. Comparison of monthly average total BrO VCD over 12 ground stations for the sensors GOME-2 B/C and TROPOMI, from July 2024 to end of 2024. Solid lines indicate absolute VCD values; the solid lines display the relative differences of the TROPOMI VCD and that of the GOME-2 instruments.

Below we repeat the results of the comparison of the GOME-2 VCDs with those from Harestua ground measurements of the Operations Report 1/2022.

The sensitivity of these measurements to the troposphere is increased by using a fixed reference spectrum corresponding to clear-sky noon summer conditions for the spectral analysis. In order to ensure the photochemical matching between satellite and ground-based observations, sunrise ground-based columns have been photochemically converted to the satellite overpass SZAs using a stacked box photochemical model (Hendrick *et al.*, 2007 and 2008).

Comparison results (150 km overpasses) for GOME-2B and GOME-2C are shown in Figure 7.13 and Figure 7.14, respectively.

Mean biases values between GOME-2B/C and ground-based data are of -15 ± 11 % and -9 ± 10 %. GOME-2B/C BrO columns are thus all within the target accuracy of 30 % and also within the optimal accuracy of 15 %, except GOME-2B which is slightly above the required optimal accuracy threshold.

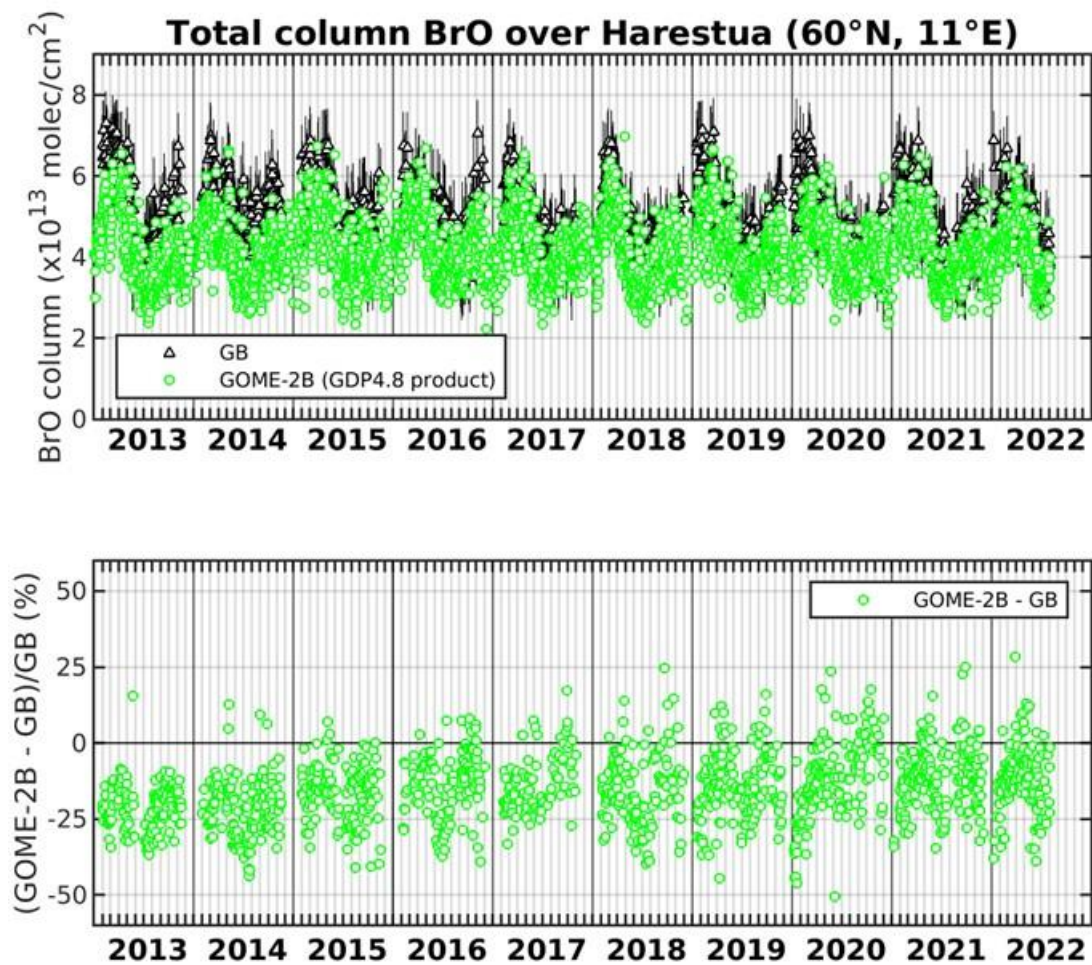


Figure 7.13. Comparison between GOME-2B GDP-4.8 and ground-based total BrO columns at Harestua (60°N, 11°E). The relative differences appear in the lower plot.

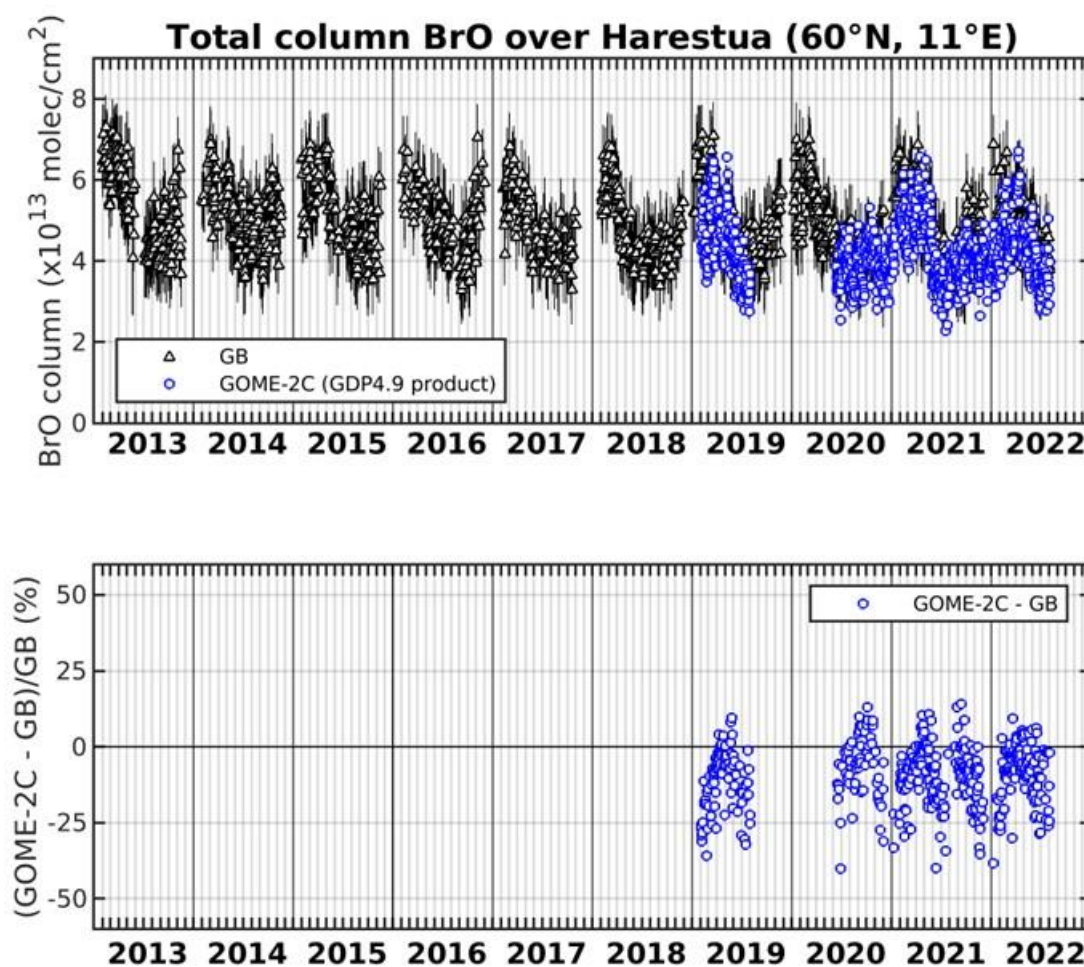


Figure 7.14. Comparison between GOME-2C GDP-4.9 and ground-based total BrO columns at Harestua (60°N, 11°E). The relative differences appear in the lower plot.

Status of GOME-2B and GOME-2C SO₂

GOME-2 SO₂ GDP-4.8 continues to be used for the near-real-time observation of volcanic activity within the SACS service. The Support to Aviation Control Service (SACS) hosted by the Royal Belgian Institute for Space Aeronomy (BIRA-IASB) aims at supporting the Volcanic Ash Advisory Centers, like Toulouse VAAC and London VAAC. This is achieved by delivering near real-time data of SO₂ and aerosols derived from satellite measurements regarding volcanic emissions by UV-VIS (OMI, GOME-2A and GOME-2B composite until 31 March 2021 and GOME-2B and GOME-2C composite since then, OMPS, TROPOMI) and infrared (AIRS, IASI-A, IASI-B) instruments. In case of volcanic eruptions, notifications are sent out by email to interested parties. The SACS notification archive service gathers all the notifications; the results can be found [here](#).

In the second half of 2024, SACS reported a moderate level of volcanic activity throughout, with only two medium-strength events of more than 20 DU in SO₂ load as shown in Figure 7.15. GOME-2B issued 130 alerts, with SO₂ loads ranging between 2 and 24.5 DU, with a mean global level of 5.33 ± 3.65 DU and median 4.45 DU. GOME-2C issued 128 alerts, with SO₂ loads ranging between 2 – 21.7 DU, with a mean global level of 5.43 ± 3.44 DU and median of 4.55 DU.

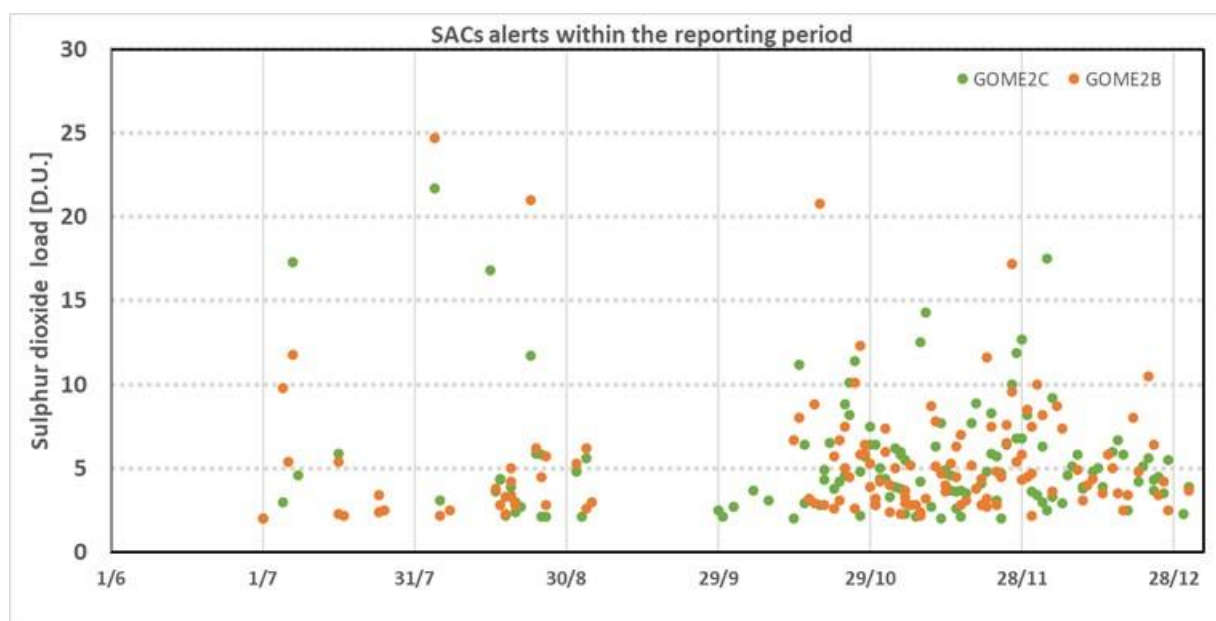
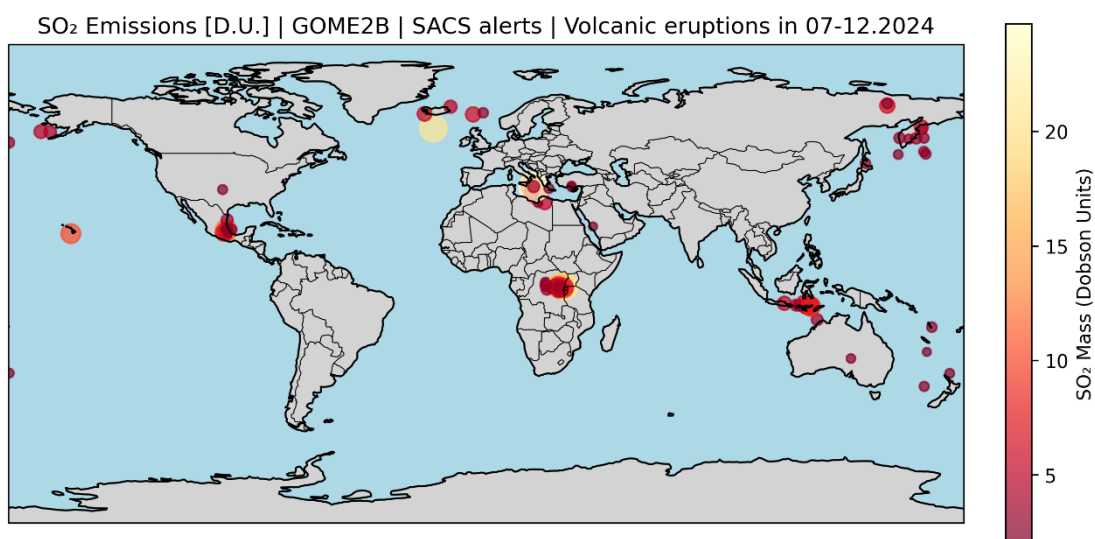


Figure 7.15. GOME-2B [orange] and GOME-2C [green] SO₂ load SACS alerts during the reporting period as a timeseries.

Dukono, a remote volcano on Indonesia's Halmahera Island, has been erupting continuously since 1933, with frequent ash explosions and sulphur dioxide plumes. The highest reported plume of the period reached 9.4 km above the summit on 14 November 2022. The Pusat Vulkanologi dan Mitigasi Bencana Geologi (PVMBG; also known as Indonesian Center for Volcanology and Geological Hazard Mitigation, CVGHM) reported that the eruption at Dukono was ongoing during the week of 17 to 23 April 2024. Gray-and-white ash plumes rose 100 – 1200 m above the summit and drifted E, N, and W almost daily. The Alert Level remained at Level 2 (on a scale of 1 – 4), and the public was warned to remain outside of the 3-km exclusion zone. In Figure 7.17 the Mt. Dukono eruptive days of April 18th and April 19th, 2024, are presented. The GOME2-B/C combined product appears to capture the event very well, both in terms of sulphur dioxide load and location of the volcanic SO₂ plume.



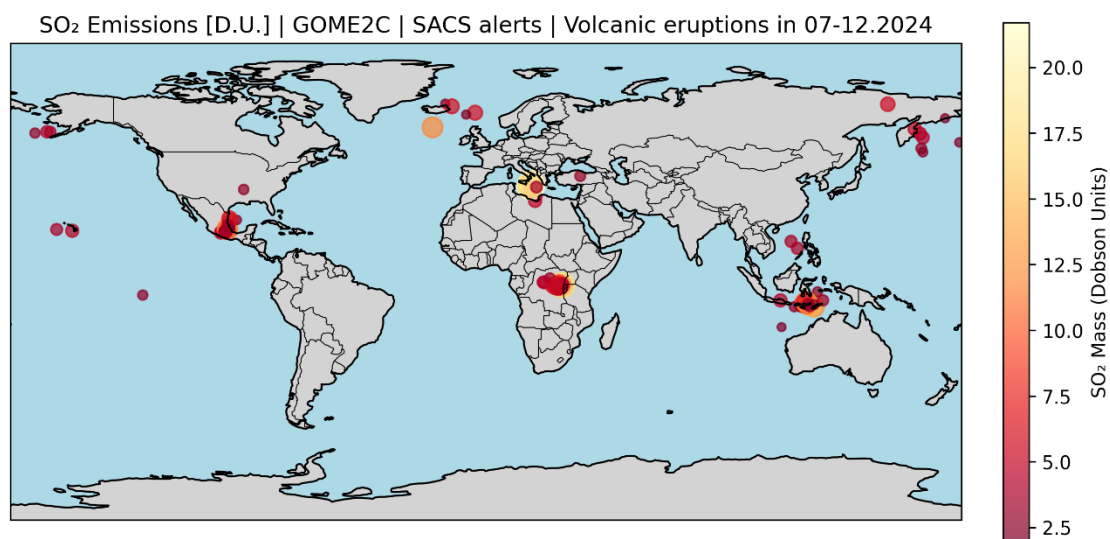


Figure 7.16. GOME-2B [upper] and GOME-2C [lower] SO₂ load SACS alerts during the reporting period. The size of the markers follows the SO₂ load reported.

During the reporting period, the main eruptions/eruptive periods identified by the GOME-2B/2C observations are shown in Figure 7.16, coloured and sized according to the magnitude of the SO₂ load sensed by each instrument. Two eruptions are noteworthy:

Mount Etna, Italy | Eruption Date: August 4, 2024 | See Figure 7.17

Mount Etna produced a vigorous explosive eruption, sending a volcanic plume approximately 5,500 meters above the summit. The eruption triggered lava fountains, ashfall across eastern Sicily, and temporary [airport closures in Catania](#). Sulfur dioxide emissions spiked to over 15,000 tons per day during the peak of activity, the highest levels observed at Etna since 2015. The SO₂ plume was observed drifting southeast across the Mediterranean, [reaching as far as Greece](#). The eruption disrupted daily life for tens of thousands and caused localized damage to crops and infrastructure. ([Etna, 2024 Mount Etna eruption](#)).

Sundhnúksígígar, Iceland | Eruption Date: August 22, 2024 | See Figure 7.18

The sixth eruption in the ongoing Sundhnúksígígar series commenced on August 22, 2024, at approximately 21:25 UTC, following a significant earthquake swarm. The eruption released an estimated 61 million cubic meters of lava, covering 15.8 km² and causing 40 cm of land subsidence. The Copernicus Atmosphere Monitoring Service (CAMS) tracked the SO₂ plume as it moved [southeast across the North Atlantic](#), reaching [northwestern Europe](#) by August 24. Satellite observations indicated that the highest concentrations of SO₂ were between 5–8 km in the atmosphere. In Iceland, elevated levels of fine particulate matter and SO₂ were detected in the capital area, leading to warnings about volcanic smog and gas pollution. The public [was advised to limit outdoor activities](#), especially for individuals with respiratory sensitivities and children. The [SO₂ plume reached as far as Edinburgh](#), Scotland, where an unprecedented increase in SO₂ levels was recorded. Measurements indicated 1,161 µg/m³ of SO₂ in the air, significantly higher than typical levels of about 0.5 µg/m³.

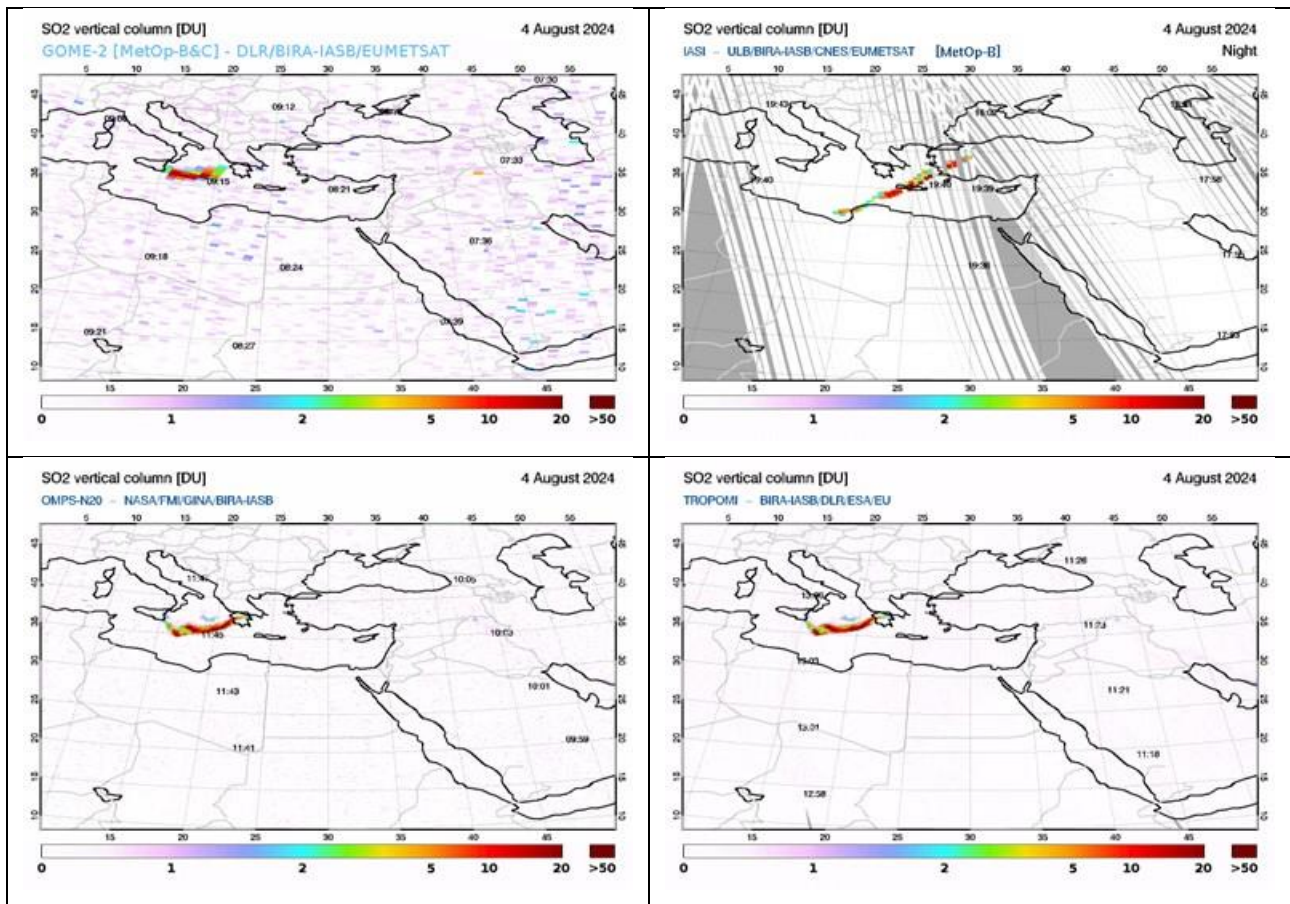
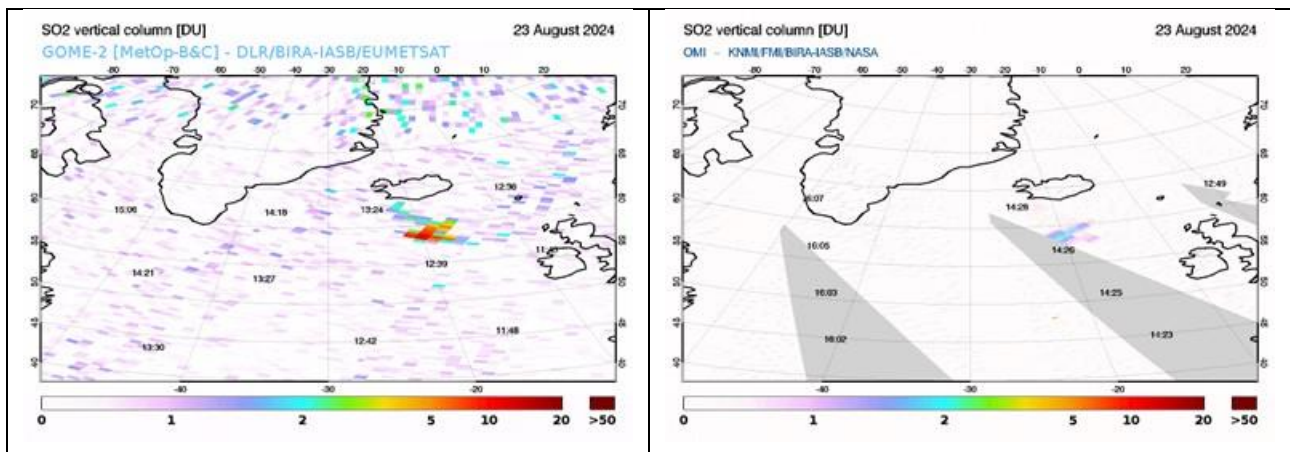


Figure 7.17. Mt. Etna, Italy eruption, on the 4th of August 2024, sensed by GOME2-B/C [upper left], IASI/Metop-B [upper right], OMPS/NPP [bottom left] and S5P/TROPOMI [bottom right] from the [SACS](#) monitoring pages.



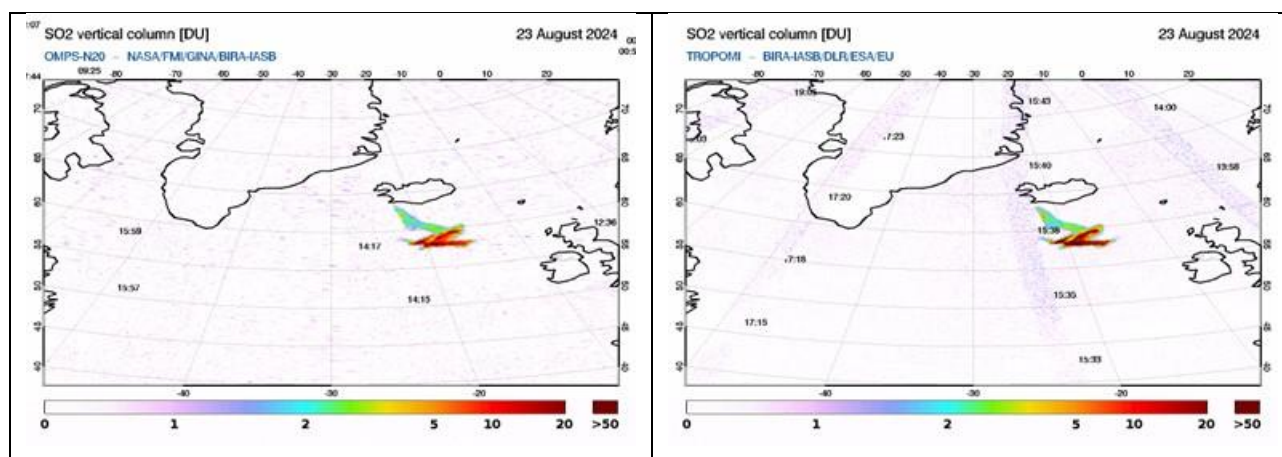


Figure 7.18. Sundhnúkur, Island, eruption, on the 23th of August 2024, sensed by GOME2-B/C [upper left], OMI/Aura [upper right], OMPS/NPP [bottom left] and S5P/TROPOMI [bottom right] from the [SACS](#) monitoring pages.

The coherence of the GOME-2B/C measurements with the other morning instruments (Figure 7.17) is clear, as is the temporal evolution with the afternoon platform instruments (Figure 7.18).

References:

Clémer, K., Van Roozendaal, M., Fayt, C., Hendrick, F., Hermans, C., Pinardi, G., Spurr, R., Wang, P., and De Mazière, M.: Multiple wavelength retrieval of tropospheric aerosol optical properties from MAXDOAS measurements in Beijing, *Atmos. Meas. Tech.*, 3, 863-878, 2010.
<https://doi.org/10.5194/amt-3-863-2010>

De Smedt, I., Stavrakou, T., Hendrick, F., Danckaert, T., Vlemmix, T., Pinardi, G., Theys, N., Lerot, C., Gielen, C., Vigouroux, C., Hermans, C., Fayt, C., Veeckind, P., Müller, J.-F., and Van Roozendaal, M.: Diurnal, seasonal and long-term variations of global formaldehyde columns inferred from combined OMI and GOME-2 observations, *Atmos. Chem. Phys.*, 15, 12519-12545, 2015.
<https://doi.org/10.5194/acp-15-12519-2015>

De Smedt, I., Pinardi, G., Vigouroux, C., Compernelle, S., Bais, A., Benavent, N., Boersma, F., Chan, K.-L., Donner, S., Eichmann, K.-U., Hedelt, P., Hendrick, F., Irie, H., Kumar, V., Lambert, J.-C., Langerock, B., Lerot, C., Liu, C., Loyola, D., Piders, A., Richter, A., Rivera Cárdenas, C., Romahn, F., Ryan, R. G., Sinha, V., Theys, N., Vlietinck, J., Wagner, T., Wang, T., Yu, H., and Van Roozendaal, M.: Comparative assessment of TROPOMI and OMI formaldehyde observations and validation against MAX-DOAS network column measurements, *Atmos. Chem. Phys.*, 21, 12561–12593, 2021.
<https://doi.org/10.5194/acp-21-12561-2021>

Gielen, C., Van Roozendaal, M., Hendrick, F., Pinardi, G., Vlemmix, T., De Bock, V., De Backer, H., Fayt, C., Hermans, C., Gillotay, D., and Wang, P.: A simple and versatile cloud-screening method for MAX-DOAS retrievals, *Atmos. Meas. Tech.*, 7, 3509–3527, 2014.
<https://doi.org/10.5194/amt-7-3509-2014>

Hendrick, F.M., Van Roozendaal, M., Chipperfield, M.P., Dorf, M., Goutail, F., Yang, X., Fayt, C., Hermans, C., Pfeilsticker, K., Pommereau, J.-P., Pyle, J.A., Theys, N., and De Mazière, M.: Retrieval of stratospheric and tropospheric BrO profiles and columns using ground-based zenith-sky DOAS observations at Harestua, 60° N., *Atmos. Chem. Phys.*, 7, 4869-4885, 2007.
<https://doi.org/10.5194/acp-7-4869-2007>

Hendrick, F., Johnston, P.V., De Mazière, M., Fayt, C., Hermans, C., Kreher, K., Theys, N., Thomas, A., and Van Roozendael, M.: One-decade trend analysis of stratospheric BrO over Harestua (60°N) and Lauder (45°S) reveals a decline, *Geophys. Res. Letters*, 35, L14801, 2008.
<https://doi.org/10.1029/2008gl034154>

Hendrick, F., Müller, J.-F., Clémer, K., Wang, P., De Mazière, M., Fayt, C., Gielen, C., Hermans, C., Ma, J.Z., Pinardi, G., Stavrakou, T., Vlemmix, T., and Van Roozendael, M.: Four years of ground-based MAX-DOAS observations of HONO and NO₂ in the Beijing area, *Atmos. Chem. Phys.*, 14, 765–781, 2014.
<https://doi.org/10.5194/acp-14-765-2014>

Pinardi, G., Van Roozendael, M., Lambert, J.-C., Granville, J., Hendrick, F., Tack, F., Yu, H., Cede, A., Kanaya, Y., Irie, I., Goutail, F., Pommereau, J.-P., Pazmino, A., Wittrock, F., Richter, A., Wagner, T., Gu, M., Remmers, J., Friess, U., Vlemmix, T., Pitters, A., Hao, N., Tiefengraber, M., Herman, J., Abuhassan, N., Bais, A., Kouremeti, N., Hovila, J., Holla, R., Chong, J., Postlyakov, O., Ma, J.: GOME-2 total and tropospheric NO₂ validation based on zenith-sky, direct-sun and multi-axis DOAS network observations, *Proceeding of the EUMETSAT conference*, 22-26 September 2014, Geneva, Switzerland.

Pinardi, G., Van Roozendael, M., Hendrick, F., Theys, N., Abuhassan, N., Bais, A., Boersma, F., Cede, A., Chong, J., Donner, S., Drosoglou, T., Frieß, U., Granville, J., Herman, J. R., Eskes, H., Holla, R., Hovila, J., Irie, H., Kanaya, Y., Karagkiozidis, D., Kouremeti, N., Lambert, J.-C., Ma, J., Peters, E., Pitters, A., Postlyakov, O., Richter, A., Remmers, J., Takashima, H., Tiefengraber, M., Valks, P., Vlemmix, T., Wagner, T., and Wittrock, F.: Validation of tropospheric NO₂ column measurements of GOME-2A and OMI using MAX-DOAS and direct sun network observations, *Atmos. Meas. Tech.*, 13, 6141-6174, 2020.
<https://doi.org/10.5194/amt-13-6141-2020>

Richter, A., Behrens, L., Hilboll, A., Munassar, S., Burrows, J.P., Pinardi, G., and Van Roozendael, M.: Cloud effects on satellite retrievals of tropospheric NO₂ over China, oral presentation at the DOAS workshop, September 2017, Yokohama, Japan.

Theys, N., De Smedt, I., Yu, H., Danckaert, T., van Gent, J., Hörmann, C., Wagner, T., Hedelt, P., Bauer, H., Romahn, F., Pedernana, M., Loyola, D., and Van Roozendael, M.: Sulfur dioxide retrievals from TROPOMI onboard Sentinel-5 Precursor: algorithm theoretical basis, *Atmos. Meas. Tech.*, 10, 119-153, 2017.
<https://doi.org/10.5194/amt-10-119-2017>

Van Gent, J. and Hendrick, F.: S5P/TROPOMI total BrO algorithm TCBRO: Validation report, issue: 1.0.0, date: 09/01/2022, https://data-portal.s5p-pal.com/product-docs/bro/S5P-L2-BIRA-VR_TCBRO_1.0.0_20220110.pdf

Verhoelst, T., Compernelle, S., Pinardi, G., Lambert, J.-C., Eskes, H. J., Eichmann, K.-U., Fjæraa, A. M., Granville, J., Niemeijer, S., Cede, A., Tiefengraber, M., Hendrick, F., Pazmiño, A., Bais, A., Bazureau, A., Boersma, K. F., Bogner, K., Dehn, A., Donner, S., Elokhov, A., Gebetsberger, M., Goutail, F., Grutter de la Mora, M., Gruzdev, A., Gratsea, M., Hansen, G. H., Irie, H., Jepsen, N., Kanaya, Y., Karagkiozidis, D., Kivi, R., Kreher, K., Levelt, P. F., Liu, C., Müller, M., Navarro Comas, M., Pitters, A. J. M., Pommereau, J.-P., Portafaix, T., Prados-Roman, C., Puentedura, O., Querel, R., Remmers, J., Richter, A., Rimmer, J., Rivera Cárdenas, C., Saavedra de Miguel, L., Sinyakov, V. P., Stremme, W., Strong, K., Van Roozendael, M., Veefkind, J. P., Wagner, T., Wittrock, F., Yela González, M., and Zehner, C.: Ground-based validation of the Copernicus Sentinel-5P TROPOMI NO₂ measurements with the NDACC ZSL-DOAS, MAX-DOAS and Pandonia global networks, *Atmos. Meas. Tech.*, 14, 481–510, 2021.

<https://doi.org/10.5194/amt-14-481-2021>

Vlemmix, T., Hendrick, F., Pinardi, G., Smedt, I., Fayt, C., Hermans, C., Piter, A., Wang, P., Levelt, P., and Van Roozendaal, M.: MAX-DOAS observations of aerosols, formaldehyde and nitrogen dioxide in the Beijing area: comparison of two profile retrieval approaches, *Atmos. Meas. Tech.*, 2, 941–963, 2015.

<https://doi.org/10.5194/amt-8-941-2015>

Wang, T., Hendrick, F., Wang, P., Tang, G., Cl  mer, K., Yu, H., Fayt, C., Hermans, C., Gielen, C., M  ller, J.-F., Pinardi, G., Theys, N., Brenot, H., and Van Roozendaal, M.: Evaluation of tropospheric SO₂ retrieved from MAX-DOAS measurements in Xianghe, China, *Atmos. Chem. Phys.*, 14(20), 11149–11164, 2014.

<https://doi.org/10.5194/acp-14-11149-2014>

7.3.1. Online quality monitoring

Online quality monitoring plots are continuously generated at DLR and published for O₃, NO₂, BrO, HCHO, SO₂, H₂O products as described in Section 7.1.3.

BIRA-IASB provides quality assessment (QA) pages for vertical column amounts of NO₂, HCHO, BrO and SO₂ derived from GOME-2B and GOME-2C. The goal is to provide an easy tool to quickly spot anomalies and trends in the L2 data, by selecting and examining geographical regions of interest. These pages are available under <https://cdop.aeronomie.be/quality-assessment/>.

The monitored L2 is provided by DLR with processor version GDP 4.8 for GOME-2B and GDP 4.9 for GOME-2C.

System developments:

- The GOME-2 monitoring page shows time-series for Metop-B and Metop-C. Metop-A data is kept internally for comparison reasons.
- The current monitoring system, based on data storage in an SQL database, remains slow in use. As mentioned in the previous report, a new system has been under development and has shown to be much faster.

Monitoring status:

SO₂

In the case of SO₂, the available geographical regions of interest are either locations with known outgassing volcanoes or locations with strong anthropogenic sources of SO₂. The resulting graphs show a history of monthly average values over the selected region.

In Figure 7.19 and Figure 7.20, two relevant panels are presented for the time period 01/01/2024 – 30/06/2024. In the upper panels, the SO₂ fitting RMS is shown, an important parameter which acts as immediate indicator to the stability of the instruments/algorithms. In the bottom panels, the total vertical SO₂ column is presented, alongside other metrics, explained in the figure caption. Both panels include smaller subpanels which show the long-term behaviour of each sensor from the beginning of the satellite mission.

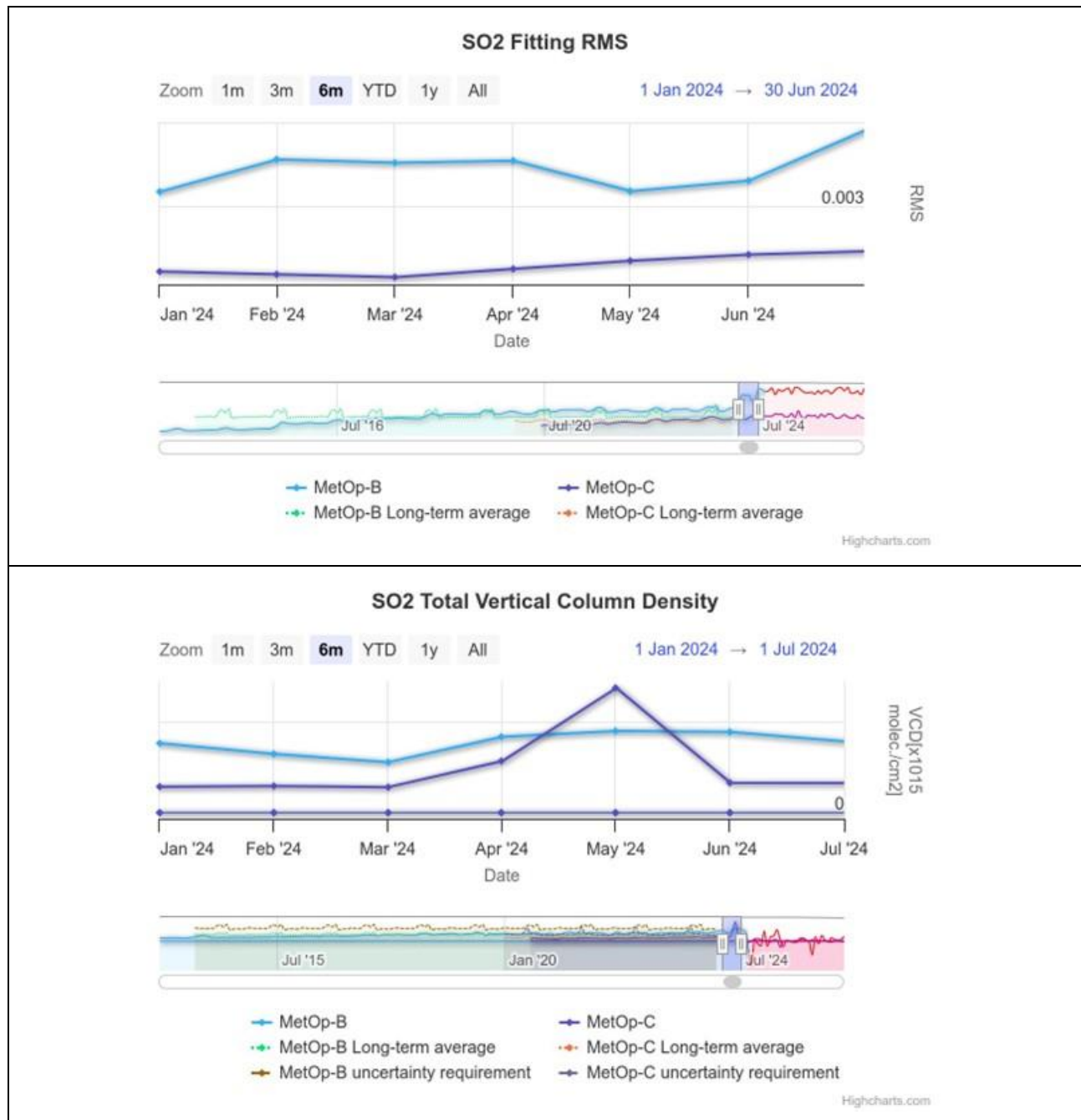


Figure 7.19. The behaviour of the GDP4.8 GOME-2B [blue curve] and GOME-2C [black curve] 6 km plume height SO₂ products between 01/01/2024 and 30/06/2024 over the region of Indonesian volcanoes. Upper panel, the SO₂ fitting RMS is shown and in the bottom panel, the total vertical SO₂ column. The equivalent long-term average is also provided [see insert legend].

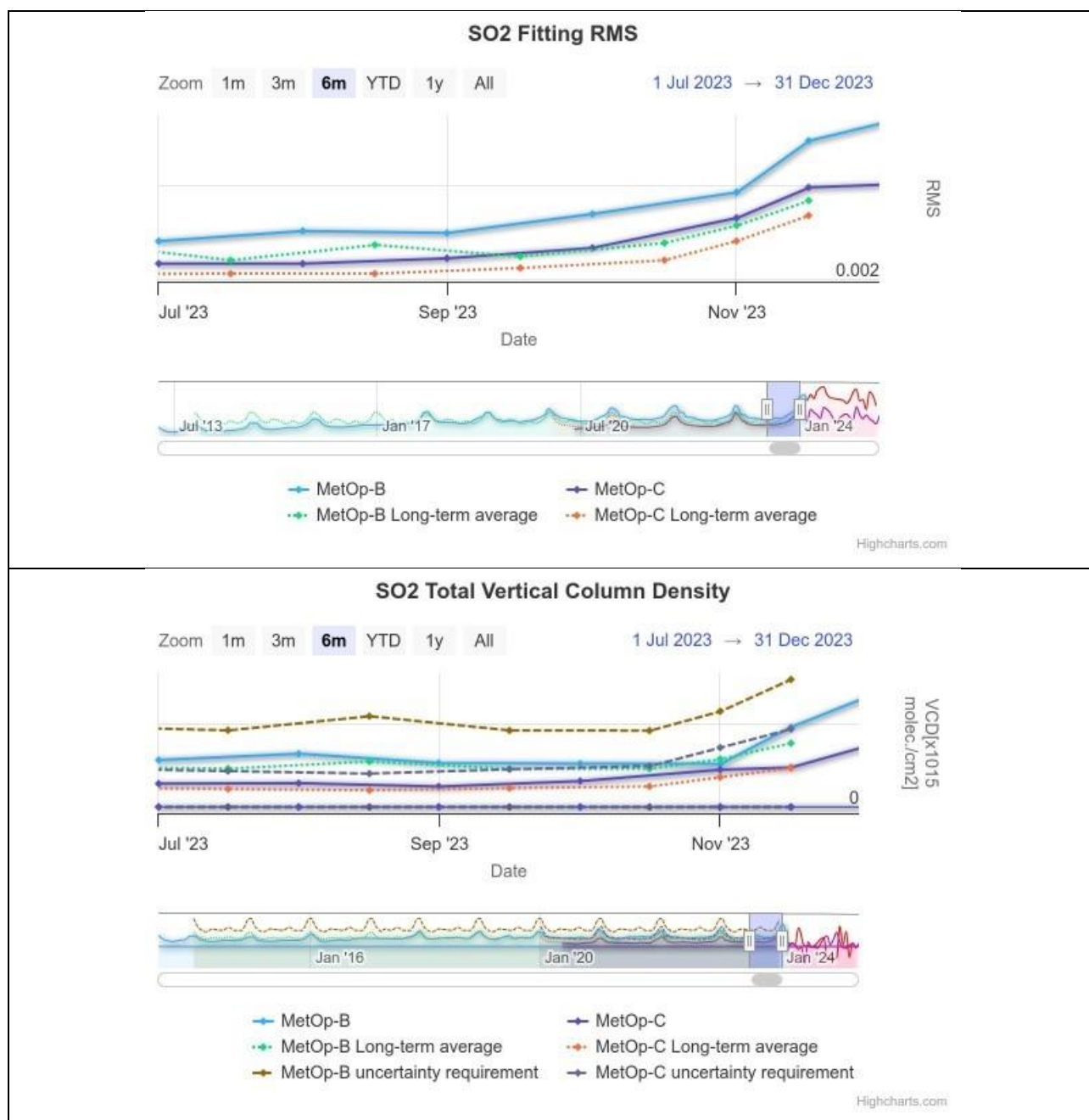


Figure 7.20. The behaviour of the GDP4.8 GOME-2B [blue curve] and GOME-2C [black curve] 6 km plume height SO₂ products between 01/07/2023 and 31/12/2023 over Indonesia. Upper panel, the SO₂ fitting RMS is shown and in the bottom panel, the total vertical SO₂ column. The equivalent long-term average is also provided [see insert legend].

From Figure 7.19 and Figure 7.20, upper panels, no spurious jumps or artefacts are observed during 2024 for either the anthropogenic or the volcanic locations in the SO₂ fitting RMS. However, not only it is said that RMS is ~20 – 25 % larger for GOME-2B than GOME-2C, but it is also equally larger from its long-term average. This points to a possible degradation effect in the GOME-2B L1b data which also affects the L2 data, as shown in Figure 7.19 and Figure 7.20, lower panels. GOME-2B has provided far larger (more than 50 %) SO₂ columnar estimates than GOME-2C and ~20 – 25 % larger than the long-term average.

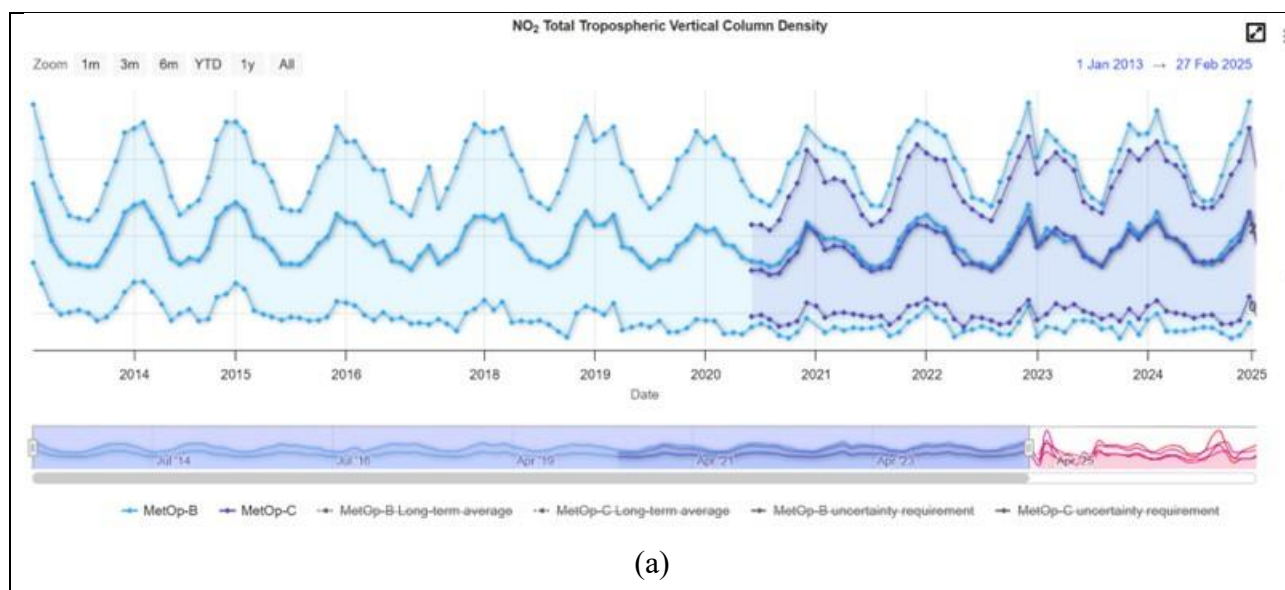
Both these issues are cause for concern and merit further investigation from the DLR L2 algorithm team. Currently, GOME-2 SO₂ retrieval uses a one fit-window approach with an improved fit-window for GOME-2C (which cannot be applied to GOME-2B due to L1b data degradation effects).

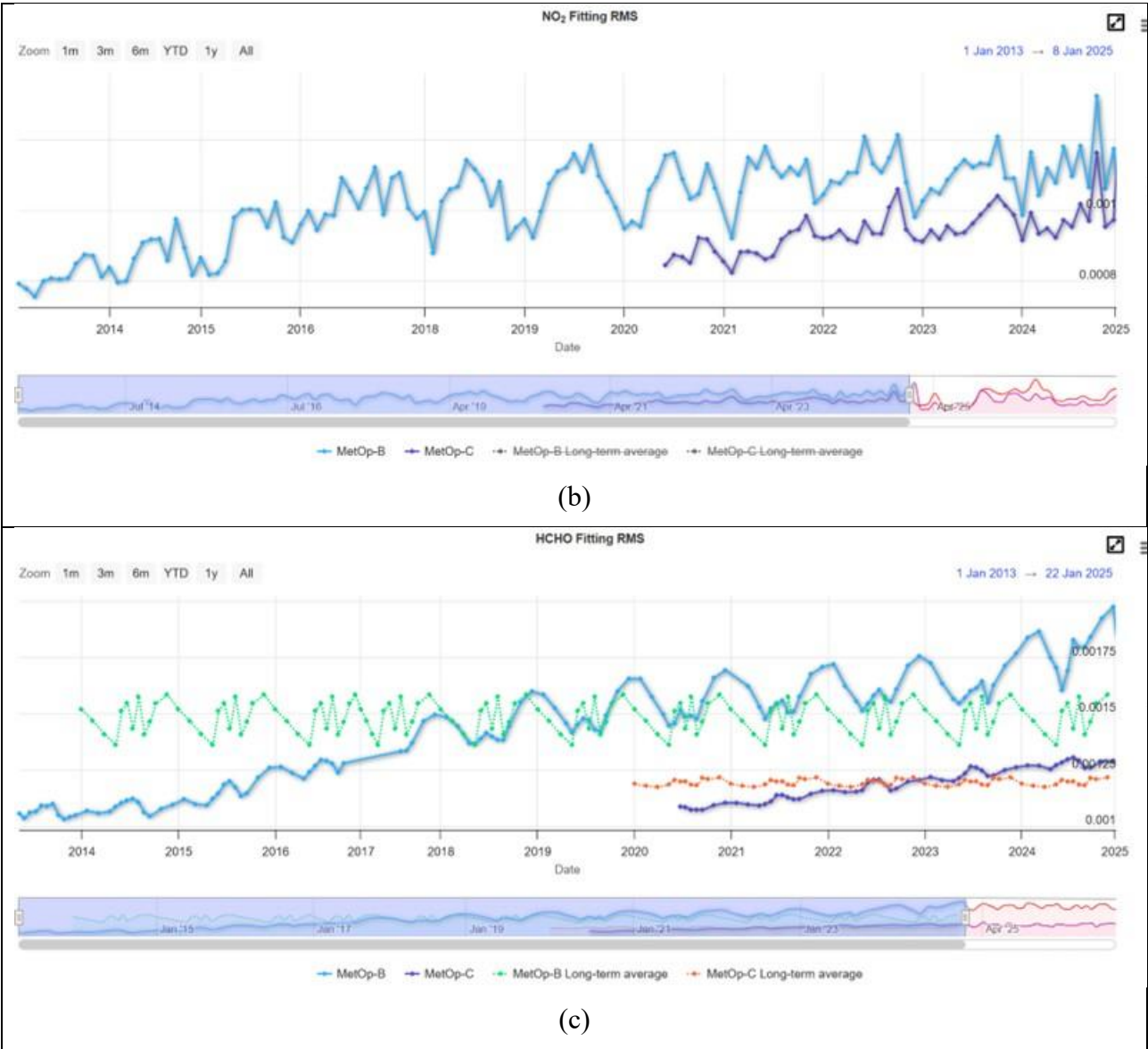
The overall quality of GOME-2B and GOME-2C SO₂ products can be improved with a 3-fit window retrieval approach (as for TROPOMI SO₂ retrieval), which is planned in the CDOP 4 for the NRT/offline products, as well as for the reprocessing.

NO₂, HCHO, and BrO

When observing the full time-series for the other monitored gases, column amounts between the two instruments agree quite well. Some examples are depicted in Figure 7.21. For NO₂, the tropospheric column amounts of both sensors show the expected annual cycle and show no systematic mutual offset (panel a, situation over the South-East US). Indications of instrumental degradation are visible in the fit residual (RMS, panel b) of both instruments. On the other hand, the raise of GOME-2B RMS seems to have flatten out over the last few years. Similar RMS patterns are observed over other geographical regions (not shown here).

Consistent patterns of total column amounts are also observed for HCHO (panel c, Indonesia). There, however, the increase of the RMS signal for GOME-2B continues also in recent years; For BrO (panel d), a flattening of the RMS-increase is also visible, be it less pronounced than for NO₂. and depending on the observed region.





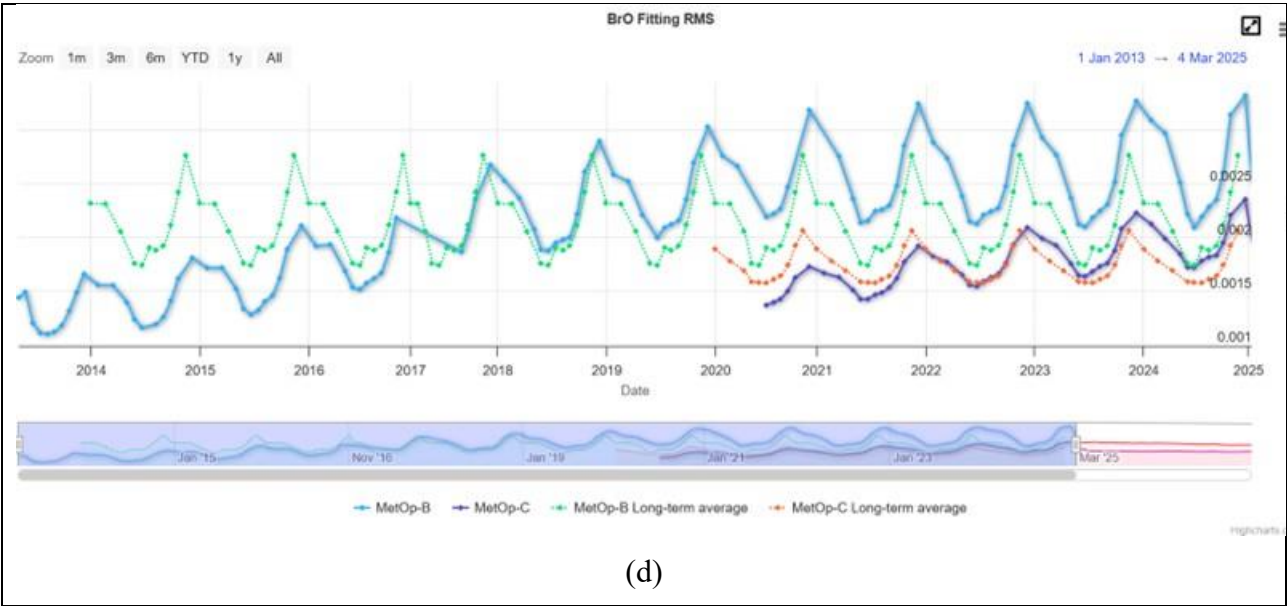


Figure 7.21. Examples of time-series from the QA monitoring page: a) NO₂ tropospheric column (plus uncertainty range) over the Southeastern US, b) NO₂ fitting RMS over S. E. US, c) HCHO fitting RMS over Indonesia, and d) Fitting RMS for BrO, averaged over the 60°-90° Arctic latitude band.

7.4. GOME-2 ozone profile products

Table 7.13. Validation status of ozone profile products

Product Identifier	Product Name	Accuracy	Reference	Validating Institute	Correlative data sources
O3M-47.1	NRT high-resolution ozone profile	Fulfil threshold accuracy requirements	RD7	KMI DWD	Ozonesonde data from SHADOZ , NDACC , NILU and WOUDC Lidar/microwave data from NDACC
O3M-311			RD22		
O3M-39	Offline high-resolution ozone profile	Fulfil threshold accuracy requirements	RD6	KMI DWD	Ozonesonde data from SHADOZ , NDACC , NILU and WOUDC Lidar/microwave data from NDACC
O3M-48			RD7		
O3M-312			RD22		

Validation results can be found in more detail on the at [AC SAF validation & quality assessment website](#).

Validation activities summary:

This summary contains validation results for the GOME-2B and GOME-2C high-resolution (HR) ozone profile products, retrieved by the Ozone Profile Retrieval Algorithm (OPERA) at KNMI. This validation section focuses on the time period January 2024 – December 2024.

The authors of this summary are Dr. Andy Delcloo from KMI and Dr. Peggy Achtert from DWD. More information on how these values are extracted is available in the [validation report](#).

There is no material difference in the content of the NRT vs. the offline vertical ozone profile data product, other than its size. The offline file is a concatenation of the NRT L2 PDUs for a particular orbit. While the validation partners are provided the L2 PDUs that were sent out in NRT for their validation, it makes no difference for the validation itself.

To report the skill scores of GOME-2 ozone profile products in a more condensed way, the statistics for the different output levels of GOME-2 are reduced to two layers: Lower Stratosphere (until an altitude of 30 km) and Upper Stratosphere (up to an altitude of 50 km).

The validation for the lower stratosphere is made with ozonesonde data, for the upper stratosphere with lidar, FTIR and/or microwave data. The stations used in this validation for the FTIR/lidar/microwave data are the Network for the Detection of Atmospheric Composition Change (NDACC) stations of Bern (microwave), Payerne (microwave), Hohenpeissenberg (lidar), Table Mountain (lidar), and Lauder (FTIR, lidar).

The collocation data used for the validation using ozonesonde data are shown in Figure 7.22.

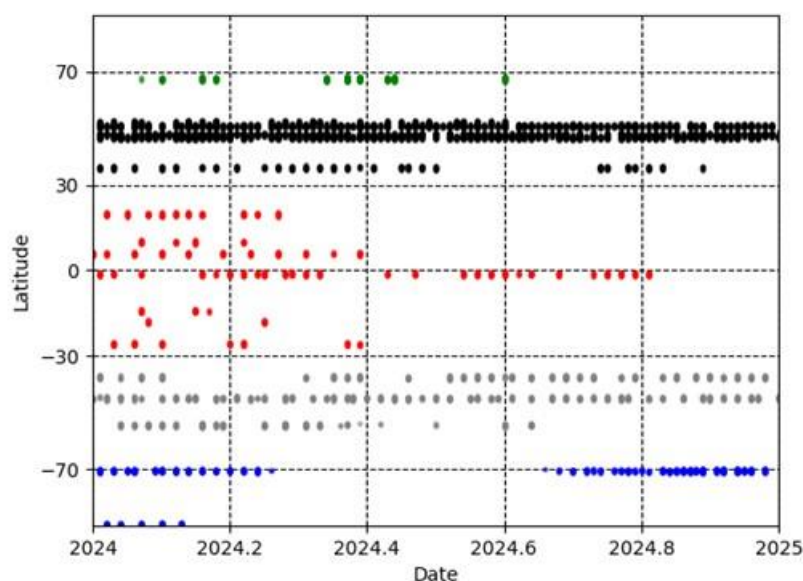


Figure 7.22. Collocation data for the validation with ozonesonde data for the time period January – December 2024.

Table 7.14 shows an overview of the obtained results for the time period January 2024 – December 2024 only for the lower and the higher stratosphere, not taking into account the tropospheric ozone column products since a dedicated product is discussed earlier in this report. The statistics for the lower stratosphere are obtained by KMI, the statistics for the higher stratosphere by DWD.

Table 7.14. Absolute Differences (AD), Relative Differences (RD) and standard deviation (STDEV) are shown on the accuracy of GOME-2B/C HR ozone profile products for the lower and the higher stratosphere for five different latitude belts for the time period January – December 2024.

GOME-2B HR						
	Lower Stratosphere			Upper Stratosphere		
	AD	RD	STDEV	AD	RD	STDEV
	(DU)	(%)	(%)	(DU)	(%)	(%)
Northern Polar Region	1.92	1.4	9.9			
Northern Mid-Latitudes	2.08	2.0	11.3	-5.8	-8.6	3.3
Tropical Region	0.96	4.8	5.7			
Southern Mid-Latitudes	1.85	7.0	12.2	-5.9	-11.3	6.6
Southern Polar Region	4.35	14.2	57.3	-	-	-

GOME-2C HR						
	Lower Stratosphere			Upper Stratosphere		
	AD	RD	STDEV	AD	RD	STDEV
	(DU)	(%)	(%)	(DU)	(%)	(%)
Northern Polar Region	1.82	0.7	9.1			
Northern Mid-Latitudes	1.51	2.7	8.9	-3.4	-4.6	6.9
Tropical Region	1.00	7.2	8.3			
Southern Mid-Latitudes	1.77	7.2	11.8	-4.4	-9.3	4.8
Southern Polar Region	2.98	8.1	41.6	-	-	-

The target value (15 % accuracy) is met in both lower and upper stratosphere for all belts under consideration for Metop-B and Metop-C, except for the Southern Polar Region. The discrepancy is highest at high latitudes. The observed differences between the GOME -2 and the ground-based observations are smaller for Metop-C compared to Metop-B.

More detailed ozone profile validation results can also be found on the AC SAF [ozone profile validation website](#).

7.4.1. Online quality monitoring

Timeline of the vertically integrated Metop-B ozone profile with respect to time is presented in Figure 7.23.

More information and images at the following web addresses

<https://www.temis.nl/acsaf/timeseries.php?sat=metopb>

<https://www.temis.nl/acsaf/timeseries.php?sat=metopc>

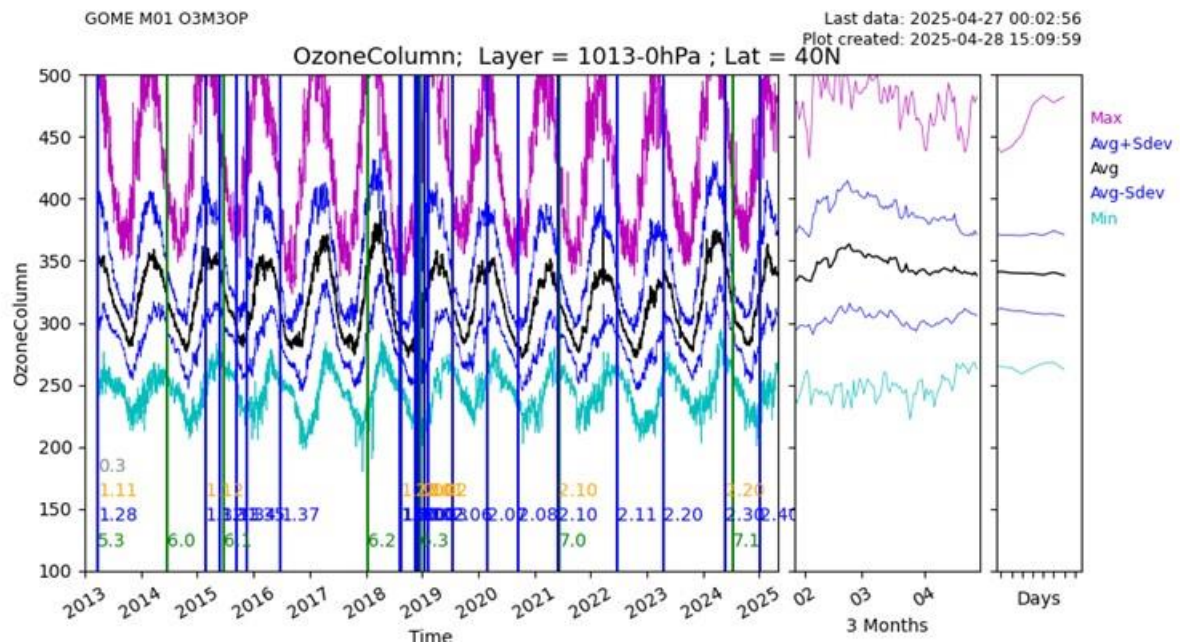


Figure 7.23. Timeline of vertically integrated Metop-B ozone profiles (=total ozone columns) and changes in data processor (vertical lines). The changes in late 2018 / early 2019, including the improved degradation correction, have resulted in much better ozone profiles and have also affected the total ozone columns shown here.

Legend of the coloured vertical lines:

- Green: PPF version
- Blue: Software version (PGE)
- Orange: Algorithm version
- Grey: Config version

7.5. GOME-2 aerosol products

Table 7.15. Validation status of aerosol products

Product Identifier	Product Name	Accuracy	Reference	Validating Institute	Correlative data sources	
O3M-78	NRT absorbing aerosol height	Fulfil threshold accuracy requirement	RD28	KMI, AUTH	CALIOP, EARLINET	
O3M-364						
O3M-72.1	NRT absorbing aerosol index from PMDs	Fulfil threshold accuracy requirement	RD13	KNMI	Comparisons with other satellite instruments: SCIAMACHY, OMI, and intercomparison of GOME-2A with GOME-2B	
O3M-362			RD29		Comparisons with the AAI products from GOME-2A and GOME-2B	
O3M-69	Offline absorbing aerosol height	Fulfil threshold accuracy requirements	RD28	KMI, AUTH	CALIOP, EARLINET	
O3M-79						
O3M-365						
O3M-63.1	Offline absorbing aerosol index from PMDs	Fulfil threshold accuracy requirements	RD13	KNMI	Comparisons with other satellite instruments: SCIAMACHY, OMI, and intercomparison of GOME-2A with GOME-2B	
O3M-73.1			RD29		Comparisons with the AAI products from GOME-2A and GOME-2B	
O3M-363						

Validation activities summary:

This summary contains validation results for the GOME-2A, GOME-2B and GOME-2C Absorbing Aerosol Height (AAH) products and is made available by the validation teams of AUTH and KMI. More information on how these values are extracted is available in the validation report [validation report](#).

AAH is a new operational AC SAF product for aerosol layer height detection, developed by KNMI within the AC SAF. It uses the AAI as an indicator to derive the actual height of the absorbing aerosol layer in the O₂-A band using the Fast Retrieval Scheme for Clouds from the Oxygen A band (FRESCO) algorithm (Wang *et al.*, 2012; Tilstra *et al.*, 2020). The AAH reported by GOME-2 onboard Metop-A, Metop-B and Metop-C, between 2007 and 2019, has been validated by AUTH against ground-based lidar data from the European Aerosol Research Lidar Network (EARLINET) database and by KMI against CALIOP aerosol layer height (De Bock, *et al.* 2020; Michailidis *et al.*, 2021).

AUTH results:

A wide choice of lidar stations (first column of Table 7.17) was made to examine the behaviour of the comparisons for different common aerosol loads around Europe. The geographical distribution

of the selected EARLINET stations depicted in Figure 7.24 indicates the domain of applicability of the validation results. All participating stations (red circles) operate high-performance multi-wavelength lidar systems. The list of stations, along with their identification codes, surface elevation, and respective references, considered for the validation of the GOME2/Metop AAH product are shown in Table 7.16.

The total number of carefully screened collocations with the EARLINET lidar measurements from the beginning of each mission to the reporting period for the three GOME-2 instruments was 410. On average, the mean absolute bias (GOME-2 minus EARLINET lidar height) was found to be -0.54 ± 2.00 km, with a near-Gaussian distribution and minimum and maximum differences of $\sim \pm 5$ km. On a per station basis, and with a couple of exceptions, their mean biases fall in the ± 1 km range, with an associated standard deviation between 0.6 – 2.4 km. For the time period between July 2024 and December 2024 for the GOME-2B and GOME-2C offline AAH products, the number of collocated cases was 25.

Table 7.16. Locations of EARLINET lidar stations and their geographical coordinates

EARLINET Station	Code	Country	Coordinates	Elevation (m)
Antikythera	AKY	Greece	23.31E, 35.86N	193
Athens	ATZ	Greece	23.78E, 37.96N	212
Barcelona	BRC	Spain	2.12E, 41.39N	115
Bucharest	INO	Romania	26.03E, 44.34N	93
Dushanbe	DUS	Tajikistan	68.85E, 38.55N	864
Évora	EVO	Portugal	7.91W, 38.56N	293
Granada	GRA	Spain	3.60W, 37.16N	680
Lecce	SAL	Italy	18.10E, 40.33N	30
Leipzig	LEI	Germany	12.43E, 51.35N	125
Limassol ^{1,2}	LIM	Cyprus	33.04E, 34.67N	10
Minsk	MAS	Belarus	27.60E, 53.91N	200
Potenza	POT	Italy	15.72E, 40.60N	760
Sofia	SOF	Bulgaria	23.38E, 42.65N	550
Thessaloniki	THE	Greece	22.95E, 40.60N	50

¹ Cyprus University of Technology (CUT) [before Oct 2020]

² Leibniz Institute for Tropospheric Research and ERATOSTHENES Centre of Excellence [after Oct 2020]

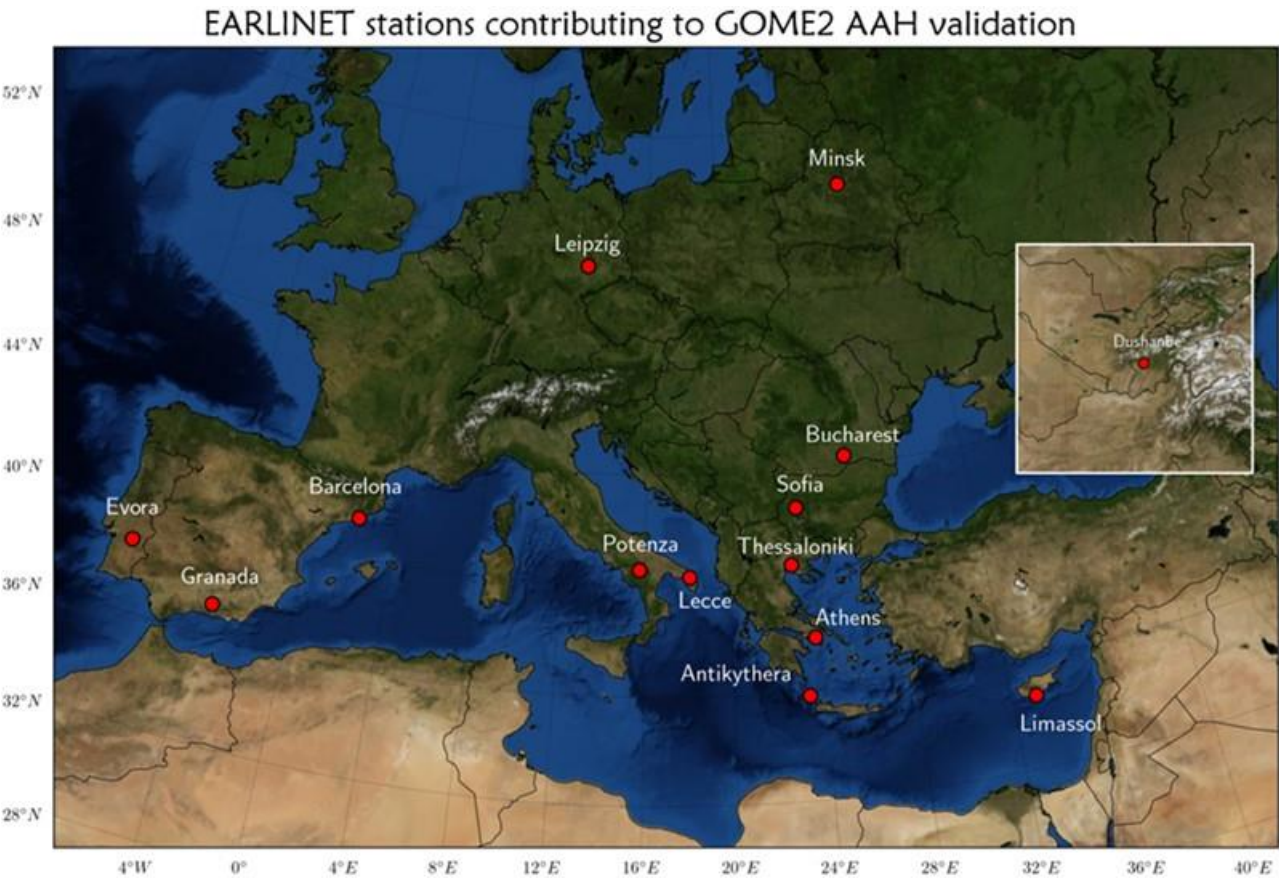


Figure 7.24. Geographical distribution of EARLINET ground-based stations for which co-locations with GOME-2 AAH data were used.

Table 7.17. Summary of statistics for the comparisons between GOME-2 AAH and LIDAR ALH for all stations

EARLINET Station	N	Statistical parameters (in km)			
		Mean absolute bias	Std	Min	Max
Athens, Greece	5	-1.98	0.78	-3.60	-1.06
Antikythera, Greece	50	-1.02	2.26	-6.77	3.84
Barcelona, Spain	36	-0.44	1.86	-4.66	2.86
Belsk, Poland	28	0.11	1.50	-3.11	3.24
Bucharest, Romania	19	-0.07	2.08	-4.81	3.37
Dushanbe, Tajikistan	36	-0.64	1.38	-3.81	1.78
Évora, Portugal	10	-0.09	1.98	-1.64	3.31
Granada, Spain	52	-0.49	2.00	-3.78	5.28
Lecce, Italy	18	-0.24	1.14	-3.47	2.05
Limassol, Cyprus	65	-1.03	2.42	-5.64	4.44
Minsk, Belarus	5	0.56	0.61	-0.05	1.51
Potenza, Italy	23	-1.25	1.68	-3.50	2.52
Thessaloniki, Greece	55	-0.12	2.07	-4.71	5.23
Warsaw, Poland	8	0.80	1.50	1.08	2.15
Summary	410	-0.56	2.00	-6.77	5.28

In Figure 7.25, the histogram of absolute differences between GOME-2 and EARLINET aerosol layer heights, calculated for all collocated cases is shown, with the associated statistics. The associated Absorbing Aerosol Index (AAI) value is color-coded. In the right panel, the scatter plot between GOME-2 AAH and aerosol layer height from EARLINET stations, for the totality of collocated cases is presented.

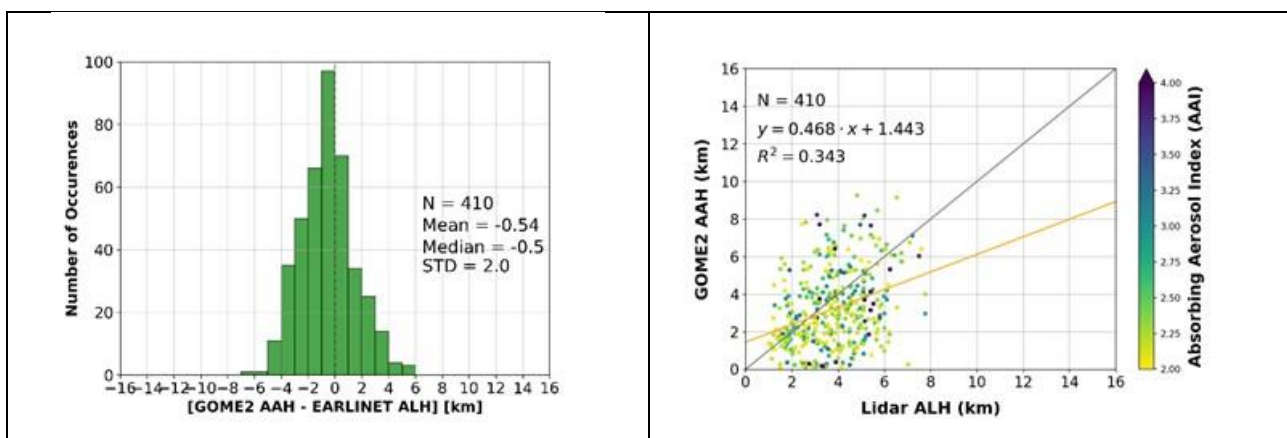


Figure 7.25. Histogram of absolute differences between GOME-2 AAH and aerosol layer height obtained from EARLINET backscatter profiles (using the WCT method), calculated for all collocated cases. The associated AAI value is color-coded. Right: Scatter plot between GOME-2 AAH and aerosol layer height from EARLINET stations, for the total of collocated cases.

Considering the possible temporal collocation mismatch and the spatial difference between the satellite pixel size and the point view of the ground-based observations, these results are quite

promising and demonstrate that stable aerosol layers are well captured by the satellite sensors. The official AC SAF requirements for the accuracy of the GOME-2 AAH product state that, for heights < 10 km, the threshold accuracy is 3 km, the target accuracy is 2 km, and the optimal accuracy is 1 km. This validation effort shows that for all cases the target accuracy is met, see Table 7.18. For the different regimes, which relate to the degree of cloud cover, please refer to the [validation report](#) and Michailidis *et al.*, 2021.

Table 7.18. Percentage of collocated lidar & GOME-2 AAH cases that fulfil the optimal accuracy criteria (first row), the target criteria (second row), the threshold criteria (third row) for Regime A in the first column, Regime B in the second, Regime C in the third and the totality of the collocations in the final column. The regimes are related to the degree of cloud cover.

	Regime A (194 cases)	Regime B (181 cases)	Regime C (35 cases)	Total (410 cases)
Optimal (1 km)	30.3 %	50.3 %	48.6 %	40.6 %
Target (2 km)	54.4 %	75.1 %	71.4 %	65.0 %
Threshold (3 km)	77.9 %	87.8 %	88.6 %	83.2 %

KMI results:

No new reference data was available when this report was published.

KMI validated the AAH only for specific case studies related to volcanic eruptions. AAH values are only included in the analysis if the corresponding AAI is higher than 4. CALIOP and GOME data are compared when the distance between both overpasses is maximum 100 km. There is currently no constraint on the time difference between both overpasses.

Compared to the results shown in the [validation report](#), new data has been added to the study (i.e. Fournaise de la Piton 11-12 February 2020, Karymsky 1-2 April 2020, Kavachi 16 March 2020 and Kikai 29-30 April 2020) in this report. The updated results are summarized in Table 7.19.

Overall, just about 50-60 % of the AAH pixels from GOME-2A, GOME-2B and GOME-2C reach the threshold requirements (see Table 7.19 and Figure 7.26). The optimal requirement threshold is reached for GOME-2A, GOME-2B and GOME-2C in 18 %, 25 % and 24 % of the cases, respectively (when comparing the AAH with the minimum CALIOP layer height). If only the tropospheric aerosol species (as defined by CALIOP) are studied, the results improve. This can also be seen in Table 7.19 (values in brackets).

Table 7.19. Percentage of data for each GOME-2 instrument that reached the threshold, target and optimal accuracy requirements. Values obtained when only considering the tropospheric aerosol species are shown in brackets

GOME-2A				
		Layer height <10 km	Layer height >10 km	Total
Threshold	AAH-minC	56.0 % (69.6 %)	53.1 % (26.4 %)	55.9 % (68.9 %)
	AAH-maxC	56.4 % (69.5 %)	46.8 % (23.6 %)	56.2 % (68.7 %)
Target	AAH-minC	39.0 % (48.5 %)	43.5 % (19.1 %)	39.1 % (48.0 %)
	AAH-maxC	38.0 % (46.9 %)	32.4 % (23.6 %)	37.9 % (46.3 %)

Optimal	AAH-minC	17.3 % (21.5 %)	29.9 % (10.0 %)	17.6 % (21.3 %)
	AAH-maxC	18.1 % (22.3 %)	15.6 % (10.0 %)	18.1 % (22.1 %)
GOME-2B				
		Layer height <10 km	Layer height >10 km	Total
Threshold	AAH-minC	51.8 % (53.6 %)	22.9 % (11.7 %)	50.9 % (51.6 %)
	AAH-maxC	52.6 % (54.4 %)	20.6 % (10.2 %)	51.6 % (52.2 %)
Target	AAH-minC	42.9 % (44.5 %)	20.6 % (5.60 %)	42.2 % (42.6 %)
	AAH-maxC	37.0 % (38.3 %)	17.1 % (7.90 %)	36.4 % (36.8 %)
Optimal	AAH-minC	25.1 % (26.0 %)	17.1 % (3.40 %)	24.8 % (24.9 %)
	AAH-maxC	20.5 % (33.1 %)	16.5 % (3.00 %)	20.4 % (31.6 %)
GOME-2C				
		Layer height <10 km	Layer height >10 km	Total
Threshold	AAH-minC	50.8 % (50.8 %)	0.0 % (0.0 %)	46.8 % (46.8 %)
	AAH-maxC	57.1 % (57.1 %)	0.0 % (0.0 %)	52.9 % (52.9 %)
Target	AAH-minC	42.2 % (42.2 %)	0.0 % (0.0 %)	38.8 % (38.8 %)
	AAH-maxC	49.1 % (49.1 %)	0.0 % (0.0 %)	45.2 % (45.2 %)
Optimal	AAH-minC	26.3 % (26.3 %)	0.0 % (0.0 %)	24.1 % (24.1 %)
	AAH-maxC	34.5 % (34.5 %)	0.0 % (0.0 %)	31.6 % (31.6 %)

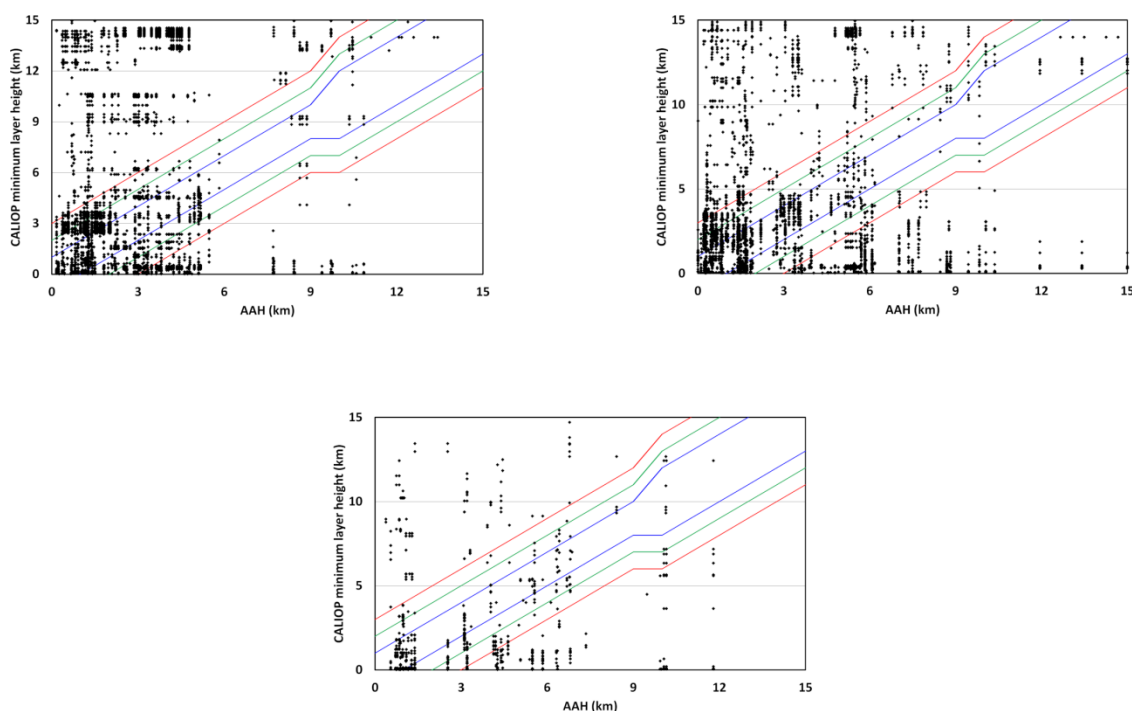


Figure 7.26. Requirement plots for GOME-2A (upper left), GOME-2B (upper right) and GOME-2C (lower middle). The red, green and blue lines represent the threshold, target and optimal requirements. CALIOP pixels are only shown up to a height of 15 km, which is the detection limit of GOME-2.

References:

Michailidis, K., Koukouli, M.-E., Siomos, N., Balis, D., Tuinder, O., Tilstra, L. G., Mona, L., Pappalardo, G. and Bortoli, D.: First validation of GOME-2/MetOp absorbing aerosol height using EARLINET lidar observations, *Atmos. Chem. Phys.*, 21, 3193–3213, 2021.

<https://doi.org/10.5194/acp-21-3193-2021>

Tilstra, L. G., Tuinder, O., Wang, P. and Stammes, P.: ALGORITHM THEORETICAL BASIS DOCUMENT GOME-2 Absorbing Aerosol Height, SAF/AC//KNMI/ATBD/005, 1.4, Royal Netherlands Meteorological Institute, de Bilt, 2019.

https://acsaf.org/docs/atbd/Algorithm_Theoretical_Basis_Document_AA_H_Apr_2019.pdf, last access: 31 March 2021.

Wang, P., Tuinder, O. N. E., Tilstra, L. G., De Graaf, M. and Stammes, P.: Interpretation of FRESCO cloud retrievals in case of absorbing aerosol events, *Atmos. Chem. Phys.*, 12(19), 9057–9077, 2021.

<https://doi.org/10.5194/acp-12-9057-2012>

De Bock, V., A. Delcloo, K. Michailidis, M. Koukouli and D. Balis, ACSAF Absorbing Aerosol Height products validation report, SAF/AC/AUTH-RMI/VR/001, 1/2020, 3 July 2020.

https://acsaf.org/docs/vr/Validation_Report_AA_H_Jul_2020.pdf, last access: 31 March 2021.

7.5.1. Online quality monitoring

The online quality monitoring of the AAI in this section shows (left duo-plot) the radiance corrections for the PMD-AAI at 340 and 380 nm, and (right duo-plot) the uncorrected residue, and the corrected residue. The rightmost plot is the result of all the corrections and should stay more or less flat when seasonal cycles and differences are removed.

The break in the curves of the latter plot in August 2018 is caused by the introduction of a combination of the ‘End-of-Orbit’ corrections and a flattening of the AAI across the swath.

The plots can also be found at: [TEMIS website](#).

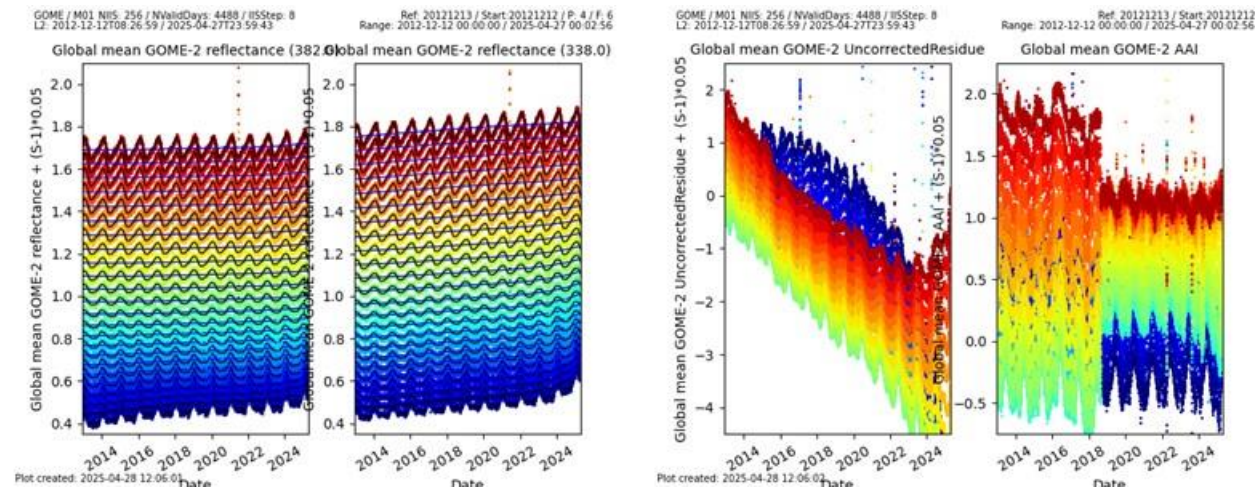


Figure 7.27. Timeline of global mean reflectances at 340 and 380 nm (left) and the uncorrected and corrected AAI from the PMDs of Metop-B.

7.6. GOME-2 UV products

Table 7.20. Validation status of UV products

Product Identifier	Product Name	Accuracy	Reference	Validating Institute	Correlative data sources
O3M-409	NRT UV index, clear-sky	Fulfils threshold accuracy requirements	RD8	DMI	WOUDC , NEUBrew , NSF
O3M-410	NRT UV index, cloud-corrected				
O3M-450 – O3M-464	Offline surface UV	Fulfils target accuracy requirements	RD14	FMI	Brewers and SUV-spectroradiometers from WOUDC , NEUBrew , NSF , NOAA , AUTH and FMI

7.6.1. Online quality monitoring

NUV:

Online quality monitoring of the NRT UV index is found on [NUV web page](#). It can be traced that the quality of the NUV products is stable since the last validation. No problems with the data quality was found in the reporting period.

OUV:

[Online quality monitoring of offline surface UV](#) has not shown any unexpected, permanent changes in the monitoring value after the latest validation, indicating that the product accuracy has remained within requirements also during the reporting period. The latest OUV validation reports were published in February 2009 covering June 2007 – May 2008 (Metop-A data) and in February 2015 covering June 2012 – May 2013 (Metop-B data).

Figure 7.28 presents the long-term monitoring graph of OUV, which illustrates seasonal variation of **global average of erythemal daily dose** (yellow markers). Any sudden changes would indicate problems with data quality. Additionally, six-month average values (January – June and July – December) are represented by red markers.

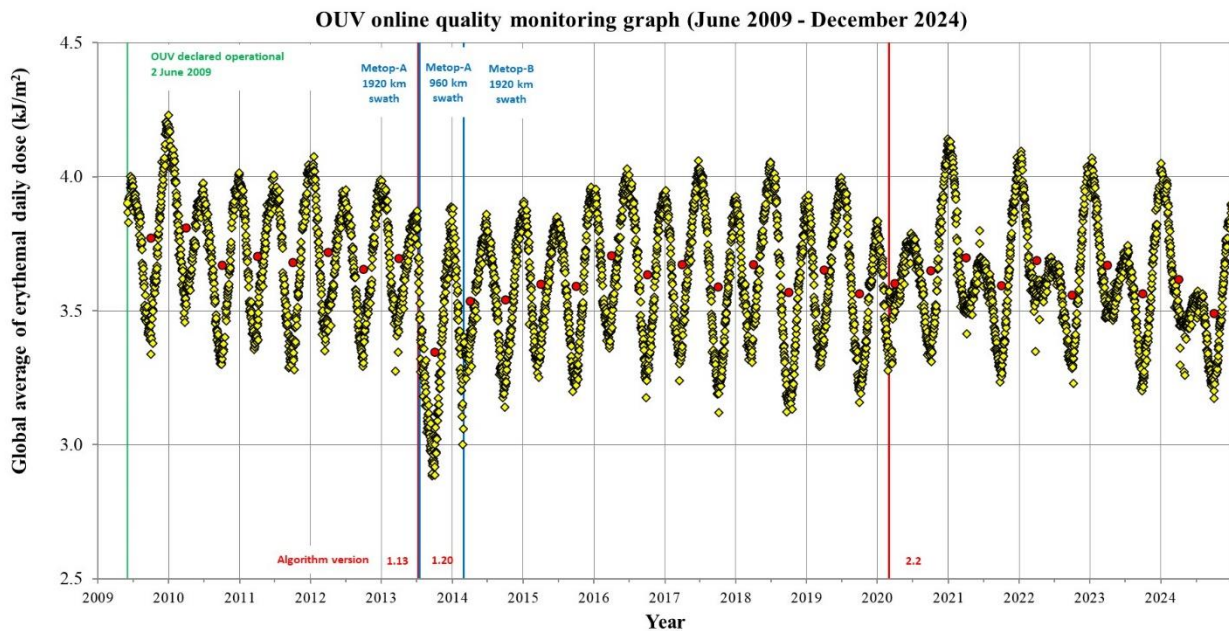


Figure 7.28. OUV long-term monitoring graph.

NOTES:

- GOME-2A was switched from nominal swath width (1920 km) to reduced swath width (960 km) 15 July 2013. The effect to OUV monitoring values can be clearly seen as more widespread global average values of erythemal daily dose. This is due to the dominance of lower EDD values in high latitudes when the satellite coverage near the equator is poor due to narrower swath width.
- OUV data processing was switched to use Metop-B data having nominal swath width of 1920 km 1 March 2014
- OUV data processing was switched to use Metop-B+C data 1 March 2020

7.7. IASI NRT products

Table 7.21. Online quality monitoring of the IASI CO, SO₂, O₃ and HNO₃ products

Product Identifier	Product Name	Accuracy	Reference	Validating Institute	Correlative data sources
O3M-80	IASI NRT CO	Fulfils threshold accuracy requirement	RD18	LATMOS	FTIR NDACC, MOPITT
O3M-57	IASI NRT SO ₂	Fulfils threshold accuracy requirement	RD19	AUTH, BIRA-IASB, LATMOS, ULB	MAXDOAS
O3M-44 O3M-49	IASI NRT O ₃	Fulfils threshold accuracy requirement	RD31	AUTH, KMI, DWD	GOME-2, balloon sonde, lidar and microwave radiometer, Brewer and Dobson
O3M-81	IASI NRT HNO ₃	Fulfils threshold accuracy requirement	RD32	BIRA-IASB	FTIR NDACC (only available in 2021)

IASI NRT O₃ and IASI NRT HNO₃ products have been released by EUMETSAT as ‘operational’ on 18 May 2022.

IASI online quality monitoring is performed at ULB and LATMOS.

IASI NRT CO online monitoring:

https://atmosphere.copernicus.eu/charts/packages/cams_monitoring/

Dissemination monitoring activities summary:

IASI CO:

The IASI NRT CO product (v6.3) has been declared operational on 2 March 2017. Here we present statistical results when comparing the EUMETSAT product disseminated by EUMETCast in BUFR format (COX) with the native product produced at ULB (FORLI-CO v20191122) for 6 days representative of 6 months: January 15th, February 15th, March 16th, April 15th, May 15th and June 15th, 2024, for Metop-B and Metop-C. This allows monitoring if any discrepancy occurs between the two, EUMETSAT and native, products. So far, the discrepancies are found within the numerical errors inherent to the use of different IT infrastructure.

CO total column and profiles are investigated. Statistics between COX data and FORLI-CO data (v20191122) are presented in Table 7.22. Profiles correlation (“Correlation”) score is computed using the discreet cross correlation integral between two profiles, normalized by the square root of the product of their auto-correlation integral. Score of 1 is expected for perfectly matching profiles, 0 for unrelated ones. Absolute and relative differences are calculated for the total columns. These tables are extracted from the Daily Reports prepared by Daniel Hurtmans at ULB.

Table 7.22. Statistics between COX data and FORLI-CO data for 6 days: January 15th, February 15th, March 16th, April 15th, May 15th and June 15th, 2024.**15/07/2024:**

		IASI-c		IASI-b	
		Native	COX	Native	COX
Individual Pixels		565678	570273	570413	568673
Common Pixels		557410 (97.74%)		567767 (99.54%)	
Correlation	Mean	0.9995±0.0019		0.9994±0.0020	
	Max	1.0000		1.0000	
	Min	0.7821		0.7604	
Total Column Differences	Mean (10 ¹⁹ mol/cm ²)	0.0052±0.0052		0.0052±0.0049	
	Max (10 ¹⁹ mol/cm ²)	1.2064		0.6805	
	Min (10 ¹⁹ mol/cm ²)	-1.0379		-0.7161	
Total Column Relative Differences	Mean (%)	2.7059±1.4481		2.7130±1.4878	
	Max (%)	84.2488		74.0229	
	Min (%)	-140.2944		-39.1749	

15/08/2024:

		IASI-c		IASI-b	
		Native	COX	Native	COX
Individual Pixels		576578	575252	495211	495111
Common Pixels		574317 (99.61%)		493262 (99.61%)	
Correlation	Mean	0.9995±0.0019		0.9996±0.0013	
	Max	1.0000		1.0000	
	Min	0.5121		0.7935	
Total Column Differences	Mean (10 ¹⁹ mol/cm ²)	0.0057±0.0050		0.0056±0.0082	
	Max (10 ¹⁹ mol/cm ²)	1.1268		0.3954	
	Min (10 ¹⁹ mol/cm ²)	-0.6876		-4.6606	
Total Column Relative Differences	Mean (%)	2.7214±1.4580		2.6410±1.4742	
	Max (%)	83.9100		52.3336	
	Min (%)	-92.4244		-66.0711	

15/09/2024:

		IASI-c		IASI-b	
		Native	COX	Native	COX
Individual Pixels		545852	545227	559749	558829
Common Pixels		544336 (99.72%)		557953 (99.68%)	
Correlation	Mean	0.9996±0.0014		0.9996±0.0013	
	Max	1.0000		1.0000	
	Min	0.7595		0.8222	
Total Column Differences	Mean (10^{19} mol/cm ²)	0.0060±0.0054		0.0061±0.0055	
	Max (10^{19} mol/cm ²)	0.6601		0.6948	
	Min (10^{19} mol/cm ²)	-0.5174		-1.3678	
Total Column Relative Differences	Mean (%)	2.6811±1.4833		2.6847±1.4423	
	Max (%)	58.9015		62.2854	
	Min (%)	-297.3937		-52.3037	

15/10/2024:

		IASI-b		IASI-c	
		Native	COX	Native	COX
Individual Pixels		547756	548852	527994	527283
Common Pixels		545825 (99.45%)		526467 (99.71%)	
Correlation	Mean	0.9996±0.0013		0.9996±0.0012	
	Max	1.0000		1.0000	
	Min	0.6960		0.7385	
Total Column Differences	Mean (10^{19} mol/cm ²)	0.0069±0.0155		0.0070±0.0184	
	Max (10^{19} mol/cm ²)	4.5965		2.5505	
	Min (10^{19} mol/cm ²)	-1.5489		-3.7393	
Total Column Relative Differences	Mean (%)	2.7289±1.4898		2.7219±1.4314	
	Max (%)	79.4211		53.1069	
	Min (%)	-44.7005		-50.1177	

15/11/2024:

		IASI-c		IASI-b	
		Native	COX	Native	COX
Individual Pixels		514677	513959	554105	553147
Common Pixels		513190 (99.71%)		552237 (99.66%)	
Correlation	Mean	0.9997±0.0009		0.9997±0.0016	
	Max	1.0000		1.0000	
	Min	0.6161		0.2856	
Total Column Differences	Mean (10^{19} mol/cm ²)	0.0054±0.0053		0.0055±0.0095	
	Max (10^{19} mol/cm ²)	1.0344		3.3964	
	Min (10^{19} mol/cm ²)	-0.1642		-0.3155	
Total Column Relative Differences	Mean (%)	2.5463±1.4694		2.4991±1.5769	
	Max (%)	74.0743		93.7199	
	Min (%)	-45.9708		-126.2271	

17/12/2024:

		IASI-b		IASI-c	
		Native	COX	Native	COX
Individual Pixels		545072	546565	533589	532777
Common Pixels		540728 (98.93%)		531929 (99.69%)	
Correlation	Mean	0.9997±0.0013		0.9997±0.0010	
	Max	1.0000		1.0000	
	Min	0.7518		0.4240	
Total Column Differences	Mean (10 ¹⁹ mol/cm ²)	0.0025±1.7024		0.0049±0.0065	
	Max (10 ¹⁹ mol/cm ²)	2.0844		0.6986	
	Min (10 ¹⁹ mol/cm ²)	-1251.8079		-3.7746	
Total Column Relative Differences	Mean (%)	2.4210±2.1696		2.4746±2.6799	
	Max (%)	80.3938		54.8417	
	Min (%)	-1084.8096		-1644.5364	

Figure 7.29 – Figure 7.34 show the correlation plots for total column between COX data and FORLI-CO for each platform. No critical deviation was found for these dates.

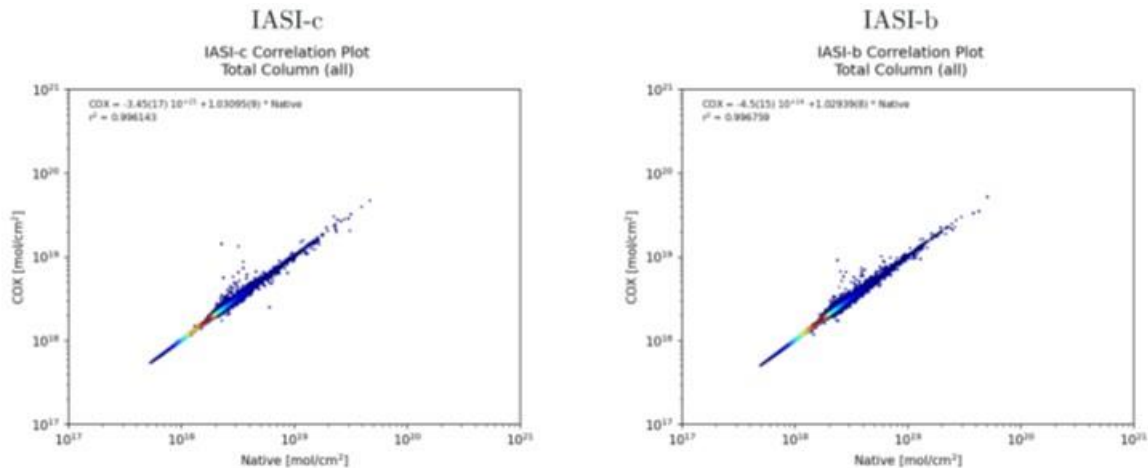


Figure 7.29. Correlation plots for total column between COX data and FORLI-CO for each platform for 15/07/2024. X-axis corresponds to native data (mol/cm²) and Y-axis corresponds to COX data (mol/cm²).

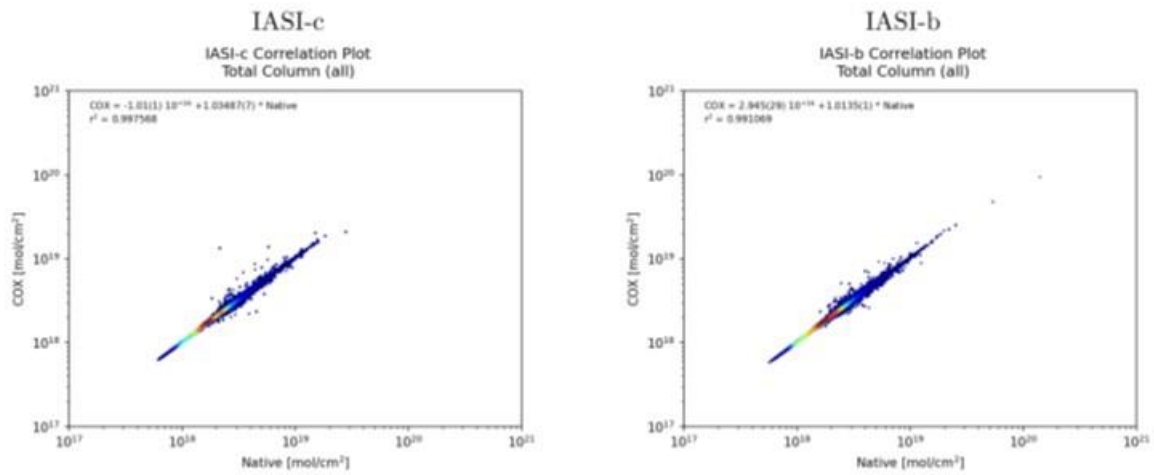


Figure 7.30. Same as Figure 7.29 but for 15/08/2024.

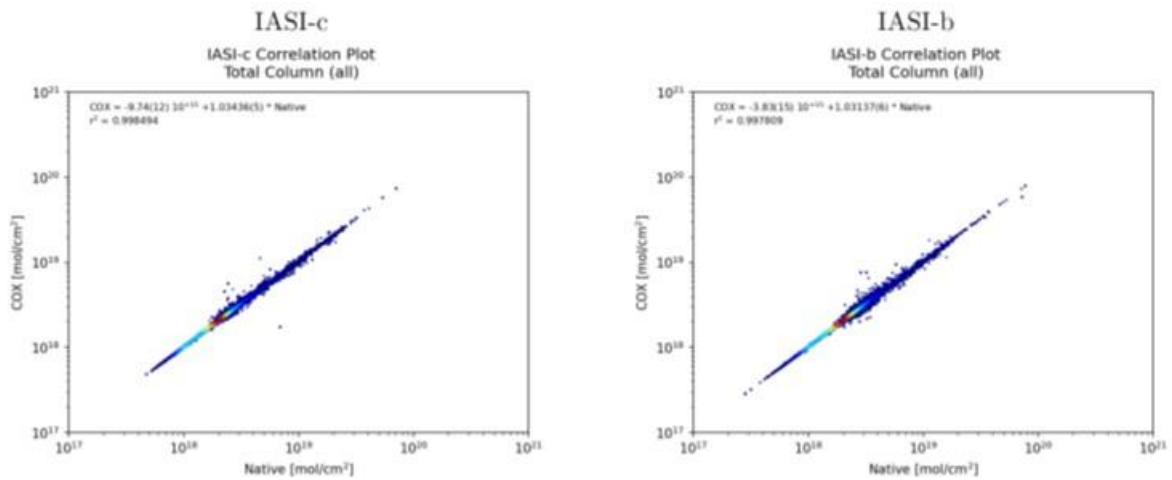


Figure 7.31. Same as Figure 7.29 but for 15/09/2024.

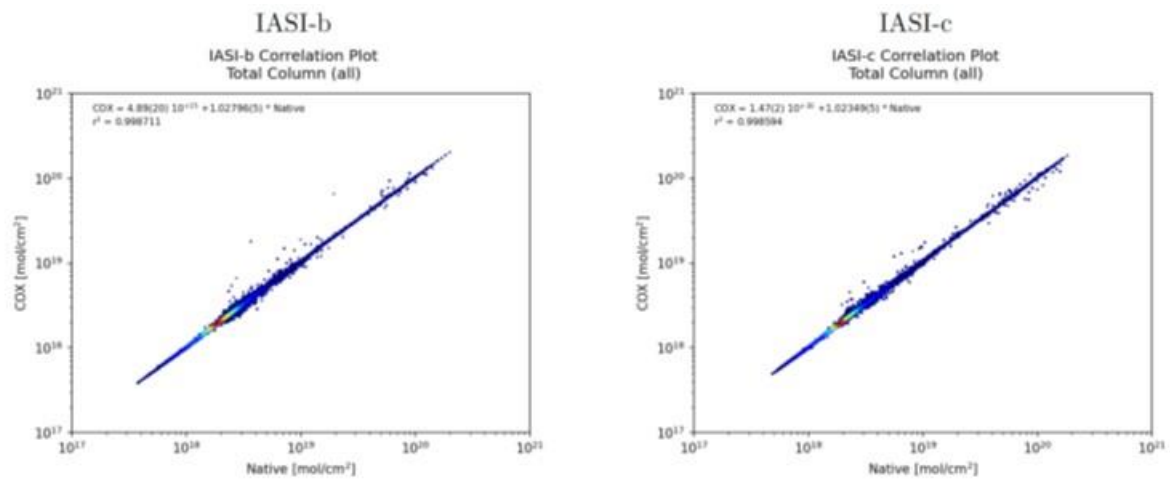


Figure 7.32. Same as Figure 7.29 but for 15/10/2024.

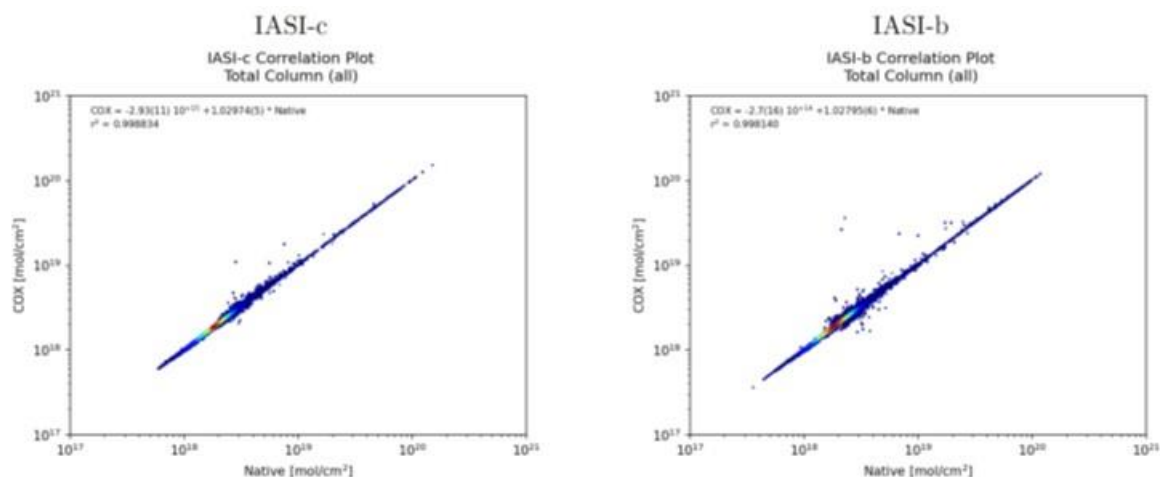


Figure 7.33. Same as Figure 7.29 but for 15/11/2024.

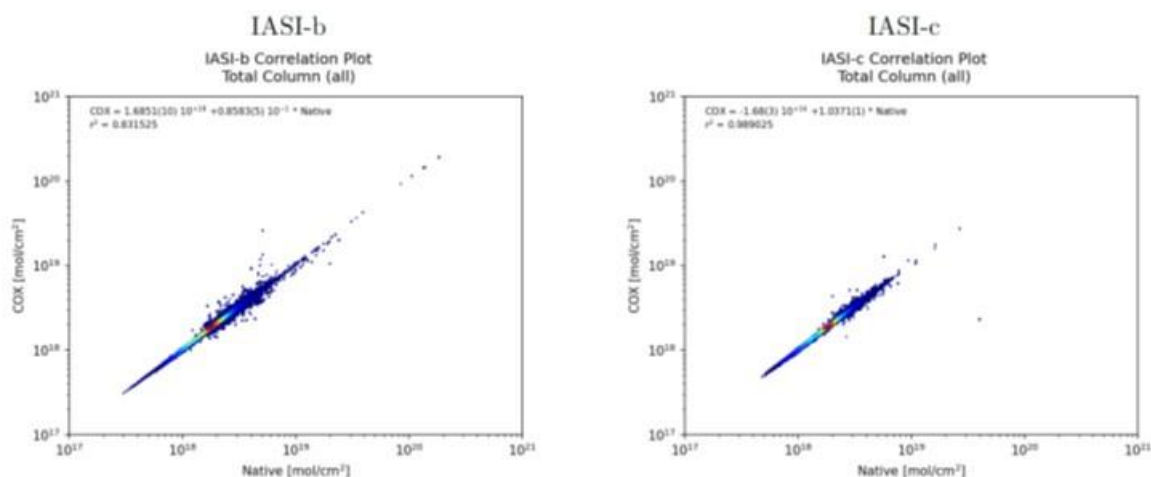


Figure 7.34. Same as Figure 7.29 but for 17/12/2024.

IASI SO₂:

The IASI BRESCIA SO₂ retrieval algorithm has been implemented in the PPF v6.3 at EUMETSAT (operational release on 18/04/2018). Here we compare the EUMETSAT product disseminated by EUMETCast in BUFR format (SO₂ EUMET) with the native product produced at ULB (SO₂ ULB) for 5 days between March and May 2024, for Metop-B and Metop-C. We choose to study 17/03/2024, 18/03/2024, 23/04/2024, 30/04/2024 and 02/05/2024.

i) Online quality monitoring for SO₂ for five estimated altitudes:

For each of the five days, scatterplots for the different estimated altitudes (7, 10, 13, 16 and 25 km) are presented (Figure 7.35 – Figure 7.39). The data have been filtered following the recommendations of the Product User Manual (Section 5.2.2, i.e. we kept the pixels in the neighbourhood (± 10 degrees) of SO₂_BT_DIFFERENCE > 1K pixels, and did not use the pixels with a SO₂_BT_DIFFERENCE < 0.4K.

We recall here that when the IASI L2 pressure and temperature profiles are not available, ECMWF forecasts (3h, interpolated in time and space) data are used in the EUMETSAT API. These pixels are flagged with SO₂_QFLAG = 11 and are not part of the comparison.

Correlation coefficients (in blue) are ~ 1 .

So far, the discrepancies are found within the numerical errors inherent to the use of different IT infrastructure.

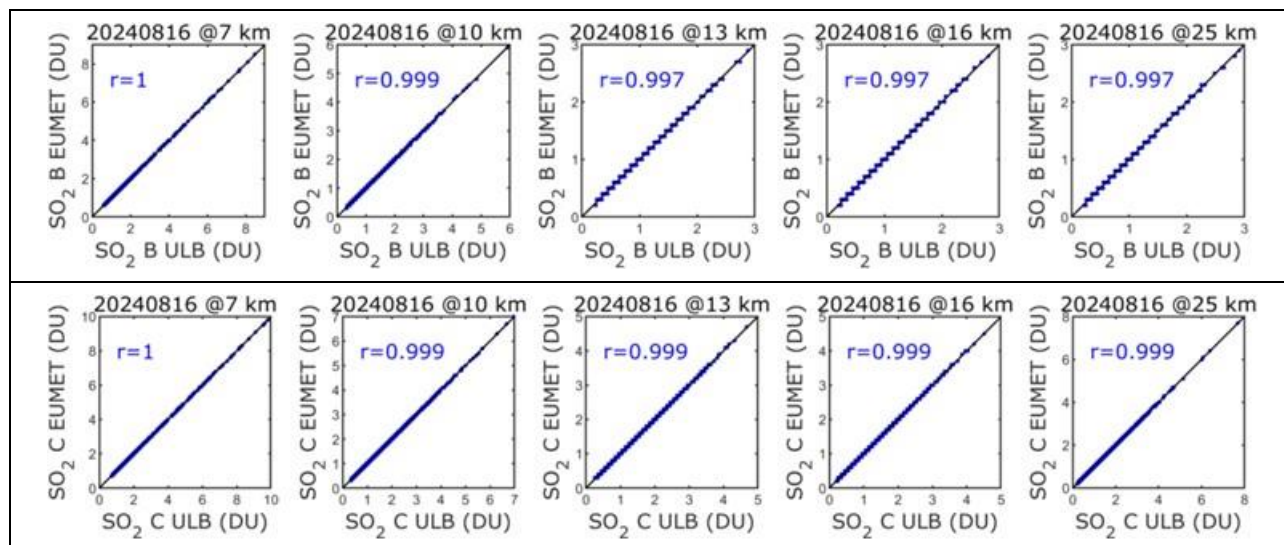


Figure 7.35. Scatterplots for Metop-B (top) and Metop-C (bottom): SO₂ EUMET versus SO₂ ULB for 16/08/2024, for the five estimated altitudes (7, 10, 13, 16 and 25 km).

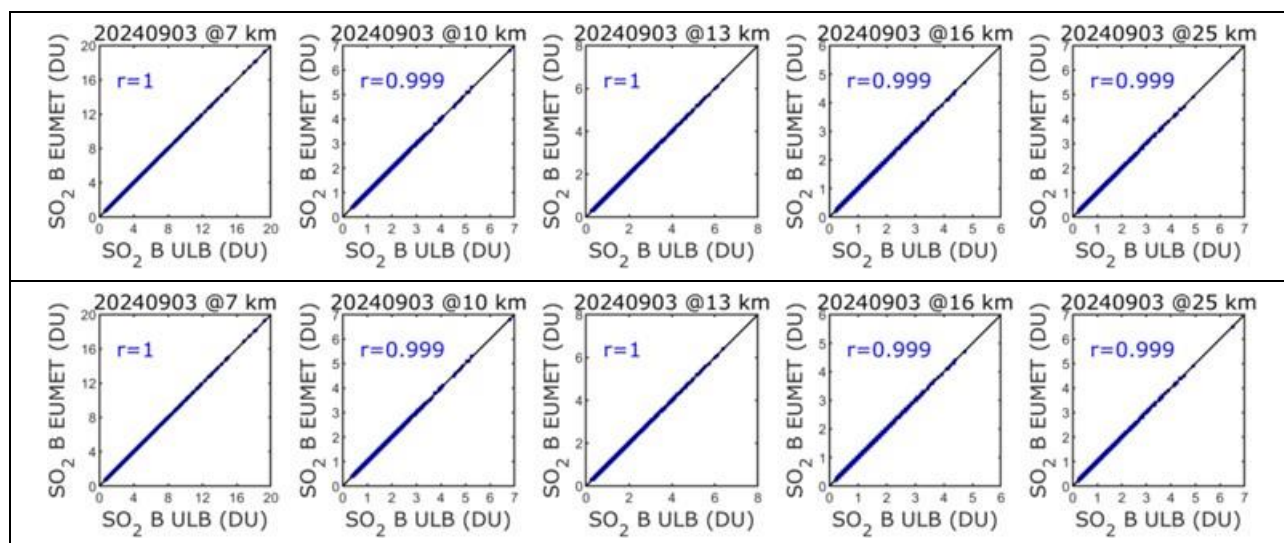
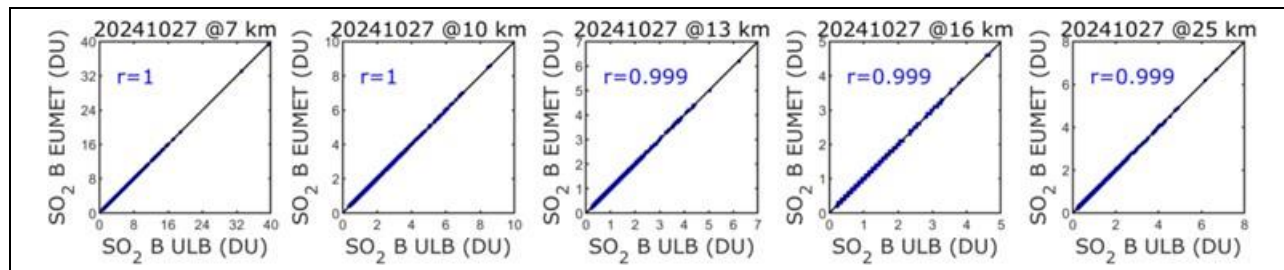


Figure 7.36. Same as Figure 7.35 but for 03/09/2024.



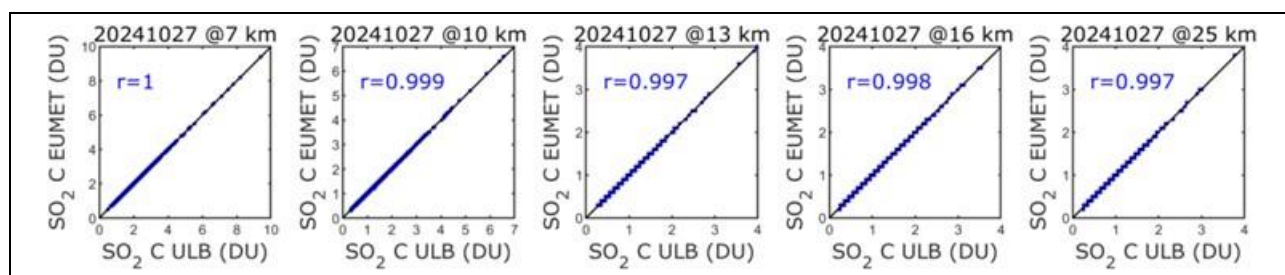


Figure 7.37. Same as Figure 7.35 but for 27/10/2024.

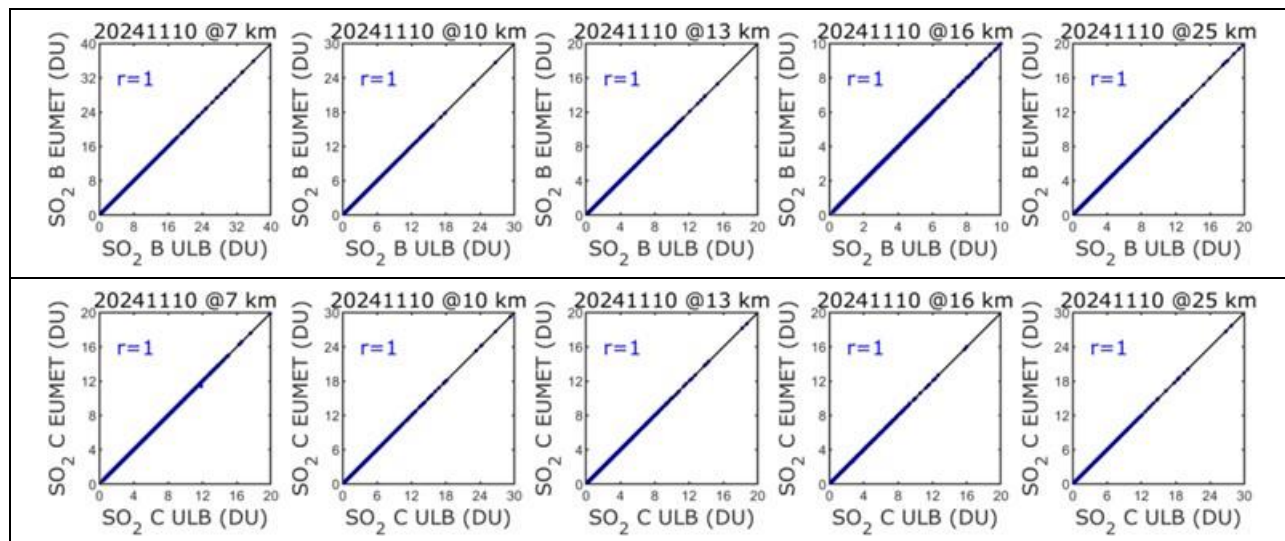


Figure 7.38. Same as Figure 7.35 but for 10/11/2024.

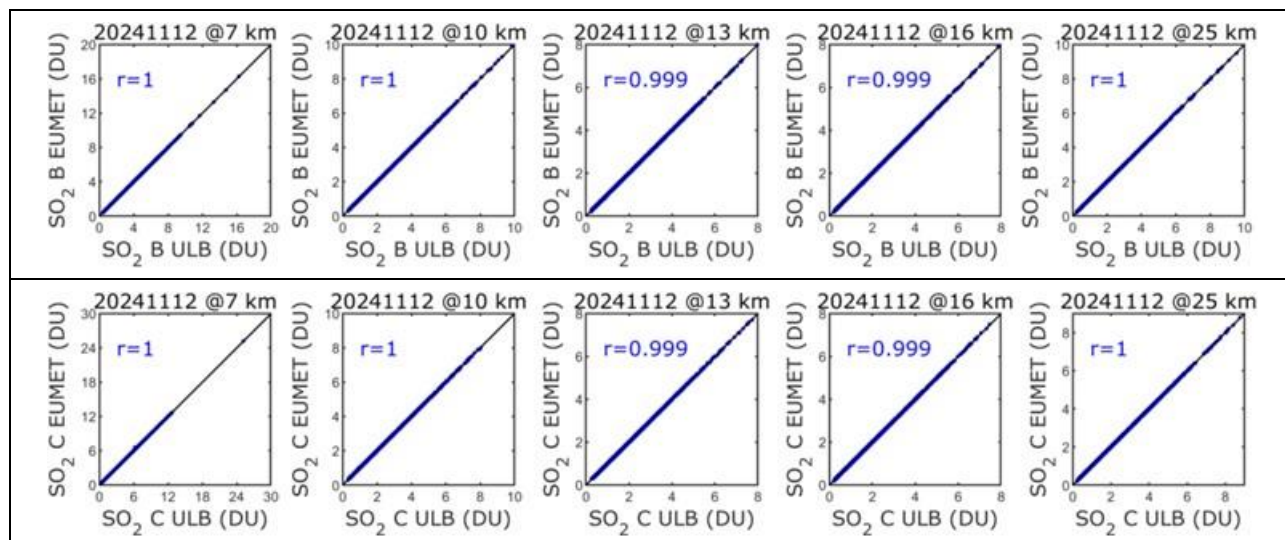


Figure 7.39. Same as Figure 7.35 but for 12/11/2024.

ii) Online quality monitoring for SO₂_ALTITUDE and SO₂_COL:

Although the two products SO₂_ALTITUDE (estimated altitude of the SO₂ plume) and SO₂_COL (SO₂ column at the estimated altitude) are operational since May 2021, **the EUMETSAT and the ULB algorithms versions are different**, with the ULB version being the latest version of the algorithm. As said in the previous report, **the EUMETSAT and ULB products are not the**

same and the comparison shows differences. Scatterplots for five dates (16/08/2024, 03/09/2024, 27/10/2024, 10/11/2024 and 12/11/2024), for Metop-B and C are shown in Figure 7.40 – Figure 7.44 to illustrate that the products do not match at all. Daniel Hurtmans provided an updated version of the Brescia algorithm (including the SO₂ altitude) for implementation to EUMETSAT, in order for the two versions to be the same. We are waiting for an update from EUMETSAT.

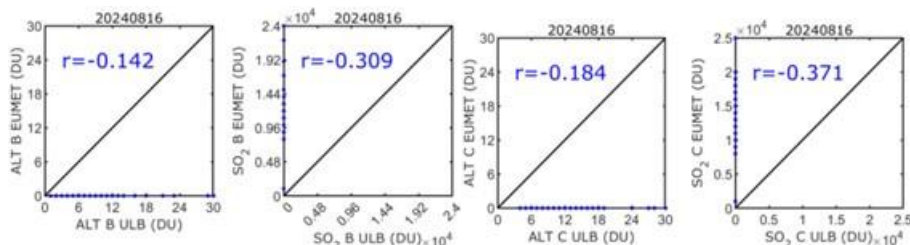


Figure 7.40. Scatter plots for Metop-B and Metop-C: SO₂_ALTITUDE EUMET versus SO₂_ALTITUDE ULB, as well as SO₂_COL EUMET versus SO₂_COL ULB, for 16/08/2024.

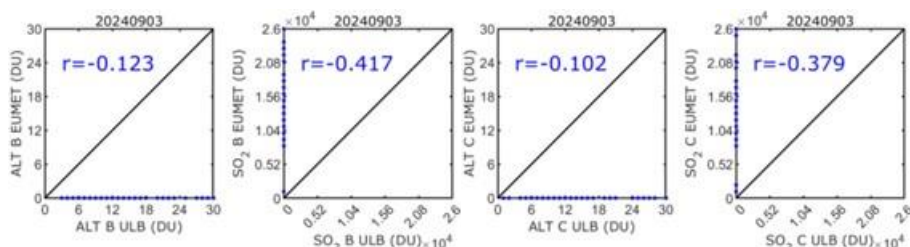


Figure 7.41. Same as Figure 7.40 but for 03/09/2024.

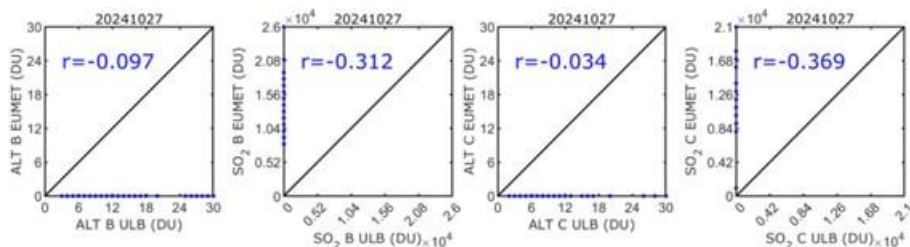


Figure 7.42. Same as Figure 7.40 but for 27/10/2024.

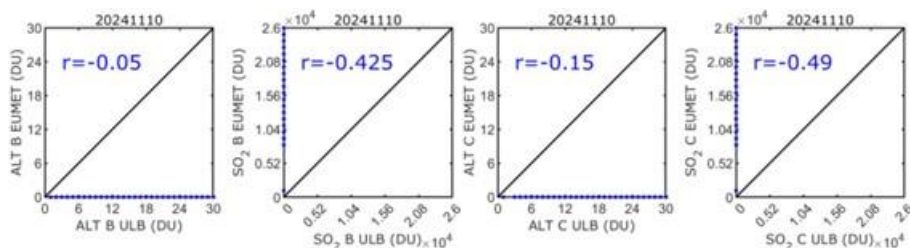


Figure 7.43. Same as Figure 7.40 but for 10/11/2024.

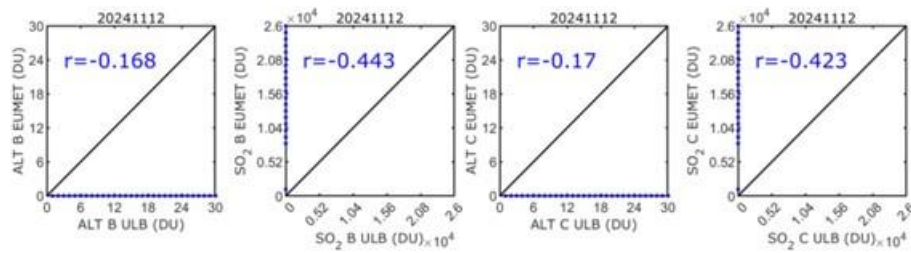


Figure 7.44. Same as Figure 7.40 but for 12/11/2024.

IASI O3:

The IASI NRT O₃ product (v6.5) has been declared operational on 18 May 2022. Here we present statistical results when comparing the EUMETSAT product disseminated by EUMETCast in BUFR format (OZO, called “bufr” hereinafter) with the native product produced at ULB (FORLI-O3 v20191122, called “native” hereinafter) for 6 days representative of 6 months: July 15th, August 15th, September 16th, October 15th, November 15th and December 17th, 2024, for Metop-B and Metop-C. This allows monitoring if any discrepancy occurs between the two, EUMETSAT and native, products. The data have been filtered following the recommendations of the Product User Manual. Furthermore, data associated with DOFS > 2 have also been filtered out.

Total and 0 – 6 km ozone column are investigated. Detailed statistics for total column between bufr and native data for each of the 6 days are presented in Table 7.23 – Table 7.28. No critical deviation was found for these dates.

The difference between individual pixels in native and bufr format is due to the fact that the NRT EUMETSAT version is the v2015, and only 1/10 pixels are treated to gain processing time, this means clearly a lower number of observations.

Table 7.23. Statistics for total ozone column between bufr and native data for July 15th 2024

O3 - 15 July 2024	IASI-B		IASI-C	
	Native	Bufr	Native	Bufr
Individual Pixels	397915	389330	399030	393013
Common Pixels	343017 (86.20 %)		345400 (86.56 %)	
Correlation	0.9992		0.9992	
Total Column Diff - Mean (DU)	2.7357 ± 1.8047		2.7785 ± 1.7713	
Total Column Diff - Max (DU)	19.6239		24.6247	
Total Column Diff - Min (DU)	-23.4864		-22.2068	
Total Column Rel. Diff - Mean (%)	0.9426 ± 0.5988		0.9605 ± 0.5952	
Total Column Rel. Diff - Max (%)	6.8002		7.5489	
Total Column Rel. Diff - Min (%)	-9.8053		-6.8771	

Table 7.24. Same as Table 7.23, but for August 15th 2024

O3 - 15 August 2024	IASI-B		IASI-C	
	Native	Bufr	Native	Bufr
Individual Pixels	350269	347810	410522	407352
Common Pixels	303957 (86.78 %)		355627 (86.63 %)	
Correlation	0.9989		0.9990	
Total Column Diff - Mean (DU)	2.8505 ± 1.5792		2.9678 ± 1.5155	
Total Column Diff - Max (DU)	27.8050		17.7753	
Total Column Diff - Min (DU)	-18.6915		-14.1225	
Total Column Rel. Diff - Mean (%)	0.9899 ± 0.5528		1.0340 ± 0.5343	
Total Column Rel. Diff - Max (%)	9.5764		6.5442	
Total Column Rel. Diff - Min (%)	-5.1282		-4.0077	

Table 7.25. Same as Table 7.23, but for September 15th 2024

O3 - 15 September 2024	IASI-B		IASI-C	
	Native	Bufr	Native	Bufr
Individual Pixels	396066	384739	387136	378979
Common Pixels	342630 (86.51 %)		336687 (86.97 %)	
Correlation	0.9993		0.9993	
Total Column Diff - Mean (DU)	2.9494 ± 1.4132		3.0420 ± 1.4124	
Total Column Diff - Max (DU)	14.9362		16.7879	
Total Column Diff - Min (DU)	-19.0016		-51.7783	
Total Column Rel. Diff - Mean (%)	1.0424 ± 0.5109		1.0738 ± 0.5065	
Total Column Rel. Diff - Max (%)	6.9002		5.5653	
Total Column Rel. Diff - Min (%)	-7.4457		-14.6273	

Table 7.26. Same as Table 7.23, but for October 15th 2024

O3 - 15 October 2024	IASI-B		IASI-C	
	Native	Bufr	Native	Bufr
Individual Pixels	379267	370527	373820	365172
Common Pixels	326079 (85.98 %)		324143 (86.71 %)	
Correlation	0.9993		0.9993	
Total Column Diff - Mean (DU)	3.0064 ± 1.7391		3.1505 ± 1.6790	
Total Column Diff - Max (DU)	27.1610		44.3984	
Total Column Diff - Min (DU)	-40.6136		-55.1571	
Total Column Rel. Diff - Mean (%)	1.1140 ± 0.6836		1.1609 ± 0.6343	
Total Column Rel. Diff - Max (%)	10.3758		14.5364	
Total Column Rel. Diff - Min (%)	-16.3002		-15.6766	

Table 7.27. Same as Table 7.23, but for November 15th 2024

03 - 15 November 2024	IASI-B		IASI-C	
	Native	Bufr	Native	Bufr
Individual Pixels	393532	379924	371464	358848
Common Pixels	337191 (85.68 %)		318930 (85.86 %)	
Correlation	0.9991		0.9991	
Total Column Diff - Mean (DU)	2.7413 \pm 1.9164		2.8549 \pm 1.8427	
Total Column Diff - Max (DU)	37.4536		48.5350	
Total Column Diff - Min (DU)	-25.5906		-30.1411	
Total Column Rel. Diff - Mean (%)	1.0109 \pm 0.7188		1.0535 \pm 0.6823	
Total Column Rel. Diff - Max (%)	10.1846		17.3518	
Total Column Rel. Diff - Min (%)	-9.4861		-7.5561	

Table 7.28. Same as Table 7.23, but for December 17th 2024

03 - 15 December 2024	IASI-B		IASI-C	
	Native	Bufr	Native	Bufr
Individual Pixels	408338	396819	nan	nan
Common Pixels	351035 (85.97 %)		nan nan	
Correlation	0.9989		nan	
Total Column Diff - Mean (DU)	2.3486 \pm 2.0854		nan	
Total Column Diff - Max (DU)	26.7863		nan	
Total Column Diff - Min (DU)	-25.5716		nan	
Total Column Rel. Diff - Mean (%)	0.8493 \pm 0.7316		nan	
Total Column Rel. Diff - Max (%)	6.9551		nan	
Total Column Rel. Diff - Min (%)	-9.5105		nan	

Figure 7.45 and Figure 7.46 present the correlation plots of bufr and native total ozone column for IASI/Metop-B and IASI/Metop-C, respectively. Similarly, Figure 7.45 – Figure 7.48 show the correlation plots of bufr and native 0 – 6 km ozone column for IASI/Metop-B and IASI/Metop-C, respectively. Correlation coefficients (in blue) are ~ 1 .

So far, the discrepancies are found within the numerical errors inherent to the use of different IT infrastructure.

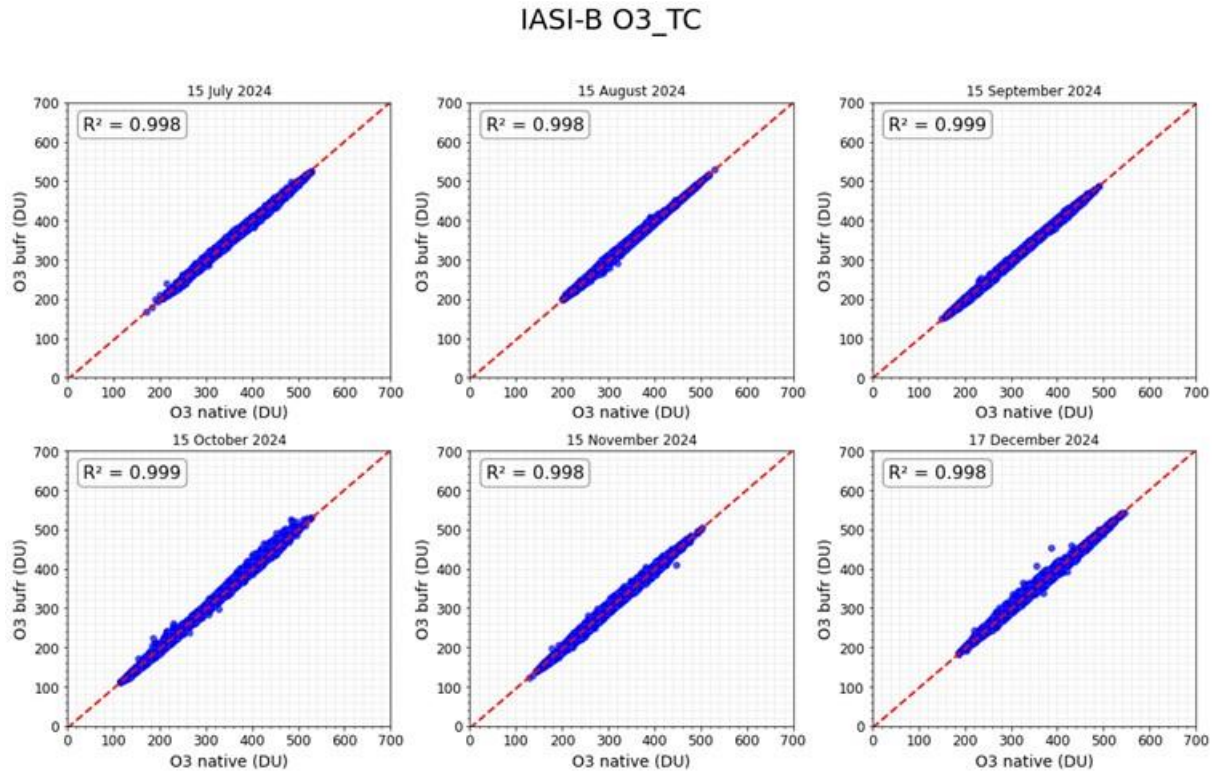


Figure 7.45. Correlation plots of bufr and native total ozone column for IASI/Metop-B for 6 days: July 15th, August 15th, September 15th, October 15th, November 15th and December 17th, 2024. X-axis corresponds to native data (DU) and Y-axis corresponds to bufr data (DU).

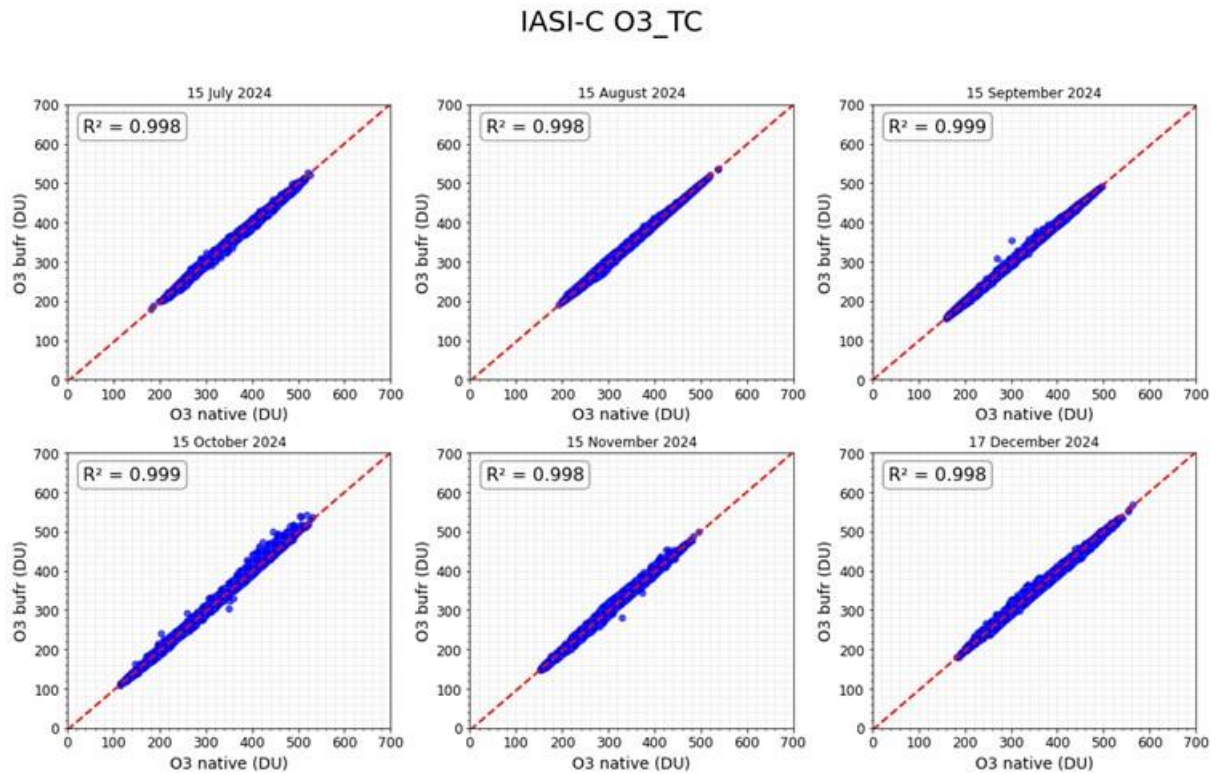


Figure 7.46. Same as Figure 7.45, but for IASI/Metop-C.

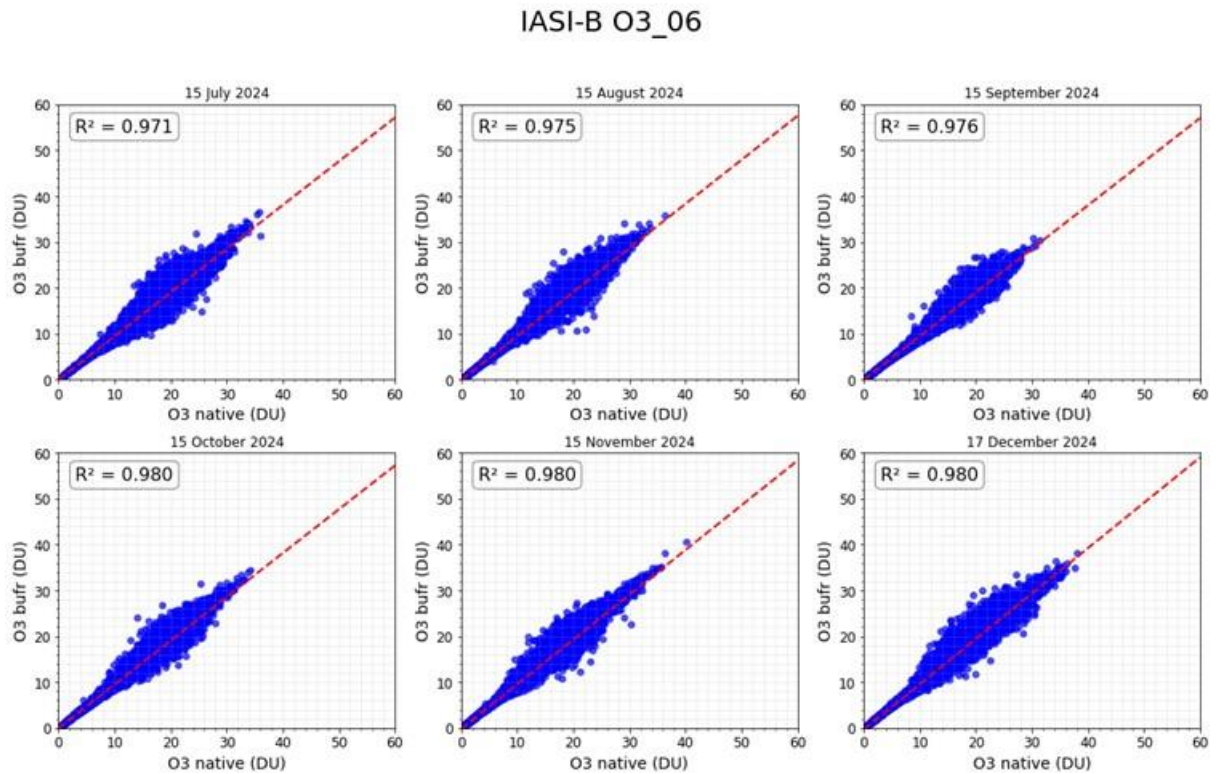


Figure 7.47. Correlation plots of bufr and native 0 – 6 km ozone column for IASI/Metop-B for 6 days: July 15th, August 15th, September 15th, October 15th, November 15th and December 17th, 2024. X-axis corresponds to native data (DU) and Y-axis corresponds to bufr data (DU).

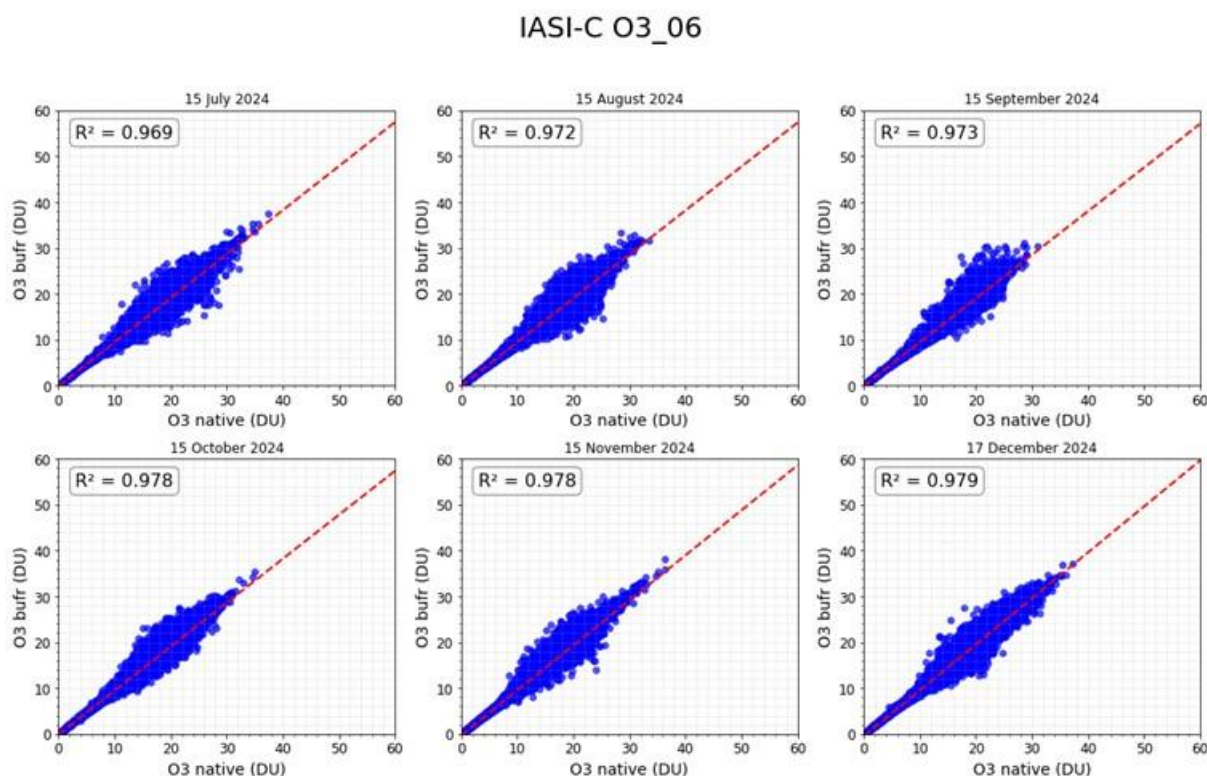


Figure 7.48. Same as Figure 7.47, but for IASI/Metop-C.

IASI HNO₃:

The IASI NRT HNO₃ product (v6.5) has been declared operational on 18 May 2022. Here we present statistical results when comparing the EUMETSAT product disseminated by EUMETCast in BUFR format (NAC, called “bufr” hereinafter) with the native product produced at ULB (FORLI-HNO₃ v20191122, called “native” hereinafter) for 6 days representative of 6 months: July 15th, August 15th, September 15th, October 15th, November 15th and December 17th, 2024, for Metop-B and Metop-C. This allows monitoring if any discrepancy occurs between the two, EUMETSAT and native, products. The data have been filtered following the recommendations of the Product User Manual.

HNO₃ total column is investigated. Detailed statistics for total column between bufr and native data for each of the six days are presented in Table 7.29 - Table 7.34. No critical deviation was found for these dates.

Table 7.29. Statistics for total HNO₃ column between bufr and native data for July 15th 2024

HNO ₃ - 15 July 2024	IASI-B		IASI-C	
	Native	Bufr	Native	Bufr
Individual Pixels	283083	279183	290929	288062
Common Pixels	249475 (88.13 %)		257405 (88.48 %)	
Correlation	0.9994		0.9993	
Total Column Diff - Mean (x10 ¹⁶ molec cm ⁻²)	0.0104 ± 0.0344		0.0089 ± 0.0327	
Total Column Diff - Max (x10 ¹⁶ molec cm ⁻²)	3.2893		1.8402	
Total Column Diff - Min (x10 ¹⁶ molec cm ⁻²)	-7.1416		-10.5982	
Total Column Rel. Diff - Mean (%)	0.9213 ± 1.6025		0.8233 ± 1.4913	
Total Column Rel. Diff - Max (%)	41.0895		30.0752	
Total Column Rel. Diff - Min (%)	-69.0598		-39.1675	

Table 7.30. Same as Table 7.29, but for August 15th 2024

HNO ₃ - 15 August 2024	IASI-B		IASI-C	
	Native	Bufr	Native	Bufr
Individual Pixels	253804	250391	298784	295085
Common Pixels	221838 (87.41 %)		261654 (87.57 %)	
Correlation	0.9963		0.9993	
Total Column Diff - Mean (x10 ¹⁶ molec cm ⁻²)	0.0068 ± 0.1274		0.0070 ± 0.0576	
Total Column Diff - Max (x10 ¹⁶ molec cm ⁻²)	9.3701		2.9726	
Total Column Diff - Min (x10 ¹⁶ molec cm ⁻²)	-41.2086		-16.8684	
Total Column Rel. Diff - Mean (%)	0.7788 ± 2.2018		0.8033 ± 1.5347	
Total Column Rel. Diff - Max (%)	576.2467		28.7453	
Total Column Rel. Diff - Min (%)	-97.6310		-91.7132	

Table 7.31. Same as Table 7.29, but for September 15th 2024

HNO ₃ - 15 September 2024	IASI-B		IASI-C	
	Native	Bufr	Native	Bufr
Individual Pixels	260057	264333	256084	259450
Common Pixels	230067 (88.47 %)		226491 (88.44 %)	
Correlation	0.9995		0.9997	
Total Column Diff - Mean (x10 ¹⁶ molec cm ⁻²)	0.0097 ± 0.0217		0.0089 ± 0.0176	
Total Column Diff - Max (x10 ¹⁶ molec cm ⁻²)	3.8617		2.0236	
Total Column Diff - Min (x10 ¹⁶ molec cm ⁻²)	-1.4225		-0.8341	
Total Column Rel. Diff - Mean (%)	0.9608 ± 1.4402		0.9129 ± 1.3612	
Total Column Rel. Diff - Max (%)	74.1519		24.9671	
Total Column Rel. Diff - Min (%)	-27.7945		-25.5136	

Table 7.32. Same as Table 7.29, but for October 15th 2024

HNO ₃ - 15 October 2024	IASI-B		IASI-C	
	Native	Bufr	Native	Bufr
Individual Pixels	256359	252538	261815	259079
Common Pixels	219547 (85.64 %)		226835 (86.64 %)	
Correlation	0.9997		0.9998	
Total Column Diff - Mean (x10 ¹⁶ molec cm ⁻²)	0.0101 ± 0.0182		0.0089 ± 0.0160	
Total Column Diff - Max (x10 ¹⁶ molec cm ⁻²)	1.4988		1.5274	
Total Column Diff - Min (x10 ¹⁶ molec cm ⁻²)	-0.6673		-0.6233	
Total Column Rel. Diff - Mean (%)	1.0393 ± 1.4493		0.9808 ± 1.3785	
Total Column Rel. Diff - Max (%)	29.6935		26.7894	
Total Column Rel. Diff - Min (%)	-31.2307		-28.3055	

Table 7.33. Same as Table 7.29, but for November 15th 2024

HNO ₃ - 15 November 2024	IASI-B		IASI-C	
	Native	Bufr	Native	Bufr
Individual Pixels	267829	243958	251560	230673
Common Pixels	216653 (80.89 %)		205246 (81.59 %)	
Correlation	0.9991		0.9972	
Total Column Diff - Mean (x10 ¹⁶ molec cm ⁻²)	0.0097 ± 0.0337		0.0076 ± 0.0571	
Total Column Diff - Max (x10 ¹⁶ molec cm ⁻²)	1.1388		1.4256	
Total Column Diff - Min (x10 ¹⁶ molec cm ⁻²)	-11.9992		-17.4483	
Total Column Rel. Diff - Mean (%)	1.0484 ± 1.6316		0.9253 ± 1.4901	
Total Column Rel. Diff - Max (%)	62.4504		25.7026	
Total Column Rel. Diff - Min (%)	-87.3696		-92.5671	

Table 7.34. Same as Table 7.29, but for December 17th 2024

HNO ₃ - 17 December 2024	IASI-B		IASI-C	
	Native	Bufr	Native	Bufr
Individual Pixels	255132	250272	268474	264428
Common Pixels	213811 (83.80 %)		227615 (84.78 %)	
Correlation	0.9994		0.9984	
Total Column Diff - Mean (x10 ¹⁶ molec cm ⁻²)	0.0084 ± 0.0395		0.0063 ± 0.0502	
Total Column Diff - Max (x10 ¹⁶ molec cm ⁻²)	12.5874		1.7990	
Total Column Diff - Min (x10 ¹⁶ molec cm ⁻²)	-1.7753		-16.6427	
Total Column Rel. Diff - Mean (%)	0.9631 ± 2.7121		0.8500 ± 1.4804	
Total Column Rel. Diff - Max (%)	986.6697		21.9427	
Total Column Rel. Diff - Min (%)	-36.4109		-85.4370	

Figure 7.49 and Figure 7.50 present the correlation plots of bufr and native total HNO_3 column, for IASI/Metop-B and IASI/Metop-C, respectively. Correlation coefficients (in blue) are ~ 1 .

So far, the discrepancies are found within the numerical errors inherent to the use of different IT infrastructure.

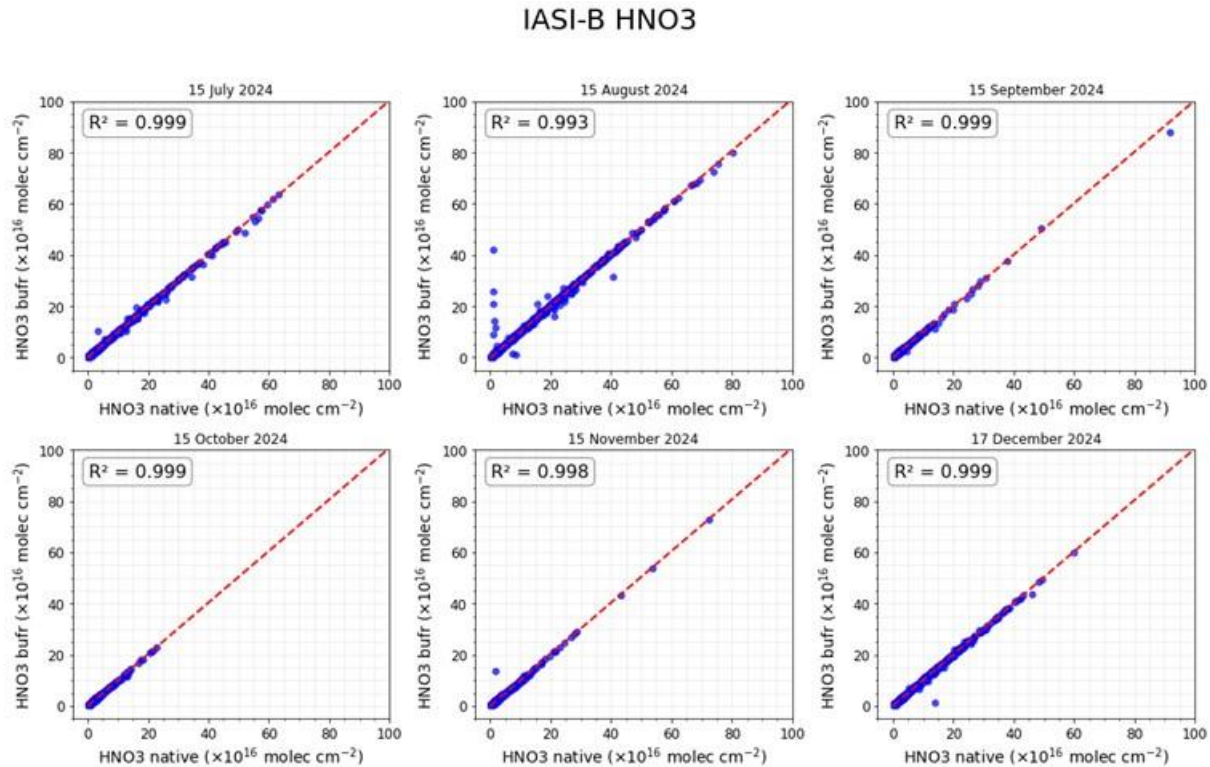


Figure 7.49. Correlation plots of bufr and native total HNO_3 column for IASI/Metop-B for 6 days: July 15th, August 15th, September 15th, October 15th, November 15th and December 17th, 2024. X-axis corresponds to native data (molec. cm^{-2}) and Y-axis corresponds to bufr data (molec. cm^{-2}).

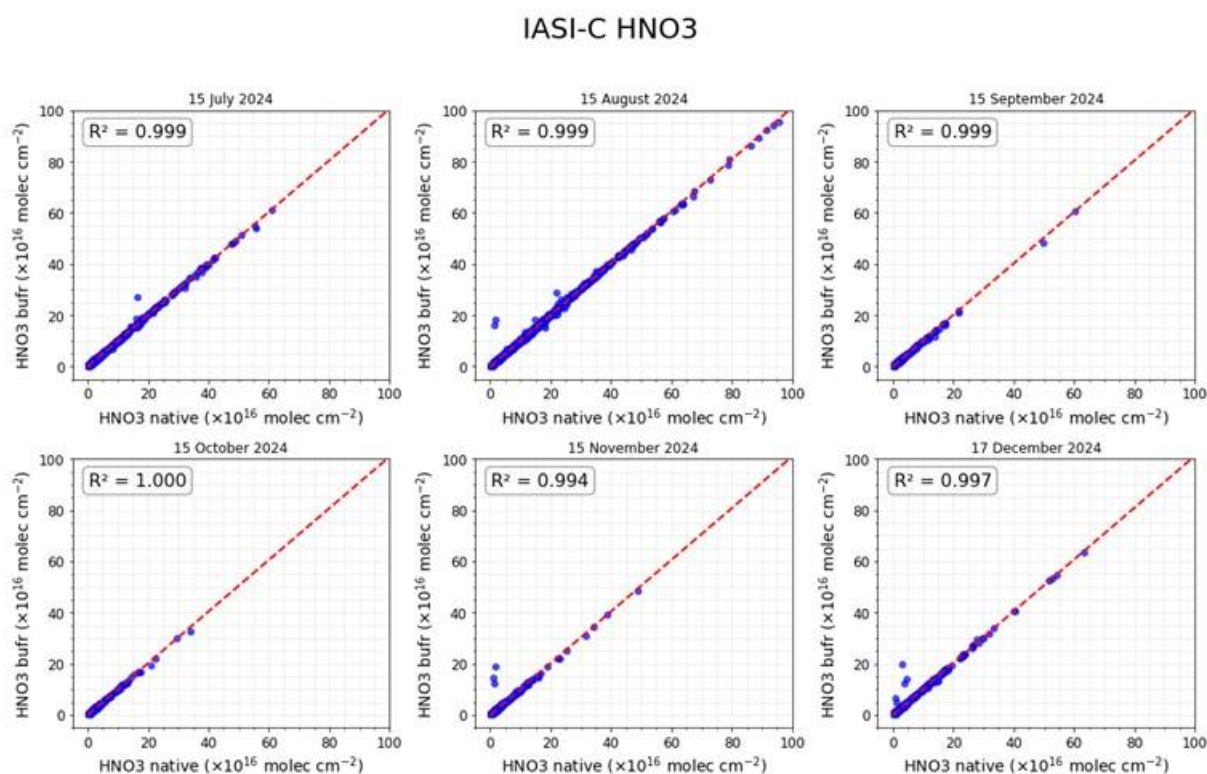


Figure 7.50. Same as Figure 7.49, but for IASI/Metop-C.

Validation with CO FTIR ground-based data

This section presents a comparison between the Metop-B/C IASI CO data and FTIR measurement data available from the NDACC (Network for the Detection of Atmospheric Composition Change) network. The Copernicus Atmosphere Monitoring Service (CAMS) projects supports selected NDACC instruments and PIs for rapid delivery of quality measurements to the NDACC data host ([contract CAMS27](#)). Recent FTIR measurement data is now available for many more sites (in this study data from 24 sites is used).

These ground-based, remote-sensing instruments are sensitive to the CO abundance in the troposphere and lower stratosphere, i.e. between the surface and up to 20 km altitude. CO total columns are validated (from surface to 100 km). A description of the FTIR instruments and retrieval methodology can be found at <https://nors.aeronomie.be>. The typical uncertainty on the FTIR CO column is approximately 3 %, which is also used in the color scale in Figure 7.52.

In this comparison each FTIR measurement is co-located to all IASI measurements within a time difference of 3 hours and within a distance of 50 km to the effective location of the FTIR measurement (this effective location is calculated along the line of sight of the FTIR measurement). The IASI *a priori* is substituted in the FTIR retrieval and subsequently the FTIR retrieved profile with the IASI *a priori* is smoothed using the IASI averaging kernel, as described in Rodgers *et al.*, 2003. In the plots the relative differences are calculated using the latter FTIR columns (smoothed with the IASI averaging kernels). This validation methodology is described in more detail in Ronsmans *et al.*, 2016. All figures for the individual stations can be browsed on <https://cdop.aeronomie.be>.

Table 7.35. Statistics between IASI-B/C and FTIR CO smoothed total columns for the entire time period January 2017 – March 2025 (the column “std” is the standard deviation of the local FTIR columns relative to the standard deviation of the IASI columns)

	Metop-B					Metop-C				
	# meas.	Std.	R	rel. Diff.	Std. Rel. Diff.	# meas.	Std.	R	rel. Diff.	Std. Rel. Diff.
Eureka	928	0.7	0.87	18.2	16.3	33	0.3	0	12.3	21.2
Ny Ålesund	209	0.9	0.91	20.4	8.51	154	0.9	0.94	20.3	7.98
Thule	7083	0.8	0.83	5.83	12.1	4182	0.8	0.85	7.45	11.8
Kiruna	1176	1.1	0.82	-2.96	7.37	720	1.1	0.83	-2.61	6.96
Harestua	217	0.7	0.80	4.80	8.87	215	0.8	0.87	3.29	6.62
St. Petersburg	1329	0.8	0.88	8.45	7.42	652	0.8	0.92	9.44	6.55
Bremen	528	0.8	0.85	8.65	7.55	275	0.9	0.82	8.47	7.42
Garmisch	3028	0.9	0.86	2.35	7.44	1386	0.9	0.89	2.23	6.87
Zugspitze	3815	0.9	0.90	-1.16	6.44	2119	0.9	0.91	-1.36	6.10
Jungraujoch	1836	0.9	0.89	-1.22	6.47	1548	0.9	0.90	-1.48	4.99
Toronto	2136	0.7	0.81	23.1	14.9	1621	0.6	0.84	23.9	14.4
Rikubetsu	109	0.9	0.84	4.76	8.26	74	1.0	0.82	2.29	8.11
Boulder	6773	0.9	0.86	-1.81	8.03	6189	0.9	0.85	-1.57	8.79
Xianghe	2569	0.6	0.84	12.0	14.9	2205	0.6	0.84	10.1	13.1
Tsukuba	519	0.8	0.81	7.22	9.94	355	0.9	0.88	5.22	6.99
Izana	1137	1.0	0.95	-0.47	4.21	573	0.9	0.96	0.80	4.41
Mauna Loa	1526	1.1	0.99	-0.80	2.81	632	1.1	0.99	-0.71	2.76
Altzomoni	1579	1.1	0.96	4.38	4.30	1027	1.1	0.96	4.17	4.53
Paramaribo	119	0.9	0.92	9.00	4.57	35	0.8	0.83	7.89	5.91
Porto Velho	278	0.9	0.98	9.82	6.64	-	-	-	-	-
La Reunion Mado	3426	1.0	0.99	4.78	3.81	1621	1.0	0.99	5.43	3.77
Wollongong	2885	0.8	0.93	7.64	8.20	2060	0.8	0.94	7.53	8.13
Lauder	3939	0.8	0.94	10.2	6.96	2836	0.9	0.96	9.96	6.21
Arrival Heights	700	0.9	0.93	16.7	8.48	559	0.9	0.93	15.6	8.54
Average for all sites		0.9	0.89	7.08	8.10		0.9	0.86	6.46	7.92

The correlation coefficients of the Taylor diagrams (Figure 7.51 and Table 7.35) are generally ranging from ~0.8 to nearly 1, showing a very good agreement between the IASI and FTIR data, for Metop-B and Metop-C. However, some sites are special:

1. Rikubetsu, Ny Ålesund, Paramaribo and Harestua have only a few co-located measurements and are statistically less relevant
2. Toronto has a lower correlation although the site has many co-locations. This may be due to some co-locations where the IASI concentration is much higher than observed by the FTIR and probably related to false co-locations during fire events. The FTIR time-series seems to suffer from outliers being too low.
3. At Kiruna, Thule and Eureka the satellite underestimates the CO columns by up to 30 % during the early spring weeks and is related to a reduced sensitivity of the IASI CO product during local spring.

The Taylor diagrams in Figure 7.51 and statistics in Table 7.35 also show that the standard deviations of the FTIR columns values are smaller compared the satellite standard deviation probably due to higher noise on the satellite time-series. Almost all site points are shifted left of the satellite reference, typically with a factor of 0.8 to 1 of the standard deviation of the satellite CO columns.

Figure 7.52 shows the time-series of bi-weekly mean relative differences for the time period January 2017 – March 2025. Red indicates a positive bias (IASI > NDACC) while blue indicates an underestimation of the satellite retrievals. The chosen color scale is based on the FTIR typical uncertainty. The IASI retrieval uncertainty should be added (typically around 4 %), so only biases above 5 % are to be considered significant. In the Northern Hemisphere a seasonal changing bias is observed: overestimation during summer and underestimation during winter months. A similar seasonal dependence but less pronounced is observed in the Southern Hemisphere. A longer time period is required to study this seasonal dependence in more detail.

We can conclude that for most of the 24 stations included in the comparison, mean relative differences, or biases, are less than 10 % (see the individual station plots at <https://cdop.aeronomie.be> under Validation Results). For the Eureka, Ny Ålesund and Arrival Heights stations, located at high latitudes, biases are larger. A similar bias is found by Buchholz *et al.* (2017) when comparing with MOPITT data. When looking at the stations between -60° and 60°, the Toronto station shows the largest biases (mean bias ± 20 %) which seems to be due to outliers.

The IASI data are generally overestimating with the overall bias of approx. 7 % being off the same order as the reported combined total uncertainty of 5 % (Table 7.35).

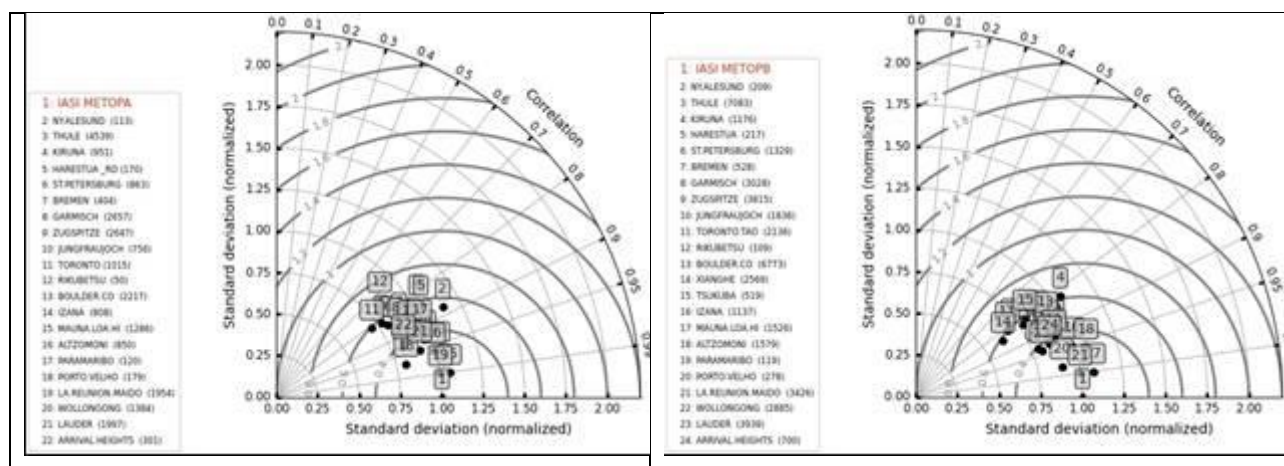


Figure 7.51. Correlation plots for IASI-B (left) and IASI-C (right) CO total columns against 23 NDACC FTIR sites (Eureka is left out due to low measurement count for Metop-C). The stations are slightly shifted to the left, indicating that the satellite time-series has a higher standard deviation (more noisy).

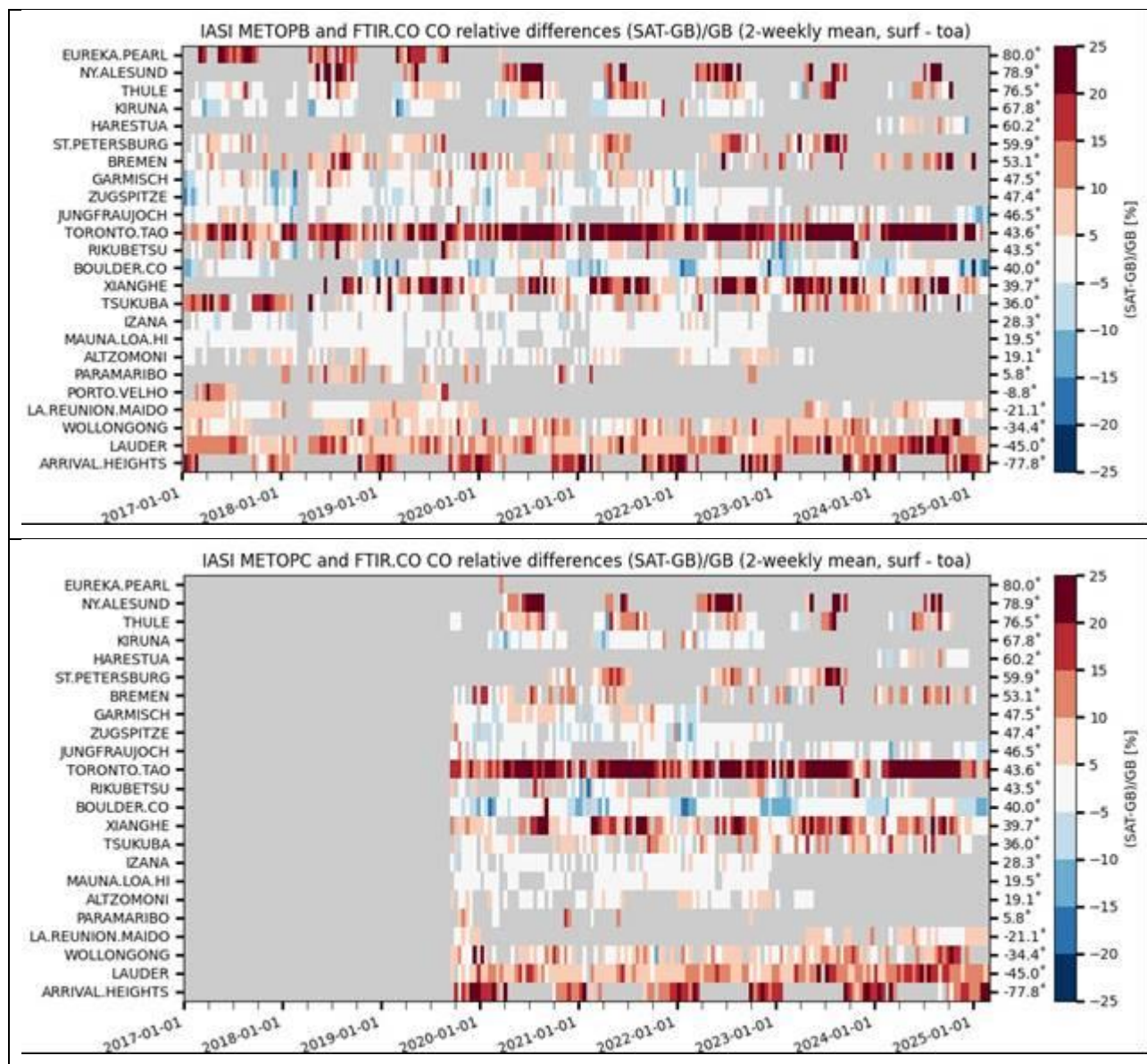


Figure 7.52. Time-series of bi-weekly relative difference for IASI-B (top) and IASI-C (bottom). The Metop-C relative bias time-series seems to correspond closely to the Metop-B time-series.

Acknowledgements: The data used in this publication were obtained as part of the Network for the Detection of Atmospheric Composition Change (NDACC) and are publicly available. Rapid delivery of NDACC data is partly supported by the CAMS-27 data procurement service contracted by ECMWF for the validation of the Copernicus Atmospheric Monitoring Service (CAMS).

References:

Buchholz, R. R., Deeter, M. N., Worden, H. M., Gille, J., Edwards, D. P., Hannigan, J. W., Jones, N. B., Paton-Walsh, C., Griffith, D. W. T., Smale, D., Robinson, J., Strong, K., Conway, S., Sussmann, R., Hase, F., Blumenstock, T., Mahieu, E., and Langerock, B.: Validation of MOPITT carbon monoxide using ground-based Fourier transform infrared spectrometer data from NDACC, Atmos. Meas. Tech., 10, 1927-1956, 2017.

<https://doi.org/10.5194/amt-10-1927-2017>

Rodgers, C. D., and Connor, B. J.: Intercomparison of remote sounding instruments, J. Geophys. Res., 108, 4116-4129, 2003.

<https://doi.org/10.1029/2002JD002299>

Ronsmans, G., Langerock, B., Wespes, C., Hannigan, J. W., Hase, F., Kerzenmacher, T., Mahieu, E., Schneider, M., Smale, D., Hurtmans, D., De Mazière, M., Clerbaux, C., and Coheur, P.-F.: First characterization and validation of FORLI-HNO₃ vertical profiles retrieved from IASI/Metop, Atmos. Meas. Tech., 9, 4783-4801, 2016.

<https://doi.org/10.5194/amt-9-4783-2016>

Validation with HNO₃ FTIR ground-based data

This section presents a comparison between the Metop-B/C IASI HNO₃ data (released Dec 2019) and FTIR measurement data available from the NDACC (Network for the Detection of Atmospheric Composition Change) network.

These ground-based, remote-sensing instruments are sensitive to the HNO₃ abundance in the stratosphere. A description of the FTIR instruments and retrieval methodology can be found at <https://nors.aeronomie.be>, and in <https://www2.acom.ucar.edu/irwg/links> (IRWG retrieval guidelines). The typical uncertainty on the FTIR columns is of the order of 10%, which is also used in the color scale in Figure 7.54. More details on the comparison methodology can be found in the dedicated validation report with reference

[SAF/AC/IASB/VR/HNO3/ValidationReport_HNO3_ORR_MetopB/C](#).

Table 7.36. Statistics between IASI-B/C and FTIR HNO₃ smoothed total columns for the entire time period Dec 2019 – Dec 2024 (the column “std” is the standard deviation of the local FTIR columns relative to the standard deviation of the IASI columns)

	Metop-B					Metop-C				
	# meas.	Std.	R	rel. Diff.	Std. Rel. Diff.	# meas.	Std.	R	rel. Diff.	Std. Rel. Diff.
Eureka	112	1.1	0.90	2.38	11.4	103	1.1	0.91	-1.30	10.3
Ny Ålesund	14	1.2	0.80	-11.1	6.97	14	1.0	0.46	-13.0	11.8
Thule	1876	1.0	0.90	-2.69	9.11	1858	1.1	0.88	-3.20	9.42
Kiruna	1142	1.0	0.95	11.0	8.59	1138	1.0	0.95	10.2	8.30
Harestua	258	0.8	0.95	16.8	7.38	255	0.9	0.95	16.8	6.95
St. Petersburg	830	0.9	0.95	16.2	8.16	825	1.0	0.96	14.3	8.00
Bremen	74	0.9	0.87	23.6	10.4	2478	1.0	0.88	24.5	13.0
Zugspitze	2478	1.0	0.87	26.2	13.1	1428	0.8	0.92	17.2	8.16
Jungraujoch	1415	0.9	0.92	19.3	8.32	2668	0.8	0.89	17.8	12.6
Toronto	2723	0.8	0.89	19.5	12.1	78	0.9	0.92	8.82	9.37
Rikubetsu	74	0.9	0.90	11.4	9.96	463	0.8	0.94	18.3	10.2
Tsukuba	473	0.9	0.93	18.6	10.5	807	0.9	0.85	13.8	11.1
Izana	837	0.9	0.83	16.0	10.8	968	1.0	0.85	17.9	11.1
Mauna Loa	957	1.1	0.84	19.2	11.8	139	0.7	0.71	21.8	12.7
Altzomoni	90	0.5	0.51	29.2	19.3	110	0.6	0.70	20.1	21.0
Maido	31	0.7	0.68	19.2	8.13	28	1.3	0.71	16.0	6.23
Wollongong	551	0.8	0.92	22.6	9.85	542	0.9	0.90	20.7	9.43
Lauder	3012	0.8	0.89	25.4	11.4	2961	0.8	0.88	23.5	11.3
Arrival Heights	851	1.0	0.92	-4.59	13.4	842	1.0	0.92	-5.99	12.6

		0.91	0.86	14.7	10.6		0.92	0.85	12.5	10.7
--	--	------	------	------	------	--	------	------	------	------

The correlation coefficients of the Taylor diagrams (Figure 7.53 and Table 7.36) are generally ranging from ~0.8 to nearly 1, showing a very good agreement between the IASI and FTIR data, for Metop-B and Metop-C. However, some sites are special:

1. Ny Ålesund, Toronto and Mado have only a few co-located measurements and are statistically less relevant.
2. Higher biases are observed in the Southern hemisphere (Wollongong and Lauder).
3. High latitude sites have a nearly vanishing bias (compared to the FTIR uncertainties) while mid-latitude sites have a positive bias of the order of 20%, which confirms the conclusions from the validation report revealing a dependence of the bias on the absolute column values.

The Taylor diagrams in Figure 7.53 and statistics in Table 7.36 also show that the standard deviations of the FTIR columns values are smaller compared the satellite standard deviation probably due to higher noise on the satellite time-series. Almost all site points are shifted left of the satellite reference, typically with a factor of 0.75 to 1 of the standard deviation of the satellite columns.

Figure 7.54 shows the time-series of bi-weekly mean relative differences for the time period Dec 2019 – Dec 2024. Red indicates a positive bias (IASI > NDACC) while blue indicates an underestimation of the satellite retrievals. The chosen color scale is based on the FTIR typical uncertainty.

The statistics reveal an overall bias of approx. 20 % for mid-latitudes and tropical sites (the combined total uncertainty on the bias is of the order of 15 %) and nearly vanishing bias at high latitude sites (Table 7.36). For all of the 19 stations included in the comparison, mean relative differences, or biases, are less than the target threshold of 35 % but larger than the optimal threshold of 10 %.

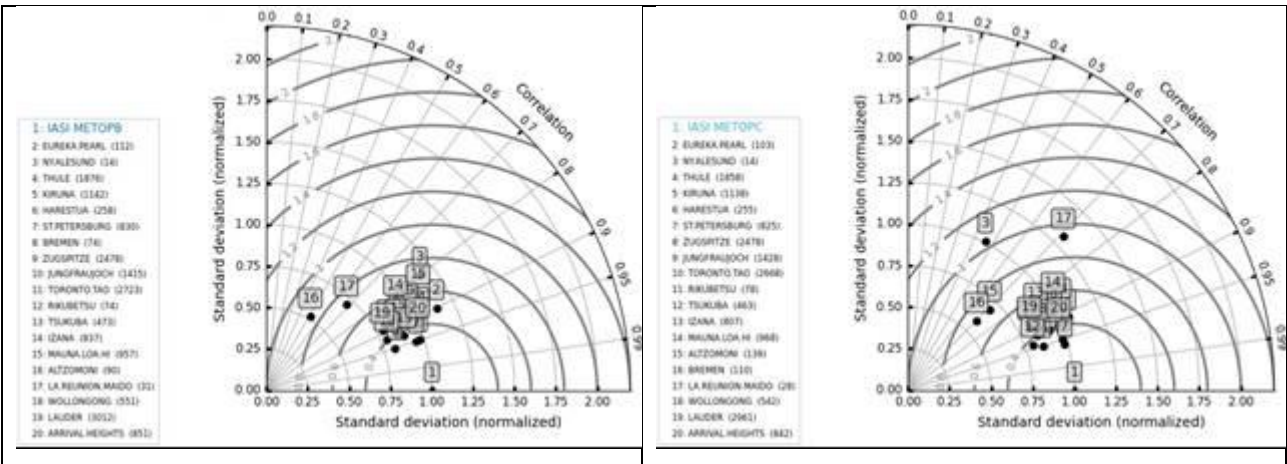


Figure 7.53. Correlation plots for IASI-B (left) and IASI-C (right) HNO_3 total columns against 19 NDACC FTIR sites. The stations are slightly shifted to the left, indicating that the satellite time-series has a higher standard deviation (more noisy).

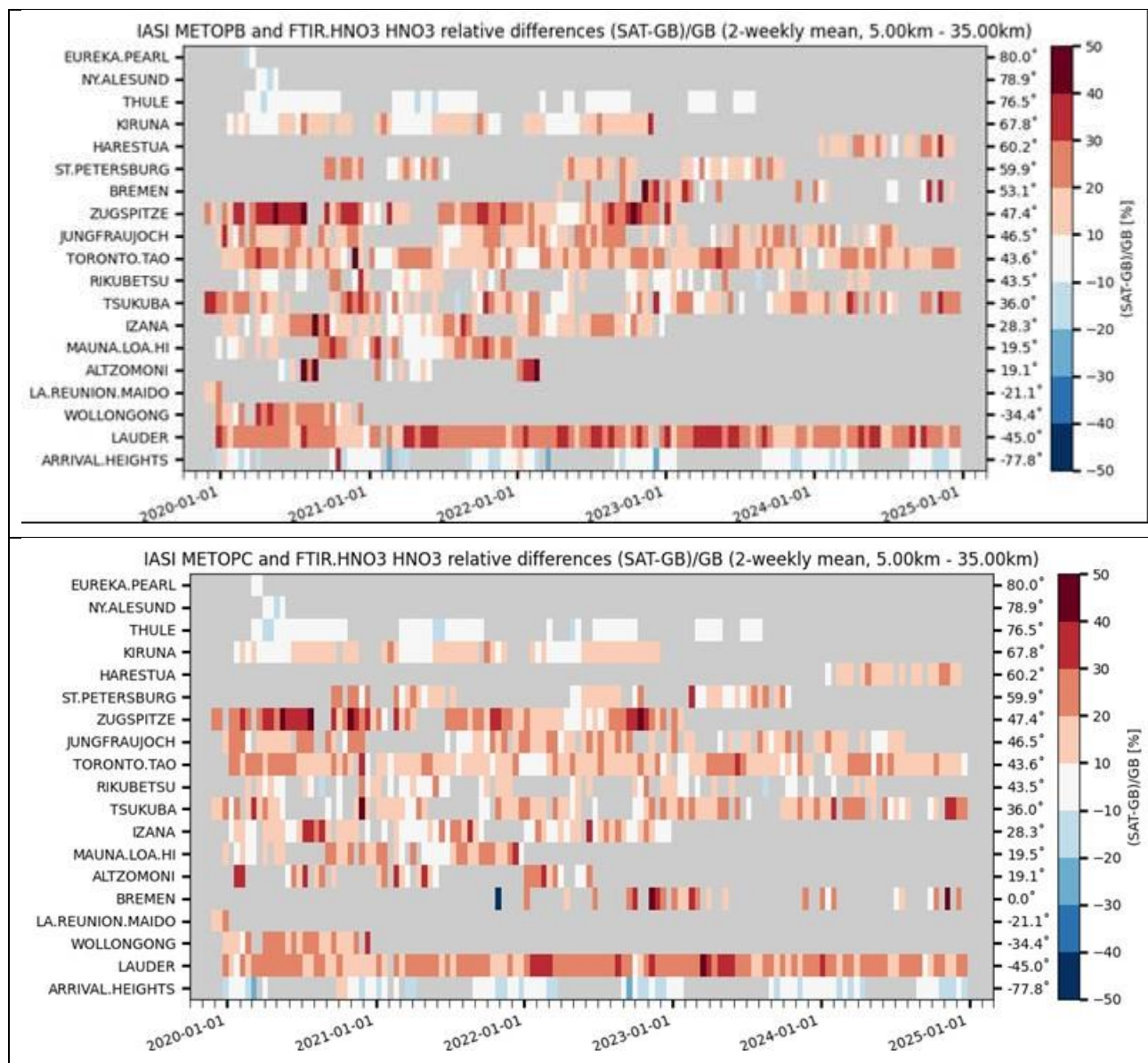


Figure 7.54. Time-series of bi-weekly relative difference for IASI-B (top) and IASI-C (bottom). The Metop-C relative bias time-series seems to correspond closely to the Metop-B time-series.

Acknowledgements: The data used in this publication were obtained as part of the Network for the Detection of Atmospheric Composition Change ([NDACC](#)) and are publicly available.

8. List of AC SAF users

The institutes of registered users of AC SAF products are listed below.

8.1. FMI archive

Europe:

Armenia:

- ICHD

Austria:

- Central Institute for Meteorology and Geodynamics
- Private individual
- Sistema GmbH
- University of Veterinary Medicine
- University of Vienna (2 users)

Belarus:

- National Academy of Sciences
- State University

Belgium:

- BIRA-IASB (2 users)
- Flanders Marine Institute
- Ghent University (15 users)
- Karel de Grote University College
- KMI (4 users)
- KU Leuven
- Novigo+
- Private individual
- ULB (3 users)

Bulgaria:

- Bulgarian Academy of Science
- Space Research and Technology Institute (2 users)

Croatia:

- J. J. Strossmayer University of Osijek

Czech Republic:

- Czech Hydrometeorological Institute (4 users)
- Global Change Research Institute

Denmark:

- Aarhus University (2 users)
- DMI (3 users)
- DTU Compute

Estonia:

- Estonian Environment Agency
- Intertrust

Finland:

- FMI (11 users)
- Häme University of Applied Sciences
- University of Helsinki (3 users)

France:

- AERIS/ICARE
- Aix-Marseille University
- CNRS (3 users)
- Grenoble Alpes University
- Laboratory of Atmospheric Optics
- Lasem
- LATMOS
- LISA (2 users)
- LISA-CNRS
- LSCE-IPSL-CNRS
- Météo France (5 users)
- Mines Paristech
- ONERA
- Open University
- Private Individual (2 users)
- Reuniwatt
- Sistema
- Sorbonne University
- Université Claude Bernard
- University of Reunion (2 users)
- University of Lille
- University of Paris Est Creteil

Germany:

- Brandenburg University of Technology
- DLR (3 users)
- DWD (4 users)
- EUMETSAT (24 users)
- Federal Office for Radiation Protection
- Forschungszentrum Jülich GmbH (5 users)
- Fraunhofer Institute
- Fraunhofer IOSB
- Gymnasium Olching
- Oldenburg University
- Potsdam Institute for Climate Impact Research
- Private Individual (2 users)
- Max Planck Institute for Chemistry (5 users)
- Sabrina Szeto Consulting
- Synwer GmbH
- Technical University of Munich
- University of Bremen (5 users)

- University of Cologne
- University of Hildesheim
- University of Konstanz
- University of Münster
- University of Potsdam

Greece:

- AUTH (5 users)
- Eratosthenes Centre of Excellence
- Hellenic Centre for Marine Research
- IESL/FORTH
- National and Kapodistrian University of Athens
- National Technical University of Athens (2 users)
- Private Individual
- Technical University of Crete
- University of Athens (2 users)
- University of the Aegean
- University of Crete (2 users)

Hungary:

- Eötvös Loránd University (2 users)
- Hungarian Academy of Sciences
- Hungarian Meteorological Service (2 users)
- Individual
- University of Szeged

Ireland:

- Trinity College Dublin

Italy:

- ARPA Valle d'Aosta
- B-Open Solutions S.r.l. (2 users)
- CNR (3 users)
- European Space Agency
- fabbricadigitale
- IFAC-CNR (2 users)
- Julia Wagemann Consulting
- LaMMA Consortium (2 users)
- MEE0 (3 users)
- National Institute for Astrophysics
- Private Individual (2 users)
- Regional Environmental Protection Agency Calabria
- University of Bologna (2 users)
- University of Milan
- University of Modena and Reggio Emilia
- University of Venice

Latvia:

- Latvian Environment, Geology and Meteorology Centre

Lithuania:

- Lithuanian National Meteorological Service
- Vilnius University

Malta:

- University of Malta

The Netherlands:

- BESSR
- Delft University of Technology
- ESA
- KNMI (6 users)
- Leiden University
- S[&]T Corporation (2 users)
- Wageningen University & Research (2 users)

Norway:

- Norwegian Institute for Air Research (2 users)
- UiT The Arctic University of Norway

Poland:

- CloudFerro
- IMGW
- Institute of Environmental Protection (2 users)
- Institute of Geodesy and Cartography
- Military University of Technology
- O3Lab
- University of Warsaw

Portugal:

- Instituto Dom Luiz
- Instituto Português do Mar e da Atmosfera (4 users)
- University of Aveiro
- University of Lisbon
- University of Trás-os-Montes and Alto Douro (2 users)

Republic of North Macedonia:

- Hydrometeorological Service

Romania:

- Babes-Bolyai University (3 users)
- Global Top Systems
- INCAS
- INOE (2 users)
- National Meteorological Administration (2 users)
- University of Galați (3 users)
- Politehnica University of Bucharest

Russia:

- Altai State University
- Daghestan Scientific Centre of Russian Academy of Sciences

- Federal Research Center Krasnoyarsk Scientific Center of the Siberian Branch of the RAS (2 users)
- Fedorov Institute of Applied Geophysics
- IG RAS
- Institute of Atmospheric Physics
- Institute of Computational Modeling of the Siberian Branch of the RAS
- Institute of Global Climate and Ecology
- Irkutsk State Transport University
- Moscow State University
- Planeta (3 users)
- Research Center of Ecological Safety
- Roscosmos
- St. Petersburg State University
- Tomsk State University of Control Systems and Radioelectronics
- V.E. Zuev Institute of Atmospheric Optics

Serbia:

- Geographical institute “Jovan Cvijic”, SASA

Slovakia:

- Private Individual

Slovenia:

- Bide-san, s.p.

Spain:

- Autonomous University of Barcelona
- Barcelona Supercomputing Center
- Basque Meteorology Agency
- Complutense University of Madrid
- CREAM-CSIC-UAB
- GREA
- I.E.S. Punta del Verde
- Modeliza
- NAITEC (2 users)
- Pablo de Olavide University
- Polytechnic University of Catalonia (2 users)
- Private Individual
- State Meteorological Agency (2 users)
- University of Alicante
- University of Barcelona (3 users)
- University of the Basque Country
- University of Extremadura
- University of Granada (2 users)
- University of Málaga
- University of Oviedo
- University of Valencia (3 users)
- University of Valladolid (2 users)

Sweden:

- Blackebergs Gymnasium
- NBI/Handelsakademin
- SMHI (5 users)

Turkey:

- Cukurova University
- Hacettepe University
- Istanbul University
- Middle East Technical University
- Turkish State Meteorological Service (2 users)
- Van Yüzüncü Yıl University

Ukraine:

- Batata LLC
- Scientific Centre for Aerospace Research of the Earth
- Taras Shevchenko National University of Kyiv
- UHE LED LLC
- UHMC
- Ukrainian Hydrometeorological Institute (3 users)

United Kingdom:

- Aggreko
- Atheras Analytics
- ECMWF (2 users)
- ESA
- IDEMS International
- London School of Economics and Political Science
- Office of National Statistics
- Private individual
- Rutherford Appleton Lab (2 users)
- Satavia Ltd.
- Satellite Applications Catapult
- Science and Technology Facilities Council (2 users)
- siHealth Ltd.
- University College London
- University of Cambridge
- University of Edinburgh
- University of Hertfordshire
- University of Leeds (2 users)
- University of Leicester
- University of Manchester
- University of Oxford
- University of Sheffield
- University of York

Asia:

Afghanistan:

- Vortil Co. Ltd.

Bangladesh:

- Institute of Forestry and Environmental Sciences
- Stamford University
- University of Dhaka

China:

- Anhui Institute of Optics and Fine Mechanics (2 users)
- Anhui Institute of Meteorological Sciences
- Anhui Normal University
- Beijing Municipal Environmental Monitoring Center
- Beijing Normal University (4 users)
- Beijing Zhixin Remote Sensing Geographic Information Co., Ltd
- Chengdu University of Information Technology
- China Academy of Sciences (8 users)
- China Meteorological Administration
- China University of Geosciences
- China University of Mining and Technology (6 users)
- Chinese Academy of Meteorological Sciences (3 users)
- East China University of Science and Technology
- Fudan University
- Guangzhou University
- Hebei University of Engineering (2 users)
- HTHJ
- Institute of Atmospheric Physics (3 users)
- Institute of Desert Meteorology
- Institute of Earthquake Forecasting
- Institute of Remote Sensing and Digital Earth (3 users)
- Jiangsu Meteorological Observatory
- Jiangsu Normal University (2 users)
- Jilin University
- Lanzhou University (2 users)
- Lanzhou Jiaotong University
- Nanjing University
- Nanjing University of Information Science & Technology (7 users)
- National Satellite Meteorological Center
- National University of Defense Technology
- Northeast Normal University
- Northwest Normal University
- Peking University (6 users)
- Private Individual
- “School”
- Shanghai University (2 users)
- Shenzhen University

- Southern University of Science and Technology (4 users)
- State Environmental Protection Key Lab of Satellite Remote Sensing
- Sun Yat-Sen University (2 users)
- The Chinese University of Hong Kong (2 users)
- The Institute of Atmospheric Physics (3 users)
- Tsinghua University (2 users)
- (unknown) (4 users)
- University of Science and Technology (5 users)
- Wuhan University (8 users)
- Xiamen University
- Zhejiang University (3 users)

India:

- Anna University
- Aryabhata Research Institute of Observational Sciences
- Banaras Hindu University
- Birla Institute of Technology
- Bose Institute
- Council of Scientific and Industrial Research
- CSIR-NIO
- CSIR-NPL
- Dibrugarh University
- “Education”
- IIT KGP
- Indian Institute of Remote Sensing
- Indian Institute of Science
- Indian Institute of Technology Delhi
- Indian Institute of Technology Kharagpur (4 users)
- Indian Institute of Technology Roorkee (2 users)
- Indian Institute of Tropical Meteorology (3 users)
- Indian Space Research Organization (3 users)
- Jawaharlal Nehru Technological University, Kakinada
- Jawaharlal Nehru University
- Malaviya National Institute of Technology Jaipur
- Mangalore University
- MSRIT
- National Atmospheric Research Laboratory (2 users)
- National Centre for Medium Range Weather Forecasting
- National Institute of Technology
- National Remote Sensing Centre
- Savitribai Phule Pune University (2 users)
- School of Planning and Architecture, Bhopal
- SIG
- Sriram Engineering College
- SRM Institute of Science and Technology
- University of Calcutta
- University of Hyderabad

- University of Kalyani
- Vikram Sarabhai Space Centre (2 users)
- Vindhyan Ecology and Natural History Foundation

Indonesia:

- Bandung Institute of Technology
- Meteorological, Climatological, and Geophysical Agency (3 users)
- National Institute for Aeronautics and Space
- Sumatera Institute of Technology

Iran:

- Sepehr Payesh

Japan:

- Chiba University
- Ibaraki University
- Japan Meteorological Agency
- Kyushu University
- National Institute for Environmental Studies
- Waseda University

Malaysia:

- Malaysian Meteorological Department
- Malaysian Space Agency
- National University of Malaysia (5 users)

Myanmar:

- Yangon Technological University

Nepal:

- International Centre for Integrated Mountain Development (2 users)
- Institute for Advanced Sustainability Studies
- Institute of Tibetan Plateau Research
- Institute of Engineering

Pakistan:

- University of the Punjab
- National University of Sciences & Technology

Philippines:

- Manila Observatory

Singapore:

- National University of Singapore (2 users)

South Korea:

- Chungnam National University (3 users)
- Gwangju Institute of Science and Technology (4 users)
- Hankuk University of Foreign Studies
- Korea Meteorological Administration (2 users)
- Korea Polar Research Institute
- National Institute of Environmental Research (2 users)

- National Meteorological Satellite Center (4 users)
- Pukyong National University
- Yonsei University (3 users)
- Kongju National University
- Seoul National University

Sri Lanka:

- Central Environmental Authority
- Private Individual

Taiwan:

- Academia Sinica
- Garmin
- National Central University (3 users)
- National Taipei University
- National Taiwan University
- Research Center for Environmental Changes

Thailand:

- Asian Institute of Technology
- King Mongkut's Institute of Technology Ladkrabang

Vietnam:

- University of Science (2 users)

Middle East:

Iran:

- Atmospheric Science & Meteorological Research Center
- Islamic Azad University
- Tabriz University
- "University"
- University of Tehran
- Unknown

Iraq:

- Al Iraqia University
- Mustansiriyah University

Israel:

- Israel Institute for Biological Research
- University of Tel Aviv (2 users)

Oman:

- Sultan Qaboos University

Saudi Arabia:

- King Abdullah University of Science and Technology (2 users)
- Private individual

United Arab Emirates:

- Amity University
- Khalifa University

- Uruk Engineering & Contracting

North America:

Canada:

- Canadian Space Agency
- Dalhousie University
- Environment and Climate Change Canada
- Environment Canada
- University of Saskatchewan

United States of America:

- Caltech
- Colorado State University
- Department of Defence
- EMDO Lab
- Florida State University
- Harvard-Smithsonian Center for Astrophysics
- Intertek
- Joint Center for Satellite Data Assimilation
- Michigan Technological University (5 users)
- Mote Marine Laboratory
- NASA (2 users)
- Naval Research Laboratory
- NOAA
- Northeastern University
- Princeton University
- Private Individual
- SpaceKnow Inc.
- Texas A&M University
- The Aerospace Corporation
- Trinity Consultants Inc.
- University of Alabama in Huntsville
- University of Alaska (2 users)
- University of Arizona
- University of California (4 users)
- University of Central Florida
- University of Colorado Boulder
- University of Kansas
- University of Maryland (2 users)
- University of North Carolina at Chapel Hill
- University of Tennessee
- University of Washington
- Unknown
- USGS
- U.S. Environmental Protection Agency

South America:

Argentina:

- National Space Activities Commission
- Universidad Nacional de Córdoba
- Universidad Nacional de Rosario

Brazil:

- Agência Pernambucana de Águas e Clima
- APAC
- Federal University of Pernambuco (2 users)
- LAPIS
- Universidade Federal de Alagoas

Chile:

- University of the Americas

Colombia:

- Universidad EAFIT

Ecuador:

- Universidad San Francisco de Quito (2 users)

Guatemala:

- ASEFOR
- INSIVUMEH

Mexico:

- Ibero Puebla
- Instituto Politecnico Nacional

Paraguay:

- Universidad San Carlos

Peru:

- Servicio Nacional de Meteorología e Hidrología del Perú

Uruguay:

- Universidad de la República

Australia / New Zealand:

- Bureau of Meteorology
- Massey University
- University of Canterbury (3 users)
- University of Melbourne (2 users)
- University of Southern Queensland (2 users)
- University of Sydney

Africa:

Algeria:

- CTS/ASAL
- Meteo Algeria

Cameroon:

- African Institute for Mathematical Sciences

Democratic Republic of the Congo:

- University of Kinshasa

Egypt:

- Egyptian Meteorological Authority (3 users)
- National Research Institute of Astronomy and Geophysics

Eritrea:

- Department of Environment

Ethiopia:

- Addis Ababa University
- Bahir Dar University

Ghana:

- Ghana Meteorological Agency
- Kwame Nkrumah University of Science and Technology
- University of Energy and Natural Resources

Morocco:

- Abdelmalek Essaadi University
- EM5D
- Maroc Météo
- University of Hassan II Casablanca

Nigeria:

- Abdou Moumouni University
- Federal University Lafia
- Federal University of Technology Akure

South Africa:

- National Chemical Emergency Centre
- North-West University
- South African Weather Service (2 users)
- Stellenbosch University
- University of KwaZulu-Natal
- University of Pretoria (2 users)
- University of the Witwatersrand

Registered users: **722**

8.2. DLR archive

Europe:

Austria:

- University of Veterinary Medicine
- University of Vienna

Belarus:

- National Academy of Sciences

Belgium:

- Antea Group
- BIRA-IASB (6 users)
- Flanders Marine Institute
- Ghent University (11 users)
- KMI (3 users)
- Novigo+
- ULB (4 users)

Bulgaria:

- Space Research and Technology Institute (2 users)

Cyprus:

- The Cyprus Institute

Czech Republic:

- Charles University
- Czech Hydrometeorological Institute (5 users)
- Global Change Research Institute

Denmark:

- Aarhus University (2 users)
- DTU Compute

Estonia:

- Estonian Environment Agency
- Intertrust

Finland:

- FMI (10 users)
- Häme University of Applied Sciences

France:

- AERIS/ICARE
- Aix-Marseille University
- CNRS (3 users)
- Grenoble Alpes University
- Institute of Environmental Geosciences
- Laboratory of Atmospheric Optics
- Lasem
- LATMOS (3 users)
- LISA
- LISA-CNRS
- LSCE-IPSL-CNRS
- Météo France (4 users)
- Mines Paristech
- Open University
- Reuniwatt

- Sistema
- Sorbonne University
- Université Claude Bernard
- University of Reunion (2 users)

Germany:

- Brandenburg University of Technology
- DLR (4 users)
- DWD (2 users)
- EUMETSAT (21 users)
- Forschungszentrum Jülich GmbH (3 users)
- Fraunhofer Institute
- Gymnasium Olching
- Heidelberg University
- Karlsruhe Institute of Technology (3 users)
- Max Planck Institute for Chemistry (4 users)
- Potsdam Institute for Climate Impact Research
- Private Individual (2 users)
- Sabrina Szeto Consulting
- Technical University of Munich
- University of Augsburg
- University of Bremen (8 users)
- University of Cologne (2 users)
- University of Hildesheim
- University of Münster

Greece:

- AUTH (4 users)
- Eratosthenes Centre of Excellence
- Hellenic Centre for Marine Research
- IESL/FORTH
- National and Kapodistrian University of Athens
- National Technical University of Athens (2 users)
- Private Individual
- Technical University of Crete
- University of Athens (2 users)
- University of Crete (2 users)

Hungary:

- Hungarian Meteorological Service (3 users)
- Individual
- University of Szeged

Ireland:

- Trinity College Dublin

Italy:

- B-open Solutions S.r.l. (2 users)
- CNR (2 users)

- fabbricadigitale
- IFAC-CNR
- Italian National Research Council
- Julia Wagemann Consulting
- LaMMA Consortium
- MEE0 (3 users)
- National Institute of Geophysics and Volcanology
- Private Individual
- Regional Environmental Protection Agency Calabria
- University of Bologna
- University of Modena and Reggio Emilia
- University of Venice

Latvia:

- Latvian Environment, Geology and Meteorology Centre

Lithuania:

- Lithuanian National Meteorological Service

Malta:

- University of Malta

The Netherlands:

- BESSR
- Delft University of Technology
- KNMI (7 users)
- Leiden University
- S[&]T Corporation (2 users)
- Wageningen University & Research (2 users)

Norway:

- UiT The Arctic University of Norway

Poland:

- CloudFerro
- Institute of Environmental Protection (2 users)
- Institute of Geodesy and Cartography
- Institute of Meteorology and Water Management-NRI
- Military University of Technology
- O3Lab
- University of Warsaw

Portugal:

- Instituto Dom Luiz (2 users)
- Instituto Português do Mar e da Atmosfera (3 users)
- University of Tras-os-Montes and Alto Douro

Romania:

- Babes-Bolyai University (3 users)
- Global Top Systems
- INOE (3 users)

- University of Galați (3 users)
- Politehnica University of Bucharest

Russia:

- Altai State University
- Institute of Computational Modeling of the Siberian Branch of the RAS
- Institute of Global Climate and Ecology
- Irkutsk State Transport University
- Planeta

Serbia:

- Geographical institute “Jovan Cvijic”, SASA

Slovakia:

- Private Individual

Slovenia:

- Bide-san, s.p.

Spain:

- Autonomous University of Barcelona
- Barcelona Supercomputing Center
- Complutense University of Madrid
- GREA
- Modeliza
- NAITEC
- Pablo de Olavide University
- Polytechnic University of Catalonia (2 users)
- Private Individual
- State Meteorological Agency (2 users)
- Universitat Politècnica de València
- University of Alicante
- University of Barcelona (3 users)
- University of Granada (3 users)
- University of Extremadura (2 users)
- University of Oviedo (2 users)
- University of Valencia (3 users)
- University of Valladolid

Sweden:

- SMHI (4 users)
- The Swedish Defence Research Agency (2 users)

Turkey:

- Cukurova University
- Hacettepe University
- Kastamony University
- Middle East Technical University
- Turkish State Meteorological Service (2 users)
- Van Yüzüncü Yıl University

Ukraine:

- Batata LLC
- Scientific Centre for Aerospace Research of the Earth
- UHE LED LLC
- UHMC
- Ukrainian Hydrometeorological Institute (2 users)

United Kingdom:

- Aggreko
- ECMWF (4 users)
- ESA
- IDEMS International
- Hibarcus
- London School of Economics and Political Science
- Private individual
- Rutherford Appleton Lab
- Satavia Ltd.
- Satellite Applications Catapult
- Science and Technology Facilities Council (2 users)
- siHealth Ltd.
- University of Cambridge
- University of Hertfordshire
- University of Leeds (2 users)
- University of Leicester (2 users)
- University of Manchester
- University of York (2 users)

Asia:

Bangladesh:

- Institute of Forestry and Environmental Sciences
- University of Dhaka

China:

- Anhui Normal University
- Anhui Institute of Meteorological Sciences University of Dhaka
- Anhui Institute of Optics and Fine Mechanics (3 users)
- Anhui University (3 users)
- Beijing Municipal Environmental Monitoring Center
- Beijing Normal University
- Beijing Zhixin Remote Sensing Geographic Information Co., Ltd
- Chinese Academy of Meteorological Sciences (2 users)
- China Academy of Sciences (8 users)
- China Meteorological Administration
- China University of Mining and Technology (7 users)
- Chinese University of Hong Kong
- East China Normal University
- East China University of Science and Technology
- Fudan University

- Guangzhou University
- Hebei University of Engineering (3 users)
- Hong Kong University of Science and Technology
- HTHJ
- Institute of Atmospheric Physics
- Institute of Geographic Sciences and Natural Resources Research, China Academy of Sciences
- Institute of Remote Sensing and Digital Earth
- Jiangsu Meteorological Observatory
- Jiangsu Normal University (2 users)
- Jinan University
- Lanzhou University
- Nanjing University (3 users)
- Nanjing University of Information Science & Technology (6 users)
- National Satellite Meteorological Center
- Northeast Normal University
- Northwest Normal University
- Ocean University of China
- Peking University (5 users)
- PIE
- Piesat Information Technology Co., Ltd.
- Private Individual
- “School”
- Shandong University (3 users)
- Shanghai University
- Shenzhen University
- South China Agricultural University
- Southern University of Science and Technology (3 users)
- State Environmental Protection Key Lab of Satellite Remote Sensing
- The Chinese University of Hong Kong (2 users)
- The Institute of Atmospheric Physics (2 users)
- Tsinghua University (3 users)
- University of Science and Technology (8 users)
- (unknown) (5 users)
- Wuhan University (8 users)
- Wuhan University of Technology
- Zhejiang Academy of Agricultural Sciences
- Zhejiang University (2 users)

India:

- Anna University
- Aryabhatta Research Institute of Observational Sciences
- Banaras Hindu University
- Birla Institute of Technology
- Bose Institute
- Central University of Hyderabad
- Central University of Rajasthan
- CSIR-NIO

- Dibrugarh University (2 users)
- “Education”
- Heritage Institute of Technology (2 users)
- IIT KGP
- Indian Institute of Remote Sensing
- Indian Institute of Science
- Indian Institute of Technology Delhi
- Indian Institute of Technology Kharagpur (3 users)
- Indian Institute of Technology Roorkee (2 users)
- Indian Institute of Tropical Meteorology (3 users)
- Indian Space Research Organization (3 users)
- Jawaharlal Nehru University
- Malaviya National Institute of Technology Jaipur
- MSRIT
- National Atmospheric Research Laboratory
- National Centre for Medium Range Weather Forecasting
- National Institute of Technology
- Savitribai Phule Pune University (2 users)
- School of Planning and Architecture, Bhopal
- SIG
- Sriram Engineering College
- SRM Institute of Science and Technology
- University of Calcutta
- University of Hyderabad
- University of Kalyani
- Vikram Sarabhai Space Centre

Indonesia:

- Bandung Institute of Technology
- Meteorological, Climatological, and Geophysical Agency (3 users)
- National Institute for Aeronautics and Space
- Sumatera Institute of Technology

Japan:

- Chiba University
- Fukuoka University
- Ibaraki University
- Japan Meteorological Agency
- Kyushu University (2 users)
- Nagoya University
- National Institute for Environmental Studies
- Remote Sensing Technology Center of Japan
- Waseda University

Malaysia:

- Malaysian Meteorological Department
- Malaysian Space Agency
- National University of Malaysia (4 users)

Myanmar:

- Yangon Technological University

Nepal:

- Institute for Advanced Sustainability Studies
- Institute of Engineering
- International Centre for Integrated Mountain Development (2 users)

Pakistan:

- National University of Sciences and Technology
- University of the Punjab

Singapore:

- National University of Singapore (2 users)

South Korea:

- Chungnam National University (3 users)
- Gwangju Institute of Science and Technology (4 users)
- Korea Meteorological Administration
- Korea Polar Research Institute
- National Institute of Environmental Research (2 users)
- National Meteorological Satellite Center (3 users)
- Seoul National University (4 users)
- Ulsan National Institute of Science and Technology
- University of Suwon
- Yonsei University (6 users)

Sri Lanka:

- Central Environmental Authority

Taiwan:

- National Central University (2 users)

Thailand:

- King Mongkut's Institute of Technology Ladkrabang

Vietnam:

- University of Science (2 users)

Middle East:

Iran:

- Khavaran Institute of Higher Education
- Sepehr Payesh
- Tabriz University
- "University"
- University of Tehran (2 users)

Iraq:

- Al Iraqia University
- Mustansiriyah University

Saudi Arabia:

- King Abdulaziz City for Science and Technology
- King Abdullah University of Science and Technology
- Private individual

United Arab Emirates:

- Amity University (2 users)
- Khalifa University
- Uruk Engineering & Contracting

North America:

Canada:

- Environment and Climate Change Canada (5 users)
- Environment Canada
- University of Saskatchewan

USA:

- Arizona State University
- Caltech (2 users)
- Colorado State University
- Department of Defence
- Florida State University
- Johns Hopkins University
- Harvard University (3 users)
- Intertek
- Joint Center for Satellite Data Assimilation
- Michigan Technological University (3 users)
- NASA (6 users)
- NOAA (4 users)
- Princeton University
- Private Individual
- Smithsonian Astrophysical Observatory
- SpaceKnow Inc.
- Texas A&M University
- Trinity Consultants Inc.
- University of Alabama in Huntsville
- University of Alaska (2 users)
- University of Arizona
- University of California (5 users)
- University of Central Florida
- University of Colorado Boulder
- University of Houston
- University of Illinois
- University of Maryland (3 users)

- University of North Carolina at Chapel Hill (2 users)
- University of Washington (2 users)
- University of Wisconsin-Madison
- Unknown
- USGS
- U.S. Environmental Protection Agency
- Utah State University

South America:

Argentina:

- Argentine Air Force
- National Space Activities Commission
- Universidad Nacional de Rosario

Brazil:

- Agência Pernambucana de Águas e Clima
- APAC
- Federal University of Pernambuco
- LAPIS
- Universidade Federal de Alagoas
- University of São Paulo

Chile:

- University of the Americas

Colombia:

- Universidad EAFIT

Ecuador:

- Universidad San Francisco de Quito

Guatemala:

- INSIVUMEH

Mexico:

- Ibero Puebla
- Instituto Politecnico Nacional

Paraguay:

- Universidad San Carlos

Peru:

- Servicio Nacional de Meteorología e Hidrología del Perú

Uruguay:

- Universidad de la República

Australia / New Zealand:

- Environmental Systems & Services
- University of Canterbury (2 users)
- University of Melbourne (2 users)
- University of Southern Queensland

Africa:

Algeria:

- CTS/ASAL
- Meteo Algeria

Cameroon:

- African Institute for Mathematical Sciences

Democratic Republic of the Congo:

- University of Kinshasa

Egypt:

- Egyptian Meteorological Authority (3 users)
- National Research Institute of Astronomy and Geophysics

Eritrea:

- Department of Environment

Ghana:

- Ghana Meteorological Agency
- Kwame Nkrumah University of Science and Technology

Morocco:

- Abdelmalek Essaadi University
- EM5D
- Maroc Météo
- National Center for Meteorological Research
- University of Hassan II Casablanca

Nigeria:

- Federal University Lafia
- Federal University of Technology Akure

South Africa:

- North-West University
- South African Weather Service
- Stellenbosch University
- University of Pretoria
- University of the Witwatersrand
- Ware Jacob Enterprises

Registered users: **650**

8.3. DMI (NUV product via FTP)

- Meteorological Institute of Romania
⇒ Several commercial companies obtain the data from MIR
- Danish Meteorological Institute, Denmark
- TrygFonden, Denmark
- Department for Health, Greenland Homerule
- The Danish Cancer Society, Denmark
- Libraries of Hjørring Community
- SunSense AS, Norway
- Richard McKenzie, New Zealand
- Elian Wolfram, Laser Research Center and Applications, Argentina
- KMI, Belgium
- By & Havn I/S, Denmark

Registered users: **11**

8.4. KNMI (unofficial NRT AAI via FTP)

- FMI, Finland
- William B. Hanson Center for Space Science, USA
- University of Leicester, UK

Registered users: **3**

8.5. Known international projects that use EUMETCast or WMO/GTS

- MACC project
- SACS service
- Temis WWW service
- ESA GlobVapour
- ESA CCI Ozone project

8.6. EUMETCast

Albania	6	Hungary	13	Poland	14
Algeria	4	Iceland	1	Portugal	7
Angola	1	India	2	Qatar	3
Armenia	1	Iran, Islamic Republic of	35	Reunion	2
Austria	22	Iraq	2	Romania	10
Azerbaijan	3	Ireland	8	Russian Federation	7
Belgium	12	Israel	5	Rwanda	2
Benin	1	Italy	290	San Marino	1
Bosnia and Herzegovina	1	Jordan	1	Saudi Arabia	2
Botswana	4	Kazakhstan	6	Senegal	6
Brazil	4	Kenya	6	Serbia	2
Bulgaria	6	Kuwait	2	Seychelles	1
Burkina Faso	1	Kyrgyzstan	1	Slovakia	7
Cameroon	3	Latvia	1	Slovenia	1
Canada	1	Lebanon	3	South Africa	7
Cape Verde	1	Lesotho	2	South Sudan	1
China	4	Liberia	1	Spain	43
Congo	2	Libya	1	Sudan	1
Congo, Democratic Republic of	1	Lithuania	2	Sweden	5
Croatia	1	Luxembourg	2	Switzerland	15
Cyprus	1	Madagascar	4	Tajikistan	1
Czech Republic	22	Malawi	2	Tanzania, United Republic of	3
Denmark	6	Mali	1	Togo	1
Egypt	3	Malta	2	Tunisia	3
Equatorial Guinea	1	Mauritania	3	Türkiye	7
Estonia	3	Mauritius	2	Turkmenistan	1
Eswatini	2	Moldova, Republic of	1	Uganda	3
Ethiopia	6	Morocco	5	Ukraine	3
Finland	5	Mozambique	2	United Arab Emirates	3
France	64	Namibia	1	United Kingdom	115
Gabon	1	The Netherlands	24	United States	2
Georgia	1	Niger	3	Uzbekistan	1
Germany	112	Nigeria	7	Vietnam	1
Ghana	6	Norway	5	Yemen	1
Greece	20	Oman	1	Zambia	3
Guinea-Bissau	2	Pakistan	2	Zimbabwe	2
Hong Kong	1	Palestine	1		
TOTAL (December 2024)	1074				

9. Updates during the reporting period

Listed below are the major configuration updates concerning operational data processing and archiving. If new versions of relevant AC SAF documents are released during the reporting period, they should be listed here also.

9.1. Software updates

Nothing to report.

9.2. Hardware updates

Nothing to report.

9.3. Documentation updates

28 October	KNMI: OPERA Software Release Note (issue 2.40)
6 November	FMI: AC SAF Operations Report 1/2024 rev. 1
19 November	KNMI: LER Algorithm Theoretical Basis Document (issue 4.3)
19 November	KNMI: LER Product User Manual (issue 4.2)
19 November	KNMI: LER Product Validation Report (issue 1/2024)
9 December	FMI: AC SAF Operations Report 2/2023 rev. 2
9 December	FMI: AC SAF Operations Report 1/2024 rev. 2

10.Changes in appearance and content of the web portal

Listed below are the major changes in the appearance and content on the [AC SAF main web pages](#).

Table 10.1. Changes in appearance and content of the main AC SAF web pages during the reporting period

Date	Description
20 September	<i>datarecords/iasi_co_cdr.php</i> and <i>datarecords/iasi_so2_cdr.php</i> published. <i>datarecord_access.php</i> updated to include IASI L2 CO and SO ₂ CDRs

In addition to updates above, following routine updates are conducted whenever necessary:

- The links to public AC SAF user documents are updated whenever new documents or new versions of existing documents become available
- The “top story” on the front page is updated
- News list on the front page is updated

APPENDIX 1

Table A.1 presents the overall summary of orders from AC SAF archive at FMI, by product type, during the reporting period.

Table A.2 presents a detailed summary of product orders from AC SAF archive at FMI during the reporting period.

Table A.1. Overall summary of product orders, by product type, during the reporting period

Product type	Number of orders	Number of distinct users	Number of files	Total size
O3MARP	11	7	243	1.74 GB
O3MARS	32	5	15834	16.3 GB
O3MOHP	9	7	1007	259 GB
O3MOUV subset	13	4	2203	35.0 GB
O3MOUV time-series	25	8	94184	14.0 MB
LER-MSD	0	0	0	-
LER-PMD	0	0	0	-

Table A.2. More detailed summary of product orders during the reporting period

JULY			
Product type	Number of products	Order size	Institute / company
OUV-BC	Time series for 17 days Selected subset: ERYDD, PLADD, UVADD, UVBDD Location: 11.20E, 43.80N (2.24 kB in total)		LaMMa consortium, Italy
ARS-B ARS-C	3977 3989	8.20 GB	AUTH, Greece
ARS-B ARS-C	99 99	204 MB	AUTH, Greece
ARS-B ARS-C	96 95	198 MB	AUTH, Greece
ARS-B ARS-C	424 424	881 MB	AUTH, Greece
ARS-B	1	1.04 MB	MEE0, Italy
ARP-B	1	4.93 MB	MEE0, Italy
OUV-BC	30 Selected subset: UVADD, UVBDD, UVI Region: 18.0E – 29.0E, 53.0N – 61.0N (916 kB in total)		Latvian Environment, Geology and Meteorology Centre
ARS-B ARS-C	171 171	453 MB	AUTH, Greece

ARS-B ARS-C	57 57	118 MB	AUTH, Greece
ARS-B ARS-C	42 43	86.9 MB	AUTH, Greece
ARS-B ARS-C	57 57	118 MB	AUTH, Greece
ARS-B ARS-C	57 57	118 MB	AUTH, Greece
OHP-B	439	110 GB	Peking University, China
OUV-B	Time series for 31 days Selected subset: ERYDD, UVADD, UVBDD, UVI Location: 16.80E, 28.20S (3.54 kB in total)		University of Pretoria, South Africa
OUV-B	Time series for 31 days Selected subset: ERYDD, UVADD, UVBDD, UVI Location: 16.87E, 28.10S (3.54 kB in total)		University of Pretoria, South Africa
ARP-A	2	12.6 MB	Michigan Technological University, USA
AUGUST			
Product type	Number of products	Order size	Institute / company
ARS-B ARS-C	436 437	907 MB	AUTH, Greece
OHP-B OHP-C	14 14	7.02 GB	Ukrainian Hydrometeorological Institute
ARS-B ARS-C	213 213	442 MB	AUTH, Greece
ARS-B ARS-C	28 29	59.4 MB	AUTH, Greece
ARS-B ARS-C	29 28	59.0 MB	AUTH, Greece
ARS-B ARS-C	43 42	87.6 MB	AUTH, Greece
ARS-B ARS-C	29 28	59.0 MB	AUTH, Greece
OUV-BC	31 Selected subset: UVADD, UVBDD, UVI Region: 18.0E – 29.0E, 53.0N – 61.0N (947 kB in total)		Latvian Environment, Geology and Meteorology Centre
ARS-B ARS-C	14 14	28.4 MB	AUTH, Greece
ARS-B ARS-C	14 15	30.1 MB	AUTH, Greece
ARS-B ARS-C	14 14	29.0 MB	AUTH, Greece

ARS-B ARS-C	14 14	29.2 MB	AUTH, Greece
ARS-B ARS-C	14 15	30.1 MB	AUTH, Greece
OUV-A OUV-AB OUV-B OUV-BC	Time series for 5843 days Selected subset: UVBDD Location: 179.5W, -90.0S (480 kB in total)		Potsdam Institute for Climate Impact Research, Germany
OUV-A OUV-AB OUV-B OUV-BC	Time series for 5843 days Selected subset: UVBDD Location: 180.0W, -90.0S (480 kB in total)		Potsdam Institute for Climate Impact Research, Germany
ARP-B ARP-C	41 42	596 MB	MEE0, Italy
ARP-B ARP-C	3 3	43.8 MB	MEE0, Italy
ARS-B ARS-C	14 14	29.0 MB	AUTH, Greece
ARS-B ARS-C	14 15	30.1 MB	AUTH, Greece
ARS-B ARS-C	15 14	30.1 MB	AUTH, Greece
ARS-B ARS-C	14 15	30.1 MB	AUTH, Greece
SEPTEMBER			
Product type	Number of products	Order size	Institute / company
ARP-B ARP-C	12 12	170 MB	FMI, Finland
ARS-C	14	14.6 MB	S[&]T, the Netherlands
ARP-C	14	102 MB	S[&]T, the Netherlands
OUV-BC	31 Selected subset: UVADD, UVBDD, UVI Region: 18.0E – 29.0E, 53.0N – 61.0N (947 kB in total)		Latvian Environment, Geology and Meteorology Centre
ARP-C	1	7.31 MB	EUMETSAT, Germany
ARS-B ARS-C	438 432	902 MB	AUTH, Greece
ARP-B ARP-C	14 13	197 MB	FMI, Finland
ARS-B ARS-C	440 439	905 MB	AUTH, Greece
ARS-B ARS-C	439 439	906 MB	AUTH, Greece
ARS-B ARS-C	411 408	842 MB	AUTH, Greece

ARP-B ARP-C	14 13	197 MB	FMI, Finland
ARS-B ARS-C	27 28	56.5 MB	CNR, Italy
ARS-B ARS-C	268 266	552 MB	AUTH, Greece
OHP-B	1	250 MB	Wuhan University, China
OHP-B	13	3.25 GB	Wuhan University, China
OHP-C	15	3.74 GB	Wuhan University, China
OHP-B	439	110 GB	Peking University, China
OCTOBER			
Product type	Number of products	Order size	Institute / company
OUV-BC	153 Selected subset: ERYDD, DNADD, PLADD, UVADD, UVBDD, ERYDR, DNADR, PLADR, VITDR, UVADR, UVBDR Region: global (944 MB in total)		University of Helsinki, Finland
OUV-BC	31 Selected subset: UVADD, UVBDD, UVI Region: 18.0E – 29.0E, 53.0N – 61.0N (914 kB in total)		Latvian Environment, Geology and Meteorology Centre
OHP-A	56	20.8 GB	CNR, Italy
OUV-BC	213 Selected subset: ERYDD, DNADD, PLADD, UVADD, UVBDD, ERYDR, DNADR, PLADR, UVADR, UVBDR Region: global (1.25 GB in total)		University of Helsinki, Finland
OUV-BC	153 Selected subset: UVADD, UVBDD, UVADR, UVBDR Region: 11.0W – 5.0W, 35.0N – 43.0N (5.01 MB in total)		University of Helsinki, Finland
OUV-BC	Time series for 153 days Selected subset: UVADD, UVBDD, UVADR, UVBDR Location: 25.0E, 60.0N (14.9 kB in total)		University of Helsinki, Finland

OUV-A	Time series for 1310 days Selected subset: DNADD, UVBDD, PLADR, UVBDR Location: 38.0E, 34.0N (238 kB in total)		Massey University, New Zealand
OHP-C	14	3.51 GB	University of Science and Technology, China
OUV-BC	Time series for 152 days Selected subset: UVADD, UVBDD, UVADR, UVBDR, UVI Location: 23.5W, 67.7S (16.5 kB in total)		University of Helsinki, Finland
OUV-BC	20 Selected subset: PLADD, UVADD, UVBDD, PLADR, UVADR, UVBDR, UVI Region: 10.8W – 4.8W, 35.2N – 43.2N (922 kB in total)		University of Helsinki, Finland
OUV-A OUV-AB OUV-B OUV-BC	Time series for 6198 days Selected subset: PLADD, UVADD, UVBDD, PLADR, UVADR, UVBDR Location: 0.8E, 77.7S (1.53 MB in total)		University of Helsinki, Finland
OUV-A OUV-AB OUV-B OUV-BC	Time series for 6198 days Selected subset: PLADD, UVADD, UVBDD, PLADR, UVADR, UVBDR, UVI Location: 77.7W, 0.8N (782 kB in total)		University of Helsinki, Finland
OUV-BC	Time series for 366 days Selected subset: PLADD, UVADD, UVBDD, PLADR, UVADR, UVBDR, UVI Location: 66.8W, 23.5S (46.9 kB in total)		University of Helsinki, Finland
OUV-A OUV-AB OUV-B OUV-BC	Time series for 6025 days Selected subset: PLADD, UVADD, UVBDD, PLADR, UVADR, UVBDR, UVI Location: 25.0E, 60.0N (760 kB in total)		University of Helsinki, Finland
OUV-A OUV-AB OUV-B OUV-BC	Time series for 6178 days Selected subset: PLADD, UVADD, UVBDD, PLADR, UVADR, UVBDR, UVI Location: 73.3W, 39.8S (779 kB in total)		University of Helsinki, Finland

OUV-BC	<p>3 Selected subset: ERYDD, DNADD, PLADD, VITDD, UVADD, UVBDD Region: 10.8W – 4.8W, 35.2N – 43.2N (123 kB in total)</p>	University of Helsinki, Finland
OUV-A OUV-AB OUV-B OUV-BC	<p>Time series for 6178 days Selected subset: PLADD, UVADD, UVBDD, PLADR, UVADR, UVBDR, UVI Location: 38.0E, 11.3N (779 kB in total)</p>	University of Helsinki, Finland
OUV-A OUV-AB OUV-B OUV-BC	<p>Time series for 6178 days Selected subset: PLADD, UVADD, UVBDD, PLADR, UVADR, UVBDR, UVI Location: 137.7E, 34.0S (779 kB in total)</p>	University of Helsinki, Finland
OUV-A OUV-AB OUV-B OUV-BC	<p>Time series for 6178 days Selected subset: PLADD, UVADD, UVBDD, PLADR, UVADR, UVBDR, UVI Location: 34.3E, 30.9N (779 kB in total)</p>	University of Helsinki, Finland
OUV-A OUV-AB OUV-B OUV-BC	<p>Time series for 6178 days Selected subset: PLADD, UVADD, UVBDD, PLADR, UVADR, UVBDR, UVI Location: 8.5W, 52.0N (779 kB in total)</p>	University of Helsinki, Finland
OUV-A OUV-AB OUV-B OUV-BC	<p>Time series for 6178 days Selected subset: PLADD, UVADD, UVBDD, PLADR, UVADR, UVBDR, UVI Location: 25.7E, 66.5N (779 kB in total)</p>	University of Helsinki, Finland
OUV-A OUV-AB OUV-B OUV-BC	<p>Time series for 6178 days Selected subset: PLADD, UVADD, UVBDD, PLADR, UVADR, UVBDR, UVI Location: 58.0W, 37.1S (779 kB in total)</p>	University of Helsinki, Finland

OUV-A OUV-AB OUV-B OUV-BC	Time series for 6178 days Selected subset: PLADD, UVADD, UVBDD, PLADR, UVADR, UVBDR, UVI Location: 3.4W, 38.3N (779 kB in total)		University of Helsinki, Finland
OUV-A OUV-AB OUV-B OUV-BC	Time series for 6178 days Selected subset: PLADD, UVADD, UVBDD, PLADR, UVADR, UVBDR, UVI Location: 38.3E, 3.4S (779 kB in total)		University of Helsinki, Finland
NOVEMBER			
Product type	Number of products	Order size	Institute / company
OUV-BC	Time series for 3 days Selected subset: UVADD, UVBDD Location: 37.3W, 8.1S (815 B in total)		Federal University of Pernambuco, Brazil
OUV-BC	Time series for 3 days Selected subset: ERYDD, DNADD, PLADD, VITDD, UVADD, UVBDD, ERYDR, DNADR, PLADR, VITDR, UVADR, UVBDR, JO1D, JNO2, UVI Location: 37.3W, 8.1S (3.59 kB in total)		Federal University of Pernambuco, Brazil
ARP-B ARP-C	15 14	205 MB	FMI, Finland
ARP-B ARP-C	15 14	205 MB	FMI, Finland
DECEMBER			
Product type	Number of products	Order size	Institute / company
OUV-BC	224 Selected subset: ERYDD, DNADD, PLADD, VITDD, UVADD, UVBDD, ERYDR, DNADR, PLADR, VITDR, UVADR, UVBDR, JO1D, JNO2, UVI Region: global (3.93 GB in total)		FMI, Finland

OUV-BC	190 Selected subset: ERYDD, DNADD, PLADD, VITDD, UVADD, UVBDD, ERYDR, DNADR, PLADR, VITDR, UVADR, UVBDR, JO1D, JNO2, UVI Region: global (3.50 GB in total)	FMI, Finland
OUV-BC	181 Selected subset: ERYDD, DNADD, PLADD, VITDD, UVADD, UVBDD, ERYDR, DNADR, PLADR, VITDR, UVADR, UVBDR, JO1D, JNO2, UVI Region: global (3.21 GB in total)	FMI, Finland
OUV-BC	944 Selected subset: ERYDD, DNADD, PLADD, VITDD, UVADD, UVBDD, ERYDR, DNADR, PLADR, VITDR, UVADR, UVBDR, JO1D, JNO2, UVI Region: global (22.2 GB in total)	FMI, Finland
OHP-C	2 504 MB	S[&]T, the Netherlands
OUV-A OUV-AB OUV-B OUV-BC	Time series for 6407 days Selected subset: ERYDD, DNADD, VITDD, UVADD, UVBDD, ERYDR, DNADR, VITDR, UVADR, UVBDR, UVI Location: 0.4W, 41.9N (2.64 MB in total)	University of Barcelona, Spain
OUV-BC	Time series for 2 days Selected subset: UVADD, UVBDD, UVADR, UVBDR, UVI Location: 34.9W, 8.1S (1.45 kB in total)	Federal University of Pernambuco, Brazil

APPENDIX 2

Table A.3 presents a detailed summary of failed product orders from AC SAF archive at FMI during the reporting period. The middle column indicates whether the failure was related to problems with AC SAF archive and/or ordering system or was the problem on the user’s side.

Table A.3. Summary of failed product orders during the reporting period

Date	Error type	Failure description and details
		Order ID: User institute: Order contents: Ordering log error message: Failure description: Corrective action: Final outcome: